

# **Quantum effects in charge control of semiconductor surfaces as elucidated by *ab initio* calculations – a review**

by Stanisław Krukowski, Paweł Kempisty and Paweł Strak

Institute of High Pressure Physics, Polish Academy of Sciences, Sokołowska 29/37,  
01-142 Warsaw, Poland

## Abstract

Recent progress in the investigations of the charge role in semiconductor surfaces is reviewed. The review includes methodologies both improvements of the calculation methods and the new type of analysis of the obtained data. The new methods include application of Laplace correction method in *ab initio* calculations. The new analysis methods incorporate: averaging of potential profiles to get its smoothed long-range variation, parallel plots of real space variation of band profiles, the use of projected density of states (PDOS) and Crystal Orbital Hamilton Population (COHP) data into the determination of the nature of the surface states. These methods provided insight into the relation between the charge distribution in space and the long-range potential variation. Thus these data have direct connection to the band profile in real space that was used to gain more insight into the bonding in the systems including the regions close to the surfaces. As a methodological supplement the spurious Coulomb interaction between the separated subsystems was discovered and presented. In the case of far distant (i.e. isolated) adsorbate and the slab they should have different Fermi levels. In *ab initio* calculations the common Fermi level is used that may cause incorrect electrons occupation of the quantum states these two subsystems. This will lead to artificial charging of both part and the purely artificial interaction. Other new methodologies incorporate applications of nonstandard quantum methods to bonding of atoms both in the bulk and at the surface. That is the concept of fractional occupation of the quantum states. They could be interpreted as resonant states that resolves existing inconsistencies between the bonding and the lattice symmetry in nitrides. This methodological set drastically improved understanding of the quantum nature of charge influence on semiconductor surfaces. Among them the delocalization of electrons is prominent as it leads to emergence of the external surface dipole. In addition to determination of the workfunction magnitude, the new role of the external dipole layer in the thermalization of the

adsorbate via electron tunneling was proposed. It was argued that the adsorbate kinetic energy loss (i.e. its thermalization) occurs via tunneling of electrons into the solid interior due to strong electric field induced by dipole at the external boundary of the crystal. The tunneling electrons carry the excess kinetic energy deep into the solid interior where it is dissipated by emission of phonons. These electrons are thermalized to Fermi energy level. At the same time the external dipole field causes deceleration of the positively charged adsorbate and its smooth attachment at the surface. The other charge related effect is the emergence of the internal dipole charge layer. The effect was already well known to exist at the surface before reported investigations. The findings reported in this review include simulations of long range variation of the electric potential within slab model. In these investigations the band bending at the surfaces of several semiconductors were obtained that led to identification of the surface states Stark effect and its role in the determination of the surface band diagrams. That elucidated the role of pinning the Fermi level at the surface and its connection to the internal dipoles. The charge balance determines occupation of surface states and the symmetry and periodicity of surface reconstructions. In connection to that it was also shown that the occupation of surface states may be drastically changed by the adsorption processes. This results from the balance between the increase of the number of the electrons donated by the adsorbate and the emergence of the new quantum states. As these numbers could be different that leads to redistribution of the electrons among the surface states. The changes of their occupation could possibly lead to the change of the pinning of Fermi level at the surface and a considerable change of the adsorption energy at some critical coverages. The coverage is critical because Fermi level becomes free, the surface dipole could disappear and the bands could become flat. At this particular coverage the adsorption energy is changed by jump-like manner as the energy contribution from the electron redistribution is changed. The typical energy changes are considerable, in case of wideband semiconductors that may reach several eVs. The effect is translated into the change of the equilibrium vapor pressure of the adsorbate by several orders of magnitude. Therefore such state of the surface is likely to occur during growth of crystals as the growth pressures are frequently located within such large pressure intervals. Thus the growth of semiconductors is conducted for the bands flat at the surface. In total the adsorption and the growth are controlled by quantum charge balance at the surface. Additional modification of the adsorbate states by quantum effects may include the change of its bonding including resonance between several states which leads to their fractional occupation. This effect is observed not only at the stability points but also at the activated complex position. The energies of the states are then affected by these quantum effects. Since the energy of quantum states are increased during the jump,

they can move into the vicinity of Fermi level or even move higher. These states are therefore fractionally or completely empty so that the quantum statistics may affect the energy barrier for diffusion severely. These numerous results proved that explicit incorporation of quantum effects demonstrate the role of the charge in the semiconductor surfaces that changes their properties considerably as described in this review.

## I. Introduction

Crystalline semiconductors are important class of the solid state systems that were in the focus of the intensive research for the recent 80 years [1,2]. They are indispensable for the development of modern civilization. This stems from their unique properties that were investigated in fundamental research first and subsequently applied in the technology. These applications are always related to the investigations, control and manipulation of the electric charge.

Therefore the charge is the most essential factor in the semiconductor physics and chemistry. The charge manipulation is indispensable in the computer logic, control of the electric current flow, detection of the changes in environment, absorption and emission of electromagnetic radiation, generation and measurements of vibration including the sound, measurements of time, frequency etc. These functions are possible due to different functionalities of specially designed semiconductor structures, built in the depth of the semiconductors and also close to and on the surface. Therefore the surface charge state is important factor affecting functioning of semiconductor devices [3].

Emergence of the locally unbalanced charge at semiconductor surfaces creates electric fields in the surrounding [3-5]. That induces the changes in the semiconductor bulk by emergence of the screening charge that limits the field penetration into the semiconductor bulk. This is a long-range effect of the charge balance related to creation of surface electric dipole on the internal side of the surface. The properties of the dipole, such as charge separation, dipole density, etc. depend on the mobile charge in the semiconductor interior. In general the dipole may have different orientation depending on the charge accumulated, located on the surface donors or acceptors. In addition to this effect, on the other side of the surface an additional, second dipole is present. The latter charge effect is related exclusively to quantum-mechanical properties of the solid state bonding. Accordingly, it is typical for all solids, with the most dramatic consequences for semiconductors. Wavefunctions of the valence band states extend behind the outermost layers of atoms, or more precisely behind the outermost layer of atomic nuclei thus creating external layer of negative charge. In conjunction with the positive charge of these atomic nuclei that creates electric dipole layer, preventing electron escape, i.e. constituting electron work function [3,7-10]. The external dipole layer was recognized fairly early by Lang and Kohn [9,10]. This phenomenon is different from the previous one as the latter generates high magnitude electric dipole field narrow layer. The field is strongly localized in the direction perpendicular to the surface. At the same time it is slowly varying, long-range in

the direction parallel to the surface [9, 10]. In contrast to the internal dipole, the outside dipole is always directed in the same direction so that the electron energy is lower in the solid interior.

These two effects are purely physical in nature, i.e. they are basically identical for all semiconductor surfaces. They could have chemical counterpart in relative secondary sense, i.e. their amplitude can be modified. In addition, the semiconductor surfaces have also the properties that are different in nature. They are related to the bonding between atoms, i.e. they are chemical in nature. These are the bonds or rather quantum states associated with the bonding between atoms, i.e. valence band (VB) states. In standard semiconductors these bonds are interpreted in terms of the overlap between  $sp^3$  hybridized orbitals of metal and nonmetal, such as Ga and As. This picture is not universal, as shown by soft x-ray emission spectroscopy of nitrides: AlN [11] and GaN[12]. From *ab initio* simulations it was found that valence band consist of the two separate subbands: the upper created by metal  $sp^3$  hybridized orbitals and nitrogen  $p$  orbitals [11-13]. The lower consists of nitrogen  $s$  orbitals and  $d$  orbitals of gallium [12,14]. In the case of AlN the latter contribution is missing. Therefore the bonding of nitrogen in tetrahedral coordination is created via four resonant states [14]. This has drastic consequences both in the bonding of the bulk and also at the surfaces.

Surface atoms have their bonds broken, i.e. with no overlap as the neighbors are missing [3]. Therefore these states have their energies higher than VB states, usually they are located in the bandgap. These states may be occupied, fully, partially or they may be empty. They can be modified by relocation of atoms that will lead to the emergence of their overlaps with the other atoms that change of their energies and occupation. That changes the surface symmetry, i.e. new reconstructions emerge [3]. In addition, adsorption of additional species could bring similar effects. These adsorption processes may also involve charge transfer between different surface states. Therefore the interplay between charge distribution, reconstruction and possible adsorption of the species is extremely complex. These phenomena are predominantly quantum in nature therefore the elucidation of these phenomena by *ab initio* calculations and their relation to other approaches and final verification by the experiment is the subject of the present review.

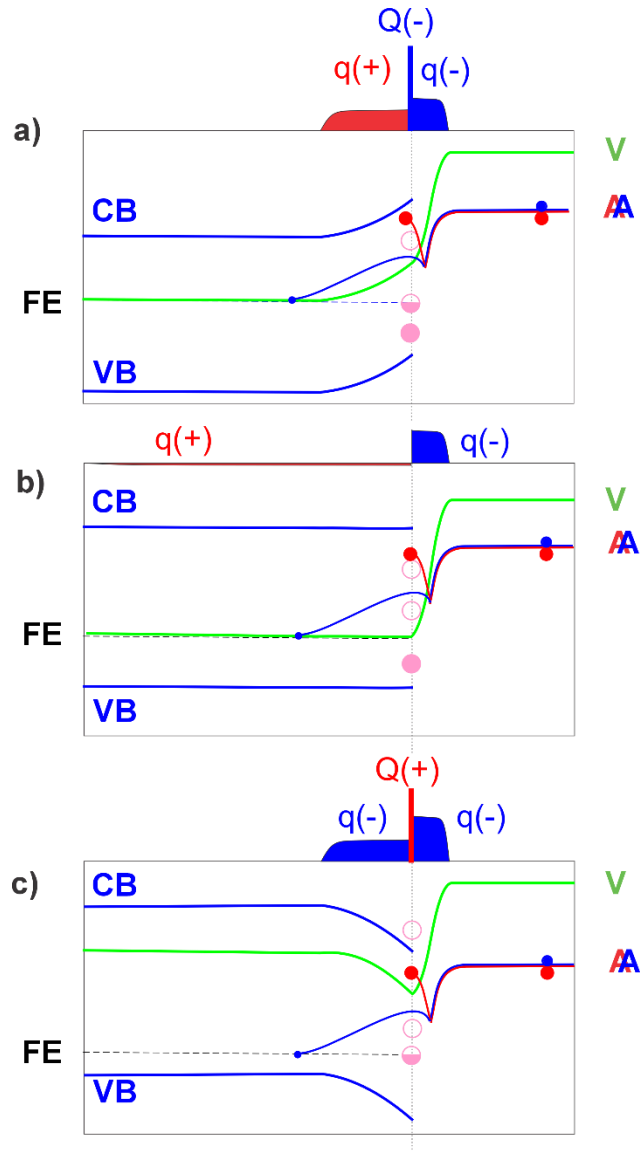


Fig. 1. Schematic presentation basic effects affecting the properties of semiconductor surfaces underlining the role of the charge. Blue lines represent the conduction band (CB) and valence band (VB), the green line presents the electric potential (V) expressed as electron energy. Broken black line represents Fermi energy (FE) in three cases: (a) FE pinned at the surface acceptor state, (b) FE free, (c) FE pinned at the surface donor state. Above the diagrams the excess charge is plotted using blue and red color to denote negative ( $q(-)$  and  $Q(-)$ ) and positive ( $q(+)$  and  $Q(+)$ ) charge, respectively. The extended charge ( $q$ ) and localized ( $Q$ ) are presented. The line marked by double red/blue colors (AA) shows the energy of electrically neutral adsorbate which is represented by two connected filled circles: large red for positive nucleus and small blue for electrons, respectively. In the high field region the adsorbate is dissociated into positive nucleus which is decelerated and negative electron accelerated, respectively. The electron tunnels into the solid interior to be ultimately thermalized to Fermi energy by emission of phonons. The rosy circles at the surface represent occupied and empty

surface states. During attachment of the adsorbate both the electrons and the states are added.

In the case of surplus of the electrons the state of the surface is shifted in the following way  $(c) \rightarrow (b) \rightarrow (a)$ , in the opposite case (i.e. electron shortage) the shift is reversed  $(a) \rightarrow (b) \rightarrow (c)$ . When the number of new electrons and states below Fermi level is equal, there is no shift.

The basic principles governing these phenomena are presented in the schematic diagram of the semiconductor surface profiles illustrated in Fig. 1. As it is shown semiconductor surface properties are affected by the presence of the charged surface states and the extended charge density on both internal and external side of the surface. The variants presented in Fig 1 (a-c) correspond to different charge present on surface states and on the internal side of the surface, i.e. internal dipole. External dipole, which is of purely quantum origin, is always directed in the same direction. This dipole is responsible for the work function, i.e. essentially the barrier keeping electrons inside the crystals. These two effects are connected to the charge density, point and extended and the corresponding band bending and potential change at the surface following from the Fermi level pinning.

Supplemental to equilibrium properties the charge effects affects also the molecular processes at the surface. As it is shown, the adsorption of new species adds the specified number of electrons and the quantum states. The relative balance of these two is crucial:

- in case of surplus of electrons the partially filled state are filled completely and the ensuing motion of the Fermi level upward from pinning state leads to free position and ultimately to the final pinning by the higher energy state. In case of Fermi level free, i.e. fully occupied states, the upward motion of Fermi level is reduced to the final part, i.e. it leads to partial filling of the higher energy surface state and pinning Fermi level there.
- in case of the surplus of newly added states, adsorption leads evacuation of the partially filled states and the Fermi level motion downward from pinned to free position, and ultimately to partial evacuation of the lower energy state and pinning the Fermi level there. In the case of Fermi level free the sequence of events is reduced the partial evacuation of lower energy state and pinning Fermi level there.

These scenario describes the final results of the adsorption process and could be treated by electron counting rule (ECR) formalism.

The external dipole plays critical role in the course of adsorption process. As shown in Fig. 1, potential energy has minimum that is necessary to stabilize adsorbate at the surface. Therefore approaching adsorbate attains kinetic energy. This has to be dissipated to thermalize

adsorbate at the surface and to avoid its reflection. The process is attained by two factors related to external dipole: acceleration and tunneling of the electron into the interior and deceleration of the positively charged adsorbate.

In addition to above, the periodicity of the surface reconstruction is controlled by the charge balance which may be affected by the adsorbate. This can be understood in the framework of resonating bond formalism which has to be applied to nitrogen component of the nitrides. This equilibrium picture will be supplemented by the analysis of the diffusion where the Fermi level position influence on the initial and the saddle point state is described, including the nitrogen bonding peculiarities.

These ideas will be presented below in detailed fashion. In order to create a coherent picture they will be preceded by the detailed presentation the calculation models, based on *ab initio* methods addressed to surfaces, and the developed analytical tools. The methodological part will be followed by the presentation of the recent development of the field along the above short description. These results will be finally summarized.

## **II. The *ab initio* calculation models of semiconductor surfaces**

The calculation models used for simulation of the properties of the surfaces stem from the difficult compromise between the limited computing resources available for calculations and the long distance coupling existing in these systems. In addition, the requirement of numerical efficiency enforces application of the mathematical methods based on Fourier transform which imposes severe limitations on the construction of the possible models. This enforces periodic boundary conditions in all three directions. In the plane parallel to the surface this is natural choice, subject to the system size only. Essentially, that choice reduces effective simulations to the flat surface only. These systems are therefore also denoted as supercells as they contain several single unit cells of the crystalline lattice. In the direction perpendicular to the surface the simulations have to overcome the long range coupling which acts against the periodicity of the potential and the wavefunctions. The solution is to use a slab of atoms, i.e. several layers of atoms in the lattice of the solid surrounded by empty space, i.e. having two surfaces. The first one is natural, i.e. the real one that is simulated, the second is artificial as it replaces the crystal bulk. In this unnatural way the basic periodicity in the dimension perpendicular to the surface is recovered. The boundaries of the simulated volume in the perpendicular direction may be selected in any way, the preferable choices are: inside the atomic layers or in the vacuum space. Note that this entails an infinite periodic chain of slabs in the direction perpendicular to the surface.

The slab as a whole has to be electrically neutral which is necessary condition for the stability of the infinite chain of the slabs. Nevertheless the three different factors can contribute to the charge separation in the slab creating electric dipole and subsequently the potential difference across the slab: a spontaneous polarization, the polarity of the surfaces and localization of the charge on the surface states. All these factors contribute to the potential difference across the slab. In the result this potential difference has to be compensated by the artificially designed opposite term. The first remedy was proposed by Neugebauer and Scheffler, who introduced compensating dipole layer in the vacuum space [15]. The next solution was proposed by Bengtsson who also proposed dipole correction [16]. Finally, Krukowski et al. proposed Laplace correction method compensating the field in the vacuum space [17]. In the latter case, in absence of any special measures, the potential difference is compensated by the additional uniform electric field in the vacuum space [17].

In fact, the Neugebauer and Scheffler solution compensates slab dipole by the additional compensating dipole which is inserted in the vacuum space at the distance close to the midpoint of the vacuum spacer between slab copies. This compensation could be affected by the error related to imprecise representation of the charge density by finite grid and miscalculation of the slab dipole [18]. In addition the presence of the dipole affects the wavefunctions of the slab, despite the fact that they are at some distance. Thus this solution could potentially deteriorate the convergence in self-consistent field (SCF) solution loop of nonlinear equations [17]. Bengtsson method is based on the periodic solution of Poisson equation with the potential jump added to Hartree potential. Therefore Bengtsson method is essentially an introduction of direct potential jump at the boundary of simulated volume obtained from the dipole calculated for the simulated volume [16]. This version again suffers from imprecise representation of the charge density field [18]. The finite size dipole is replaced by potential jump. Finally, in the paper by Krukowski et al. Laplace correction is used as a field compensation method [17]. The method adds solution of Laplace equation, i.e. uniform electric field, opposite to the field in the vacuum space. Therefore the field is compensated, within the precision of the determination of the field in the empty space. Naturally this is with the finite precision only which creates a possible source of errors in the application of this method. In summary, in any situation the electric potential has the difference between both sides of the slab which is exactly in the case of the surface finite layer of atoms at the real semiconductor surfaces. Therefore no additional energy term has to be added to Laplace correction method [17].

As mentioned, the surface dipole in the slab calculations may be related to several factors. First is the spontaneous polarization of the crystals having the symmetry permitting

emergence of the vectorial quantity. In wurtzite semiconductors the spontaneous polarization is possible while in cubic zinc blende lattice it is not [19,20]. The spontaneous polarization of the wurtzite nitrides was simulated theoretically and investigated experimentally by a number of authors [18,21-29].

*Table 1. Fundamental properties of group III nitride wurtzite semiconductors: experiment and theory*

MeN <sub>exp/th</sub>	$a$ (Å)	$c$ (Å)	$S_{wz}$ (Å <sup>2</sup> )	$P_3$ (C/m <sup>2</sup> )	$q$ (10 <sup>-3</sup> e)	$E_g$ (eV)
BN <sub>exp</sub>	2.550	4.227	5.631			6.8
BN <sub>th</sub>	2.5417	4.2019	5.595	0.061	3.81	6.77
AlN <sub>exp</sub>	3.111	4.981	8.382			6.09
AlN <sub>th</sub>	3.1126	4.9815	8.390	0.059	3.68	6.19
GaN <sub>exp</sub>	3.1890	5.1864	8.807			3.47
GaN <sub>th</sub>	3.1955	5.2040	8.843	0.011	0.687	3.41
InN <sub>exp</sub>	3.5705	5.703	11.040			0.90
InN <sub>th</sub>	3.5705	5.7418	11.040	0.014	0.874	0.65

The “exp” and “th” mark the experiment and theory, respectively. The x-ray data were collected from: BN [30], AlN [31], GaN [32], InN [33]. The area for single site for MeN(0001) surface was calculated from  $S_{wz} = a^2\sqrt{3}/2$ . The spontaneous polarization are not accessible in experiment, the theoretical values were collected from Ref 25 [25]. The other theoretical values are given in Refs 21-29 [21-29]. The polarization charge for the single site was calculated from the formula:  $q_{sp-pol} = P_3/S_{wz}$ . The experimental bandgaps were collected from: BN [34], AlN [35], GaN [36,37], InN [37-40]. The theoretical bandgaps depend on the potential used, the quoted data are collected from the authors publications.

From these data it follows that a relatively good agreement is obtained for the lattice parameters. In case of polarization values, the theoretical values obtained from Ref 25-27 are close, the values obtained in Ref 28 are much larger. The obtained polarization values are relatively low, especially for GaN and InN, indicating that the electric fields associated with the spontaneous polarization are relatively small. This was confirmed by the work by Kempisty et al. for GaN(0001) surface where the compensation of the leftover polarization field was achieved using small, fractional charge hydrogen pseudoatoms of the charge  $\Delta Z \approx 0.01$  [41].

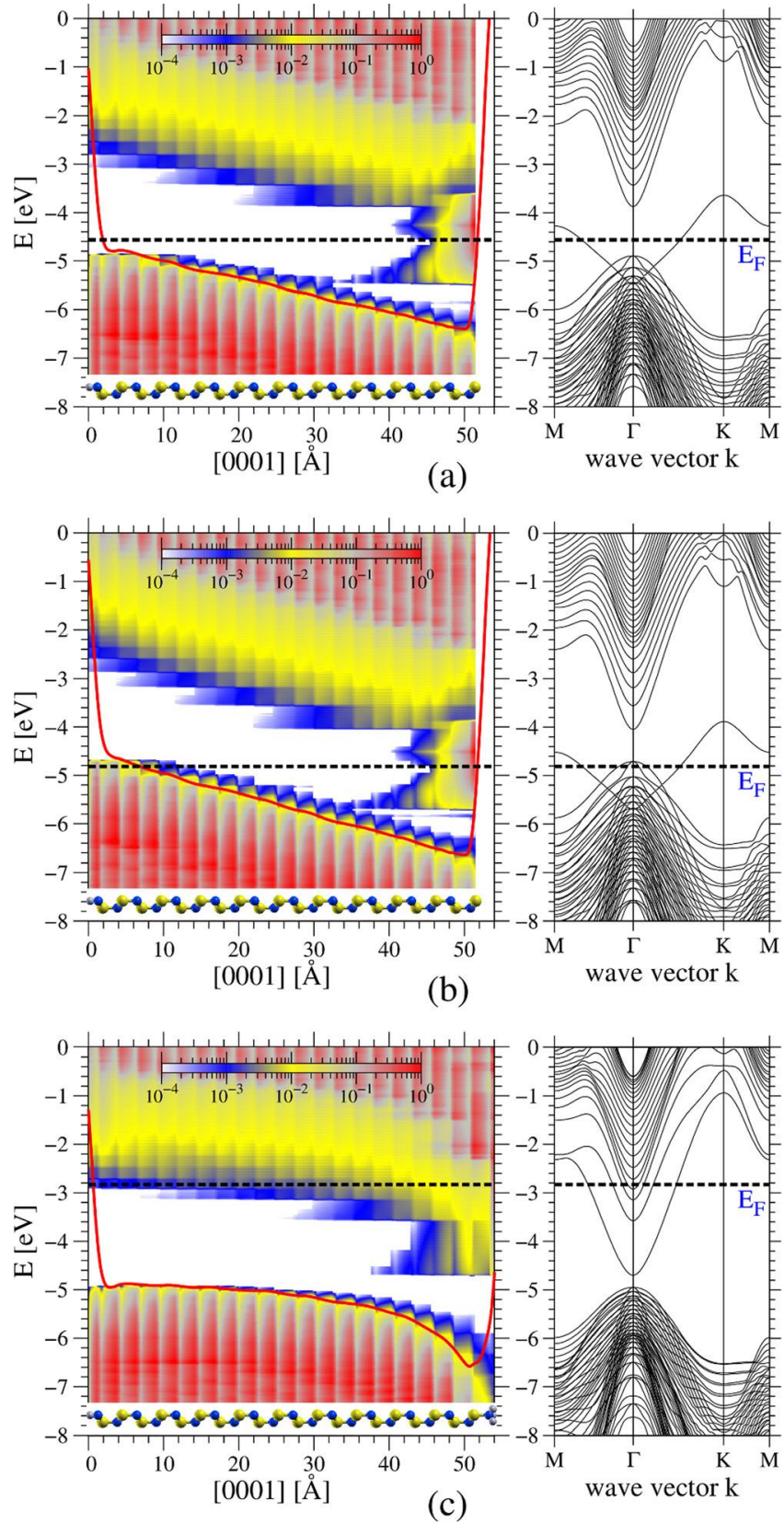


Fig. 2. Left diagram—the electric potential distribution, averaged in the plane perpendicular to c-axis, shown as electron energy (red line), and the density of states projected on the atom

quantum states (P-DOS), showing the spatial variation of the valence and conduction bands in the slabs having 20 DALs used for a simulation of a surface donor. The shades are (in arbitrary units): red—above 0.5, grey—0.1 yellow—0.01, blue— 0.001, white below 0.0001. Right diagram—the band diagram of the slab. The diagrams represent: (a) clean GaN(0001) surface with termination by  $Z = 0.715$  hydrogen pseudoatoms ; (b) clean GaN(0001) surface with termination by  $Z = 0.635$  hydrogen pseudoatoms; (c) GaN(0001) surface covered by 1 ML of ammonia with  $Z = 0.735$  hydrogen termination pseudoatoms. The schemes of the GaN slabs are presented beneath the spatial band variation diagrams. Reproduced Fig. 9 from Ref. 29 [29].

The use of hydrogen pseudoatoms at the opposite, termination surface was proposed to reduce the effect of broken bonds states both in quantum mechanical and electric potential aspects [42,43]. This is related to the presence of the charge located on the surface states, and ensuing emergence of the electric field at the surface [4, 5, 29]. The simulations recover such fields in finite thickness layer, therefore the obtained energies of the states within the slab are affected in function of their position. The effect is illustrated in Fig. 1 copied from Ref 29. where this effect was discussed.

Similar results were obtained recently by Yoo et al. in simulations of ZnO slab supercell calculations [44]. Natural consequence of the field presence is the skewed band diagram in which the projection of the states, necessary to create the typical band diagram in momentum space, leads to apparent reduction of the bandgap as shown in Fig. 2. This effect was not considered in the early publications dealing with semiconductor surfaces. The composed volume-surface band structure of ideal and relaxed nonpolar GaN surfaces calculated in local density approximation (LDA) was presented first by Northrup and Neugebauer [45]. In their diagram the band states are presented as shaded area while the surface states are presented as line in energy- momentum (parallel) coordinate system. This approach, necessary to avoid overshadowing of the surface states, was employed in number of later publications [45-50]. These diagrams are not incorrect, nevertheless they do not capture the complexity of the semiconductor surfaces.

In fact, the surface states are a part of the total band structure of the surface slab that is composed of the bulk states and the surface states. The examples of such diagram are presented in Fig. 3 where the band diagrams of the slab presenting clean polar AlN (0001) and AlN(000 $\bar{1}$ ) surfaces are presented [51]. The calculated slabs contained 24 double atomic layers

(DAL) of Al-N slabs, without any coverage on both sides. The image presents band diagrams in momentum and real space and also partial density of states (PDOS).

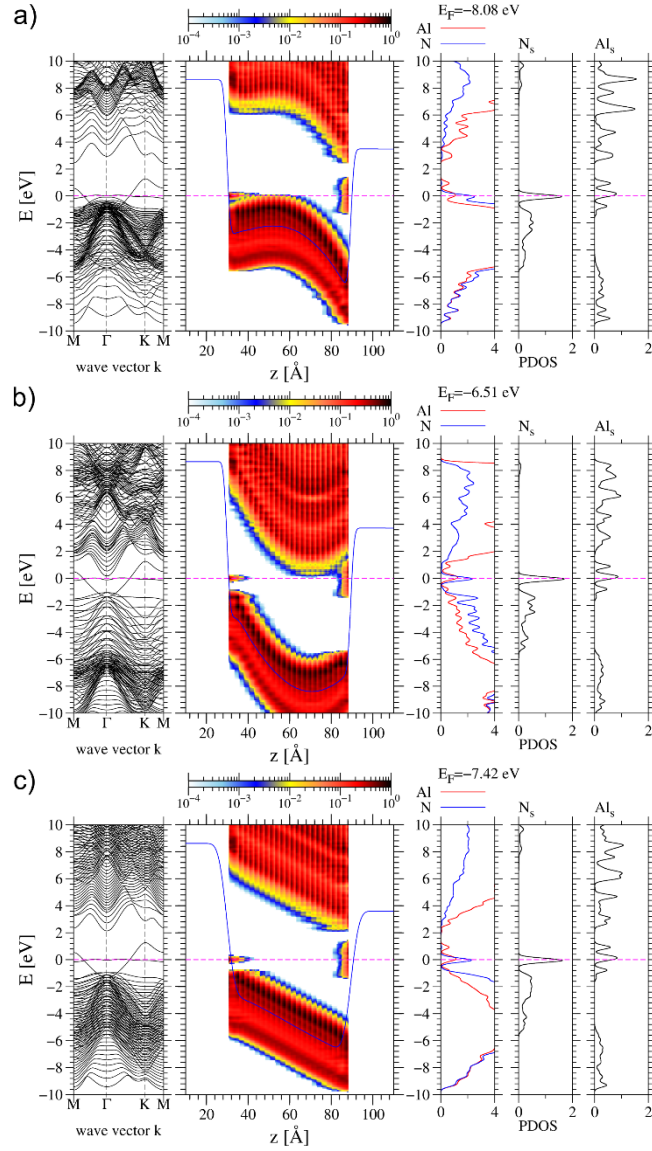


Fig. 3. Band diagram in momentum (left) and position space (middle) of the WZ 24 DALs AlN slabs and the density of states (DOS) of surface Al atoms (right): (a) p-type, (b) n-type, (c) SI. The blue line superimposed on the position space diagram is electric potential, derived as above, plotted in units of electron energy. The colors in the central panel represent electron density according to the scale at the top. Reproduced Fig. 4 from Ref. 51 [51].

As it is shown, the surface states exist on both surfaces. The states associated with Al-terminated surface, located close to conduction band minimum (CBM), have large dispersion,

about 2 eV wide. This is related to the overlap of Al states between neighboring top Al atoms. The states associated with N-terminated surface have reduced dispersion, of order of 0.3 eV and they are located close to valence band maximum (VBM). Their dispersion is smaller, related to small size of nitrogen wavefunctions and much smaller overlap between neighbors. These three diagrams represent p-type, n-type and semi-insulating (SI) AlN bulk, which is reflected by the position of the Fermi level inside the slab, close to conduction band, valence band, and in the gap center, respectively. The latter diagram is specific which is associated with the absence of the bulk charge, leading to linear dependence of the electric potential. The two other diagrams have strongly nonlinear potential profiles, confirming the presence of the charge in the bulk [51]. In addition, the field is present at both edges of the slab, leading to the energy shift of the surface and the band states which was identified as surface states Stark effect [41,52,53]. The identification is correct as the surface states energies are affected by the electric field present in the slab.

The presence of the field inside the slab is closely related to the partial occupation of the surface states. In fact these surface states are broken bond states, i.e. states without overlap with the states of the neighboring atoms as they are missing. In essence they originated from the valence band, their higher energy is due to absence of the overlap. Thus their energies are located typically in the bandgap. The example of such states are the surface states of AlN(0001) polar slabs, presented in Fig. 3. These states are partially filled thus the Fermi energy has to be there so that they are pinning the Fermi level.

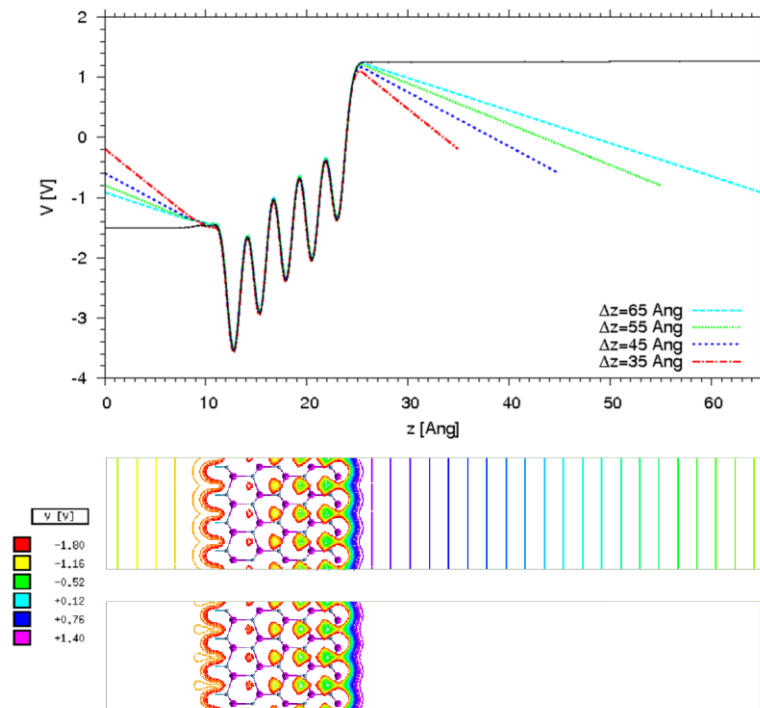


Fig. 4. Electric potential distribution (SIESTA) for different thickness of the spacer, obtained with and without Laplace correction. Top diagram presents the potential profiles along the channeling path. The black line correspond to the solution with, the color lines - without Laplace correction. Lower two diagrams show the potential sections across the slab with (upper) and without (lower) gradient correction, drawn for the largest width of the spacer. Reproduced Fig. 4 from Ref. 17 [17].

In general, the presence of Fermi level pinned at both slab sides stabilize potential difference with respect to the external field applied. Such result, plotted in Fig. 4, was obtained by Krukowski et al. in Ref. 17 [17]. The potential difference may be manipulated by the change of the electron charge in the termination hydrogen pseudoatoms, or by the distance between these atoms and the bottommost slab atoms. That will lead to the difference in the field within the slab as it is shown in Fig. 5.

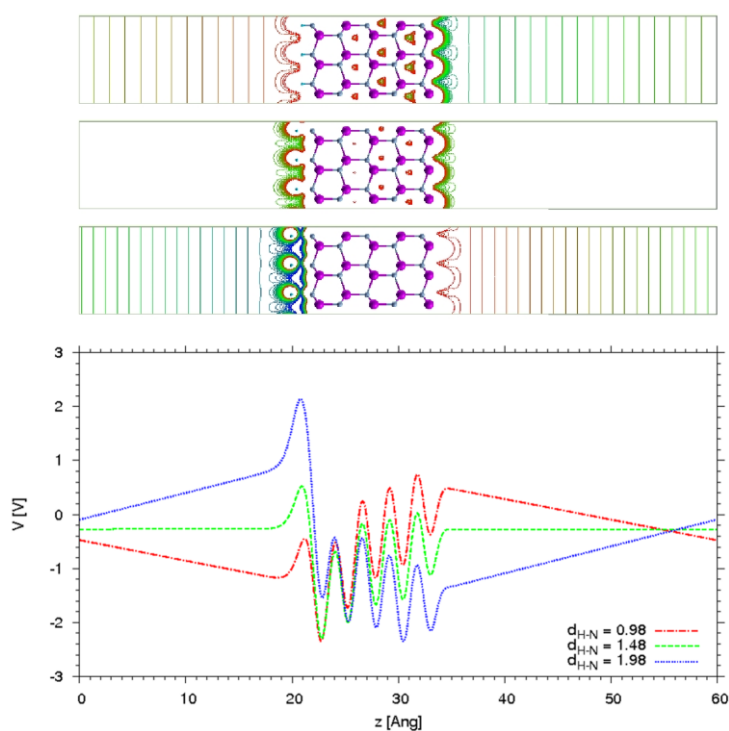


Fig. 5. Electric potential distribution in 3x3 Ga-N slab, fulfilling PBC, obtained for three different distances between N bottom atoms and H saturation atoms in SIESTA: a) 0.98 Å, b) 1.48 Å and c) 1.98 Å. Top- the sections across the slab, bottom - the potential profiles along the channeling path. Reproduced Fig. 2 from Ref. 17 [17].

The potential profiles, presented in Figs. 4 and 5, are affected by the presence of atomic cores, giving rise to high amplitude fluctuations. These fluctuations were removed by the averaging methods described in Ref. 54 [54]. The method allows one to obtain long range variation of the electric potential which, presented as electron energy in Fig. 3, proves that the bands variation in the real space follows strictly the change of the electric potential, confirming identification of the surface states Stark effect.

At both slab edges, the diagram show steep change of electric potential, of order of several volts. This is evidence of the external surface dipole contributing to the work function of the semiconductor, identified first by Lang and Kohn [9,10]. This dipole may be affected by the adsorption of the species at the surface, which is sometimes related to the charge transfer and creation of additional dipoles. Both dipoles contribute to overall dipole of the slab as shown in Fig. 3.

It has to be added, that in the investigations of the adsorption processes, additional spurious effects may arise which can affect adversely the precision of the obtained results. In fact, the separation of the quantum system into two isolated subsystems may lead to different positions of Fermi levels in both parts. This is pure quantum effect, in fact it is a combination of quantum state energy and the Fermi-Dirac statistics. Formally, the overlap always exist as the wavefunction asymptotic behavior at the far distance is always exponential. Thus formally the subsystems have coherent single wavefunction at any distance. This weak mathematical link is destroyed by thermal fluctuation, as the systems are in partial equilibrium. Therefore in reality the remote subsystems are essentially independent, having possibly different Fermi energies. The standard DFT procedures use single common position of the Fermi level for the entire system. That may entail artificial redistribution of the charge between subsystems, such as the slab and the separate adsorbate. This effect is not due to the tunneling of the electrons, in fact this is mere reshuffling of the electrons. Nevertheless this may create significant physical effect, such as an electric interaction between the charged species and the slab. This is illustrated in the case of Ga atom close to GaN slab presented in Fig. 6.

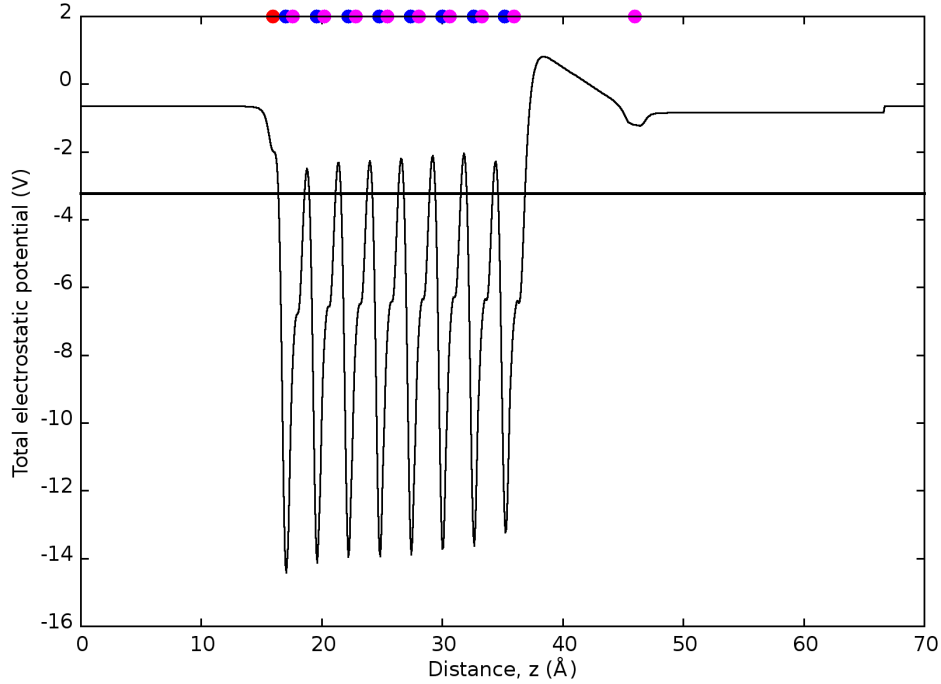


Fig. 6. Electric potential profile averaged in a plane perpendicular to the  $c$ -axis, plotted across the slab representing a bare GaN(0001) surface and  $d$  Ga atom at the distance of 10 Å from the surface. Positions of atoms are denoted by circles (blue – Ga, magenta – N, red – H) on top of the diagram. Reproduced Fig. 4. from Ref 55 [55].

The effect may be used for simulations of interaction of the plasma charged species: atoms and molecules. In fact this charge redistribution may affect the calculations of the adsorption energy using standard procedure of translation of the species away from the surface and determination of the total system energy in function of the distance. It is assumed that above critical distance, at which the overlap of the wavefunctions of the slab and the adsorbate is negligible, the energy attains the constant asymptotic value. In the case of the charged species this is not observed as the Coulomb interaction is long ranged. This is demonstrated in Fig. 7, where the energy of the GaN(0001) surface – Ga system is plotted [55]. The total energy has considerable variation at far distances, so that precise determination of the adsorption using this procedure is not possible. The other procedure based on separate calculation of the species and the slab is evidently superior.

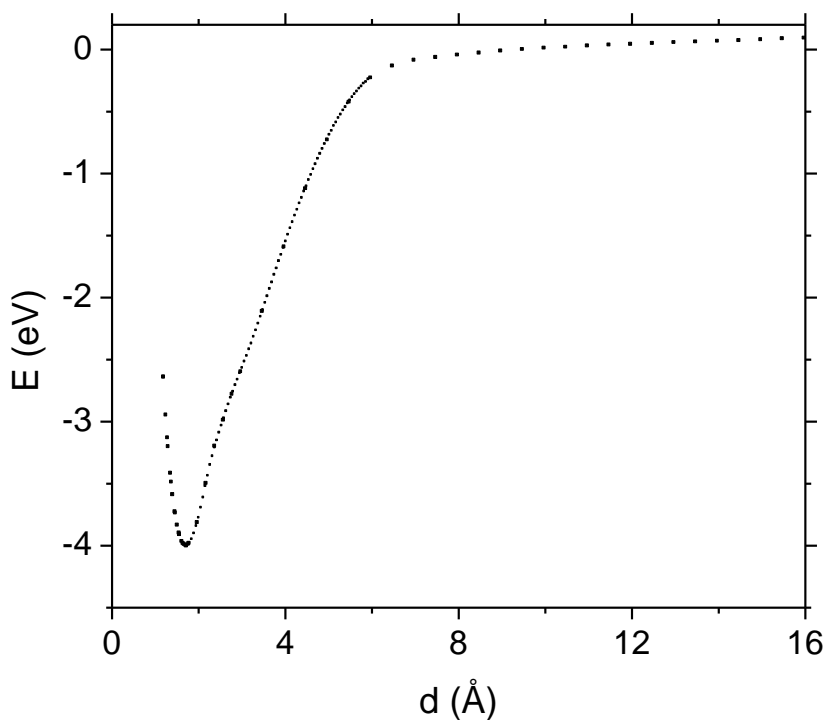


Fig. 7. Energy  $E$  of the system as a function of the distance  $d$  between Ga adatom and the bare GaN(0001) surface. Zero energy level is set for a large distance from the surface. The distance is measured as a difference between the position of the Ga adatom and a position of the topmost layer of Ga surface atoms. Reproduced Fig. 3 from Ref. 55 [55].

In the critical discussion of the slab representation of the semiconductor surfaces it is necessary to repeat that the separation of the two quantum subsystem could not be complete. Therefore the residual overlap is always present. This is visible in the overlap of the wavefunctions of the real and termination (opposite) surface atoms of the slab, shown in Fig. 8. From these data it follows that the far distance decay of wavefunction is exponential, always universal as it is the solution of the linear equation. Therefore the overlap between two surfaces does not vanish, it is reduced in exponential asymptotic way. Therefore the statements claiming that the interaction between these two surfaces is not observed are not precise. This influence is reduced in the exponential manner with no critical width of the slab present. This indicates that the requirement for the number of the atomic layers in the slab simulations are severe, requiring large number of the atomic layers. This increases the considered system to several hundreds of atoms. This is particularly unfortunate as high precision calculated employing Heyd-Scuseria-Ernzerhof (HSE) are not possible for such large number of atoms [56]. The other approximations like PBE or PBESol are much less precise in the determination of the energy of quantum states, leading to the bandgap error or order of 30% [57,58]. On the other hand,

they recover mechanical properties well, so they are useful in determination of the surface structures, e.g. surface reconstruction. The other possible choice is to use the band correction scheme of Ferreira et al. known as GGA-1/2 approximation that gives the proper band gap energies, effective masses, and band structures [59,60]. This approach provides incorrect mechanical properties, so these calculation may be used only in the final determination of the energy of quantum states, without any relaxation of the atomic positions.

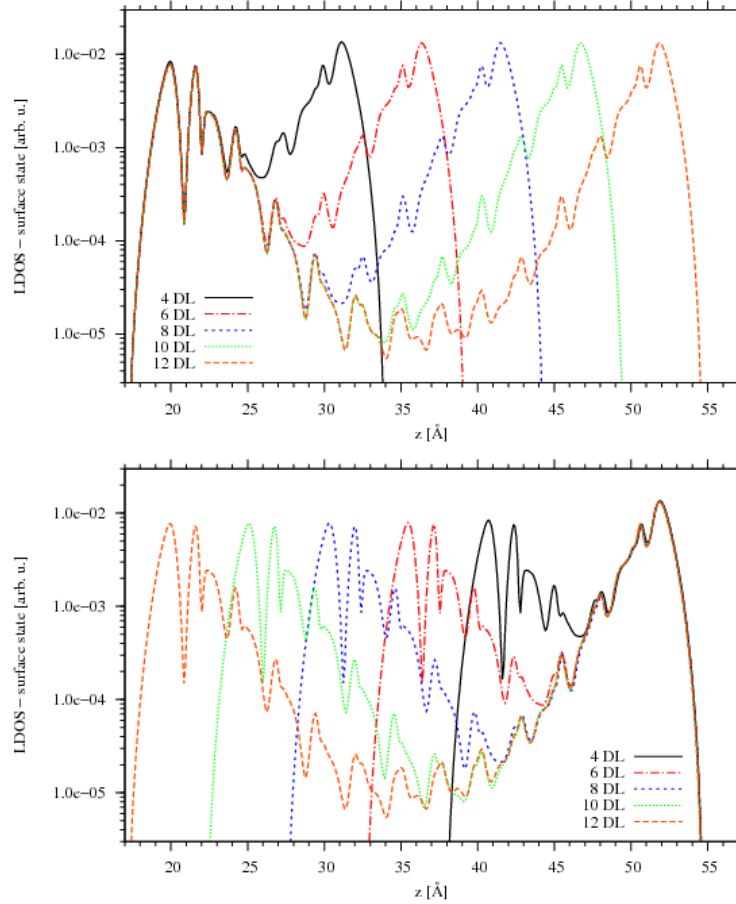


Fig. 8. Electron density profiles of the sum of the surface states related to real and artificial surfaces. The colors denote (1 x 1) GaN (0001) slabs, having four (black), six (red), eight (blue), ten (green) and twelve (yellow) double atomic layers, all terminated by H atoms. The plots correspond to left and right-adjusted diagrams. Reproduced Fig. 4 from Ref. 52 [52].

From the above plotted diagram it follows that the wavefunction overlap of the real and termination surfaces is considerable for the slab thickness of 4 and 6 DALs. In case of 8 10 and DALs this is much lower. The extension from 8 to 10 DALs brings relatively smaller reduction, while the shift to 12 DALs brings only minor improvement. Thus the slab for high precision

calculation should have at least 8 DALs while 10 or 12 DALs can be used for verification purposes.

These considerations prove that the *ab initio* simulations of the properties of semiconductor surfaces still face considerable obstacles in the route towards full precise determination of their properties. The goal is to simulate relatively thick slab of the size in plane large enough to capture basic symmetry properties of the surfaces. As it will be shown, the size of the simulated slab may severely distort the symmetry of obtained results. The same condition applies to the slab thickness. Here, the quantum independence should be correlated with the proper electric potential and charge modelling that again increases the size of the simulated systems. The precise requirement depends on the properties of the simulated system as they differ from one case to the other considerably. Nevertheless, the standard requirement for simulations of the semiconductor surface properties is several hundreds of atoms. This effectively precludes application of highly precise calculations such as in HSE approximation. Thus less precise versions of *ab initio* calculations, such as PBE and related approximation is the proper choice. On the other hand, the insight into the properties and processes on semiconductor surfaces is evidently incomplete. Therefore the optimal approach is to direct research towards understanding of the basic processes and phenomena, even at the cost of high precision. In the following Sections we will describe the state of knowledge in several aspect showing that the basic understanding of the physics and chemistry of the semiconductor surfaces need basic research and formulation of the basic ideas in the first instance.

### **III. Bonding in semiconductors – charge in the bulk and at the surface**

It is widely accepted that the tremendous majority of semiconductor crystals, both elemental such as diamond, silicon or germanium and compound such as GaAs, InSb, AlP or CdSe, HgTe are characterized by cubic symmetry of the lattice (i.e. zinc blende or diamond) and tetrahedral coordination. This is intimately related to the hybridized  $sp^3$  bonding of both elemental and compound [61, 62]. In the latter, the covalent bonding is supplemented by partial ionic contribution. Due to symmetry of zinc blende lattice, the ionic contribution is neutralized in the bulk, so that charge separation effect does not manifest itself in the form of spontaneous polarization [19,20].

In fact the ionic contribution is directly proportional to the energy difference of the hybridized  $sp^3$  states [61]. It is absent in the case of elemental semiconductors and relatively small in the majority of the II-VI and III-V compounds. This is directly related to cubic lattice structure of the crystals. In the case of the group III metal nitrides: BN, AlN, GaN and InN the

ionic part is considerably larger. In the result, the lattice structure is changed to hexagonal, tetrahedrally coordinated wurtzite. In this structure the spontaneous polarization is permitted both in the pure compounds and also in the mixed crystals [14-19]. These effects are accompanied by the different bonding in these semiconductors. Despite tetrahedral structure, the GaN bonding include hybridized  $sp^3$  orbitals of gallium and separated  $s$  and  $p$  orbitals of nitrogen. In addition  $d$  orbitals of gallium are involved. Therefore bonding overlap include separate overlaps of gallium  $d$  and nitrogen  $s$  orbitals. The second bonding involve hybridized  $sp^3$  orbitals of gallium and  $p$  orbitals of nitrogen. That creates two separate sub-bands of valence band (VB) which was measured experimentally by soft x-ray spectroscopic measurements by Magnuson et al. [12]. By *ab initio* calculations the existence of two subbands was confirmed and the nature of the bonding was identified [12,13]. In the case of AlN the subband separation was also identified, with the lower subband due to nitrogen  $s$  orbitals only [11].

The subband identification does not solve problems, in fact it creates more. The nitrogen atom is in tetrahedral surrounding, connected to four Ga neighbors. But the bonding in upper subband is created from 3 nitrogen  $p$  states. The lower  $d-s$  subband is not compatible with the tetrahedral coordination at all. Therefore four bonds are necessary. This is in fact possible due to existence of resonant bonds proposed long ago by German chemist F. A. Kekule [63]. The concept of delocalization of electrons within  $sp^2$  bonds was formulated in terms of probability of occupation of the nonorthogonal states, fully compatible with the quantum field theory. In addition  $\pi$  bonds in the direction perpendicular to the ring were incorporated [64]. Slightly different formulation was proposed by P. W. Anderson that involved the different feature of quantum mechanics, namely wave theory. This described the quantum states as the resonant, i.e. the wave states in full mutual resonance thus. having the same frequency, i.e. the energy [65]. This formulation was subsequently applied to the description of high temperature superconductivity of the copper oxide structures [65]. Subsequently the concept was extended to other systems [66].

GaN case was considered only recently during study of N adatom at GaN(0001) surface [14]. Accordingly, the quantum states of N atom in GaN bulk were obtained and are presented in Fig. 9. As it is shown in PDOS diagram in the case of N atom in the bulk the two basic states are present at approximately  $E = -5 \text{ eV}$  and at  $E = -9 \text{ eV}$ . As proved by COHP data these subbands are created: first by hybridized  $sp^3$  orbitals of gallium and the second by  $p$  orbitals of nitrogen and gallium  $d$  and nitrogen  $s$  orbitals, respectively.

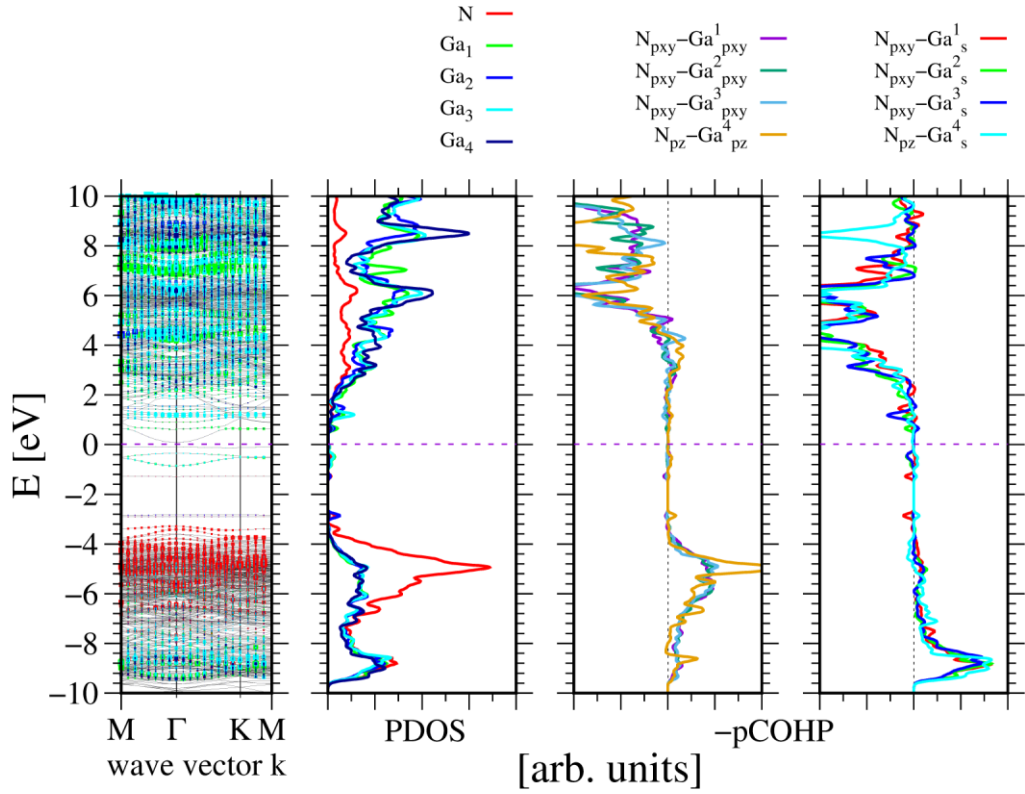


Fig 9. Energies of the quantum states of nitrogen and gallium states located in the GaN bulk of  $(2\sqrt{3} \times 2\sqrt{3})$  slab representing clean GaN(0001) surface with single N adatom located in H3 site. The panels represents, from the left: energy of the quantum states in the momentum space, projected density of states (PDOS) of the N and Ga atoms, and the right two panel - Crystal Orbital Hamilton Population (COHP) [67,68]. The COHP data correspond to N adatom and the closest topmost Ga atoms. The Fermi energy is set to zero. COHP positive values correspond to the bonding overlap.

The COHP data indicate that upper state is due to four states created by overlap of  $|N_{2p}\rangle$  states and  $|Ga_{4sp^3}\rangle$  of four atoms. Thus this number is four while they are created from the three  $|N_{2p}\rangle$  states. Thus the number is extended to four because these states are resonant states, as in the case of benzene [63-65]. Naturally these states have to be nonorthogonal, they are occupied with the probability  $P = 3/4$ . As the number is four it is sufficient to create tetrahedral bonding pattern in the wurtzite lattice symmetry. This is confirmed by the angles created by these bonds which are in the plane:  $\varphi = 110.14^\circ$  or  $\varphi = 109.73^\circ$ , i.e. close to the ideal tetrahedron. The c-axis angles are slightly different,  $\varphi = 106.92^\circ$  or  $\varphi = 109.32^\circ$ . It is worth to underline that these states are located deep below Fermi energy, their occupation

probability stems from electron distribution among large number of states. The number of the electron on these resonant states is 6 thus occupation probability  $P = 3/4$ . These states have important consequence for the charge analysis of the surface states.

#### IV. Work function

Wide applications of electron vacuum devices require creation of the cold cathodes that are effective sources of electrons. For some advanced applications the necessary condition is to emit the electrons efficiently of approximately equal kinetic energy. Thus cold emission is needed as it is the optimal way. Therefore the electron affinity (EA), i.e. energy difference between conduction band minimum and the vacuum should be possibly low, or even negative [3-5,7,8]. The two other, EA related quantities, i.e. work function (WF) and the ionization energy (IE) are defined using the energy difference between the Fermi level and of the valence band maximum, respectively [3-5,7-8]. In the case of the metals these values are identical, or more precisely, the two of them could not be defined properly so the common value defined by work function is adopted [7,8]. In fact EA and IO are independent of the band bending, caused by internal dipole surface layer discussed below. This is because the internal dipole shifts the energy of quantum states with respect to the energy of surface states. The latter remain unchanged with respect to the vacuum level i.e. far distance energy value. But these values are derived from the measurements of the work function which is affected by the surface states pinning, adsorbate etc. [73,74]. In fact this causes problems both in experiment and in the theory, so the ionization energy of AlN was disputed in severely [69-74]. Thus the absolute values of these three quantities (EA, IO and WF) are derived from the emission experiments which may be affected by number of factors [73]. Their absolute values, were finally determined to be  $EA[AlN(0001)] = 1.9 \text{ eV}$  [48] and  $3.2 \text{ eV} \leq EA[GaN(0001)] \leq 3.4 \text{ eV}$  [51]. The *ab initio* calculations gave for GaN  $EA^{DFT}[GaN(0001)] \cong 3.73 \text{ eV}$  [51]. More extensive *ab initio* calculation give smaller value for different surface coverage  $EA^{DFT}[GaN(0001)] \cong 2.93 \text{ eV}$  [51].

In fact the *ab initio* calculations could provide more precise assessment, limited by the calculation precision only. This could be illustrated by the calculation test made for pure Al which is presented in Fig. 10. The diagram may seem superfluous but it is nevertheless useful for the presentation of the calculation procedure. The difference in the potential profile at the infinity and at the interface is obtained, i.e. workfunction. In case of pure Al the profile is symmetric with the workfunction value  $WF[Al] = 3.94 \text{ eV}$ .

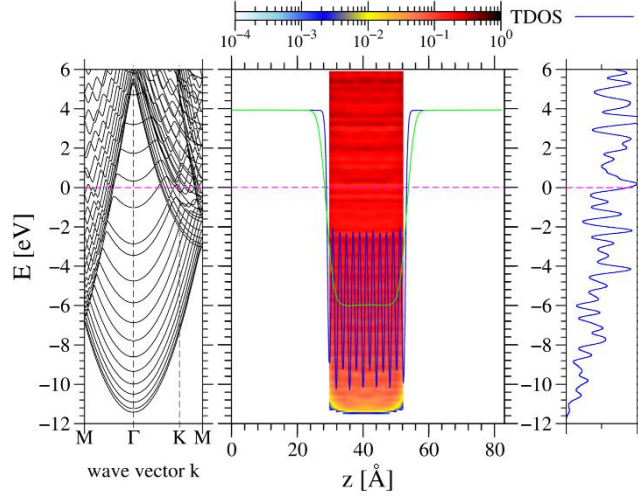


FIG. 10. Band diagram in momentum (right) and position space (middle) of face centered cubic (fcc) Al slab and the total density of states (total DOS) of the slab (right). The blue line superimposed on the position space diagram is electric potential, averaged in the plane parallel to surface of the slab, plotted in the units of electron energy whilst the green line is curve additionally smoothed along  $c$ -axis. The colors in the central panel represent electron density according to the scale at the top. Reproduced Fig. 2 from Ref 51 [51]

An important issue is related to the workfunction determination definition. Formally it is defined as the potential energy of the motion of the unit charge  $q = 1$  from the cluster (finite solid) surface to infinity. In fact this is burdened by the error caused by the Coulomb attraction contribution because the cluster need to have the opposite charge. For the conductors this can be calculated using mirror charge ( $q_m = -1$ ) with the mirror located at the position where the external potential is totally screened. In fact the contributions is the largest for the closest position of the unit and the mirror charge. Therefore the location of the mirror surface is critical. This is determined by the screening inside the conductor, i.e. density of mobile charge. Nevertheless this can be remedied by redefinition of the procedure. The unit charge has to be replaced by the infinitely small charge in the potential energy determination, i.e.  $q \rightarrow \varepsilon \rightarrow 0$ . Since the Coulomb interaction energy is proportional to both charges  $E_{Coul} \sim q q_m \sim \varepsilon^2$  therefore the interaction contribution scaled by the charge is  $V_{Coul} = E_{Coul}/q \sim \varepsilon \rightarrow 0$ . Therefore the Coulomb error in such defined procedure disappears in the limit and the procedure is precise.

It has to be noted that the potential profiles, plotted in Fig. 3 cannot be used directly for determination of these three surface characteristics (EA, WF and IE). These potentials were calculated in the case of periodic potential along  $c$ -axis, therefore far distance value is absent. The potential is corrected by the additional compensation gradient in the vacuum space [15,16] or the Laplace correction field [17]. Therefore the potential level is different on both sides of the slab presented in Fig. 3.

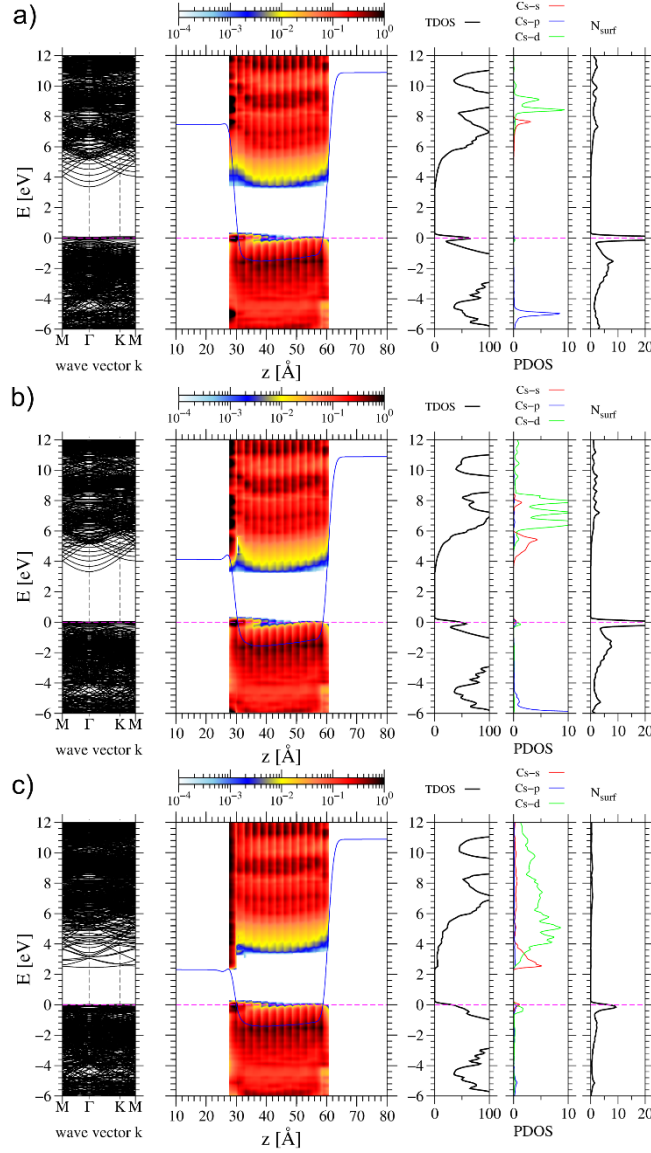


Fig. 11. Band diagram in momentum (left panel) and position space (middle panel) of the following number of Cs atoms: (a) single, (b) four, (c) eight atoms, attached to  $4 \times 4$  slab representing wurtzite N-side GaN(0001) surface (i.e. 0.0625, 0.25 and 0.5 ML coverage). The panels on the right present density of states (DOS): total, Cs adatom and N surface atoms. The

blue line superimposed on the position space diagram is electric potential, derived as above, plotted in units of electron energy. The colors in the central panel represent electron density according to the scale at the top. Reproduced Fig. 8 from Ref 51 [51].

The obtained potential profile is still very useful in different aspect. Adsorption of additional species may affect surface characteristics (EA, WF and IE) by additional surface dipole, in case when the adsorbed species are charged. This was studied in case of nitride surfaces covered by cesium adsorbed layer [51]. It is well known that the Cs  $6s$  state has low binding energy, locating this level high in the absolute energy scale. In fact Cs atom attached to  $GaN(0001)$  surface is stripped of the electron and attached by electrostatic force only [51]. That creates additional electric dipole opposite to the fundamental dipole of the solid. Therefore the electric potential barrier is reduced from  $9V$  to  $5V$  i.e. by about  $4V$  (Fig. 11). Nevertheless the charge is compensated by the opposite charge at the surface thus not changing the potential profile within the slab as presented. The identified effect which is in fact creation of the opposite dipole by the positive charge of electron stripped Cs atoms explains the drastic decrease of the workfunction by Cs coverage of the AlN surface.

The external surface dipole layer and associated potential jump may be important for the course of adsorption processes at solid surfaces. Solid surfaces in contact with the vapor undergoes constant bombardment by vapor species. In the result, a fraction of these is attached, the others are repelled. The attachment at the surface requires energy loss during scattering, i.e. in relatively short time. Then the adsorbate could be immobilized in the potential well at the surface attaining the vibrational energy in accordance with the temperature of the solid, i.e. the adsorbate is thermalized [75]. The kinetic energy of the adsorbate at the temperature  $T = 1000 K$  is of order of  $kT = 86.17 meV$ . The benchmark energy of the adsorbate attachment is  $\Delta E = 1 eV$ , i.e. at least one order of magnitude higher. Thus the parallel motion of the adsorbate is relatively slow, i.e. the adsorbate moves almost perpendicular to the surface. Therefore the other proposed scenario of the creation of the “hot” atoms [76 - 80], i.e. the adsorbate sliding along the surface over large distance to dissipate the kinetic energy does not capture the essence of the kinetic energy loss. The duration of the scattering event may be estimated assuming that the extension of the potential well is  $d = 0.5 nm$  and the velocity  $v_{th} = \sqrt{\frac{\Delta E}{2M}} \approx 450 m/s$  thus the collision time is  $\tau_{coll} \approx 10^{-12} s$  [75]. Therefore the duration of the entire collision process is no longer than the typical frequency of the Brillouin zone boundary phonons in GaN which is of order of 15 - 20 THz [81,82]. Thus the collision time is of order of single phonon

frequency. The emission of phonon bunches was also proposed as thermalization channel [82]. The thermalization require emission large number of phonons in this period, thus nonlinear effects would result in creation of surface defects.

The bombardment is intense, nevertheless creation of surface defects is not observed therefore other, faster more effective mechanism should be responsible for the effect. This channel should involve electronic degrees of freedom as only these processes are fast to be effective in so short time scale. Therefore the electron tunneling mechanism was proposed [75]. The existence of strong electric field induced by dipole layer causes electron jump from the approaching atoms into the solid interior. The estimated time of the jump is  $\tau_{jump} \leq 10^{-14}$  s, therefore fast enough to be completed within collision time. Afterwards the high electron remains in the solid interior, that can dissipated the excess kinetic energy. This process may last longer but the essential for the course of the collision process is the retardation of the positively charged adsorbate. This is due to the interaction with the dipole layer electric field which act repulsively due to the opposite, positive charge of the adsorbate. The scheme of electric potential is presented in Fig. 12.

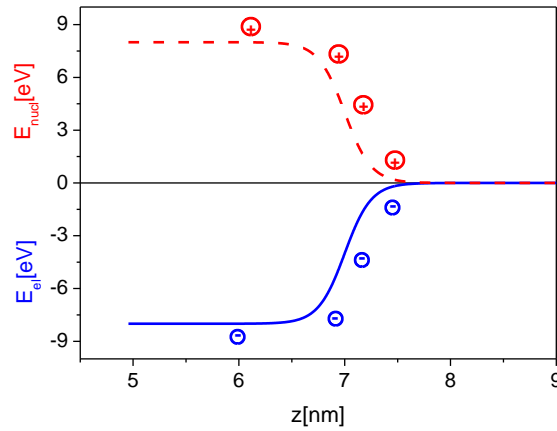


Fig. 12. The potential energy of the electron (blue solid line) and the positive ion (red dashed line) derived from AlN slab by *ab initio* method modeling. Reproduced Fig. 5 from Ref 75 [75].

It has to be added that these are preliminary investigations. The proposed scenario assumes that Born-Oppenheimer approximation, customarily used for description of the adsorption processes should be abandoned. In this approximation, the kinetic energy of the atomic motion is neglected, the energy is calculated with the immobile atoms. This is equivalent to the incorporation of additional, imaginary external force which stops adsorbate at each point along the adsorption path. In reality this is not the case, the adsorbate attains the kinetic energy. The dissipation by the proposed electrostatic repulsion involves the potential collectively so

that the force is exerted on large number of the surface atoms directly and also via indirectly via interaction with electron charge. This new scenario needs to be further investigated as it could be helpful in the understanding of number of properties. This involves inevitably the surface dipole layer and associated electric potential.

## V. Surface-internal charged dipole layer formation

In striking contrast to the external dipole layer influence discussed above, the internal surface dipole layer effects are well described for a long time [3 - 5]. The layer emerges as a consequence of pinning of Fermi level by fractionally occupied surface states. The band bending, necessary to attain uniformity of Fermi level over the entire conductive solid is related to accumulation of the mobile charge, i.e. screening. That leads to creation of internal surface dipole. In contrast to the earlier described external dipole of Lang and Kohn, the internal dipole is partially classical effect. The effect is described by screening length determined from Lindhard theory of charged gas screening [83]. In long distance limit this result is compatible with Thomas-Fermi screening length  $\lambda_{TF}$  for degenerate electron gas [3]:

$$\lambda_{TF} = \sqrt{\frac{2\varepsilon\varepsilon_0 E_F}{3ne^2}} \quad (1a)$$

and in the case of nondegenerate electron gas this is the Debye-Huckel screening length  $\lambda_{DH}$  [3]:

$$\lambda_{DH} = \sqrt{\frac{\varepsilon\varepsilon_0 kT}{ne^2}} \quad (1b)$$

where  $\varepsilon$  is the dielectric constant which for the case of GaN is:  $\varepsilon = 10.28$ . Other quantities are:  $k$  – Boltzmann constant,  $\varepsilon_0$  – permittivity of vacuum,  $e$  - elementary charge,  $n$  – charge density and  $T$  – temperature in kelvins. The screening length depends on the temperature and the charge density. This value may be evaluated for typical conditions: for  $T = 300 K$  and typical electron density for n-type GaN, i.e.  $n = 10^{18} cm^{-3}$  and  $n = 10^{19} cm^{-3}$  these lengths are:  $\lambda_{DH} = 3.83 nm$  and  $\lambda_{DH} = 1.21 nm$ , respectively. Thus these conditions could be recovered in *ab initio* simulations. Therefore such simulations were made for GaN(0001) surface by Kempisty and Krukowski [84]. In these simulations two different cases of GaN(0001) surface was considered: bare and under full H – coverage. Both p – type and n-type doping was considered. The doping was made by the addition of the uniform charge background over the part of the volume occupied by the cores of the functional basis set in SIESTA, such that the total charge added is equivalent to a single electron. Thus for positive charge background additional electron

has to be added for the occupation numbers which is equivalent to n-type doping. In the case of negative charge the number of the electrons occupying quantum states is smaller by one so that this corresponds to p-type doping. The doping level may be therefore estimated assuming single charge for 20 elementary cells, where the cell volume for GaN is  $V_{\text{GaN}} = 46.0 \text{ \AA}^3$ . The calculations were made for the 20 GaN DAL slab therefore the doping level was  $n = p \cong 10^{21} \text{ cm}^{-3}$ . In order to achieve the convergence, the electron temperature was set to  $T = 1000 \text{ K}$ . From the estimate it was that  $\lambda_{\text{DH}}(10^{21} \text{ cm}^{-3}, 1000 \text{ K}) = 2.2 \text{ \AA}$ . The simulation results for clean GaN(0001) surface are presented in Fig. 13.

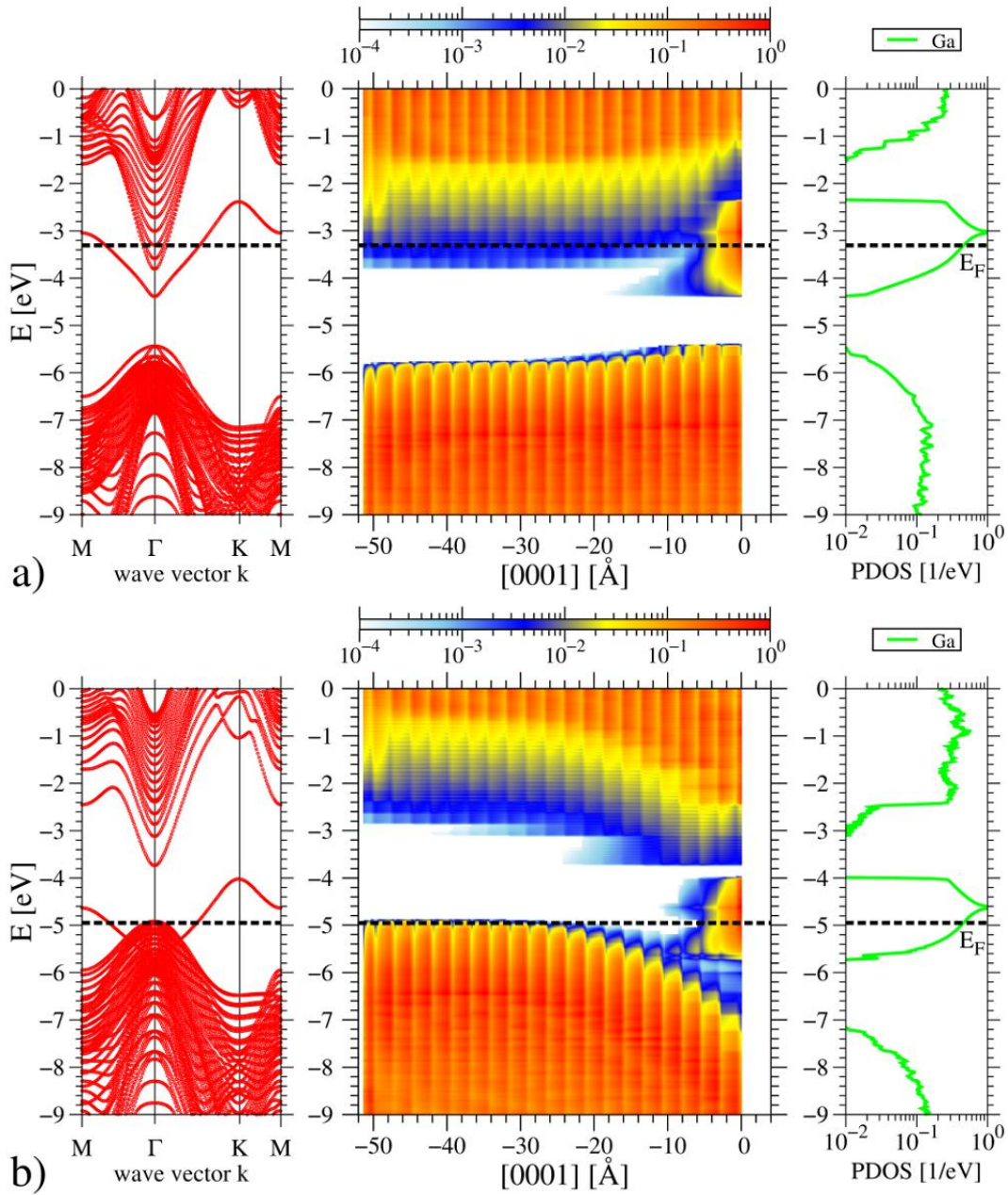


Fig. 13. Dispersion relations (left), space alignment of the bands derived from atom projected density of states (P-DOS) (middle) and DOS projected on surface gallium atoms (right) for clean GaN(0001) surface: a) n-type; b) p-type, obtained from 1 x 1 slab. The electronic temperature was 1000K. Reproduced Fig. 1 from Ref 84 [84].

It is well known that clean GaN(0001) surface, terminated by Ga-broken bond atoms has the surface with its energy located close to CBM. The state has wide dispersion about 2 eV wide and is partially filled. In case of n-type doping the Fermi level is pinned close to the CBM so that there is no band bending or nonlinear potential profile as the opposite side is not pinned. Drastic difference is observed for p-type doping. Here again the Fermi level is pinned by Ga-broken bond state, close to CBM. Thus the amplitude of the band bending is close the bandgap, i.e.  $E_g \sim 3.47 \text{ eV}$ . This is high difference so that the linear theory is not precise. The estimated screening length is  $\lambda_{DH}(10^{21} \text{ cm}^{-3}, 1000 \text{ K}) = 2.2 \text{ \AA}^3$ . In the simulation this length is close to  $\lambda_{DH} \sim 10 \text{ \AA}^3$ . Naturally, the doping level was estimated only, so that this could also contribute to the observed results.

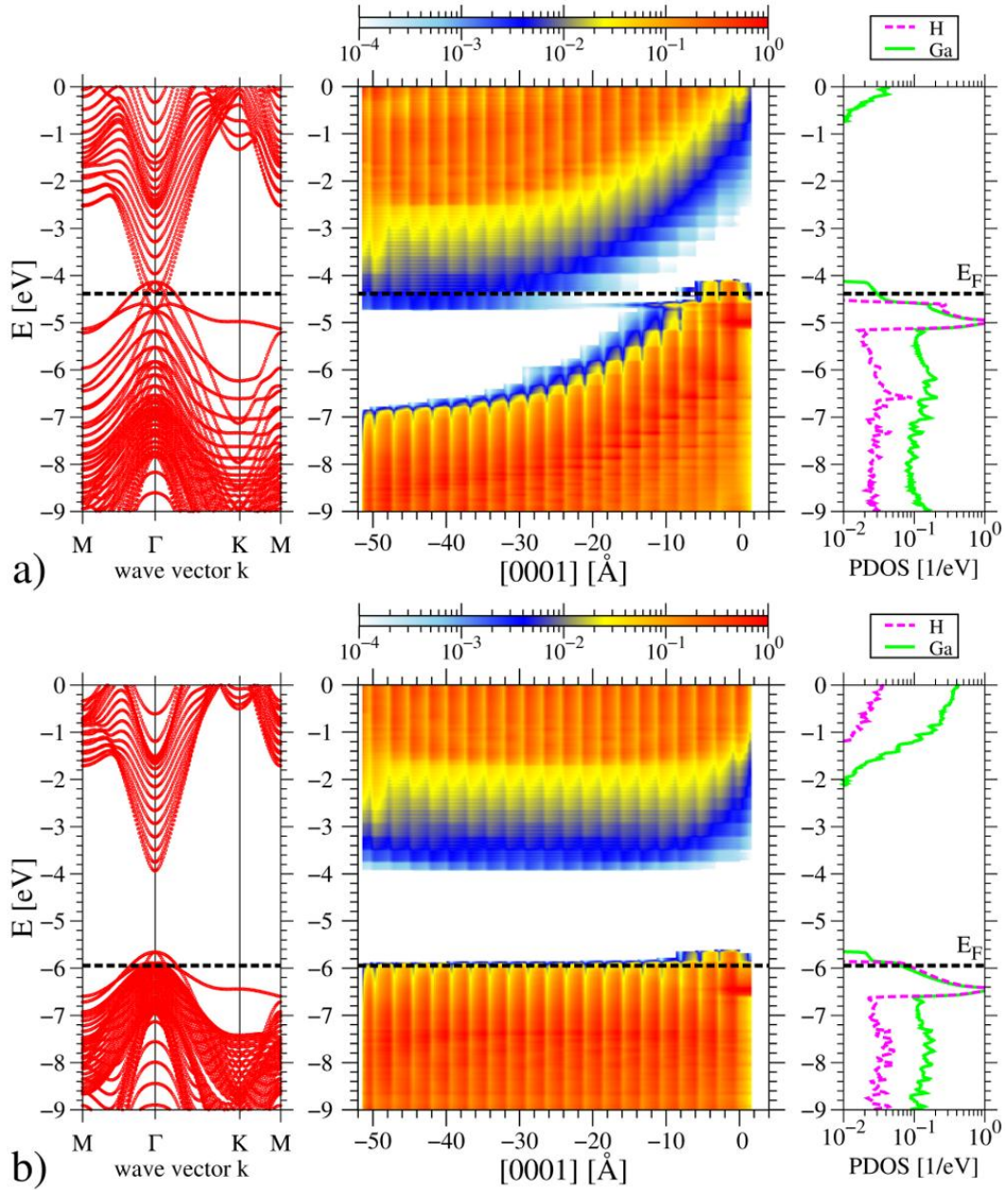


Fig. 14. Dispersion relations (left), space alignment of the bands derived from atom projected density of states (P-DOS) (middle) and DOS projected on surface gallium and hydrogen atoms (right), for fully hydrogen-covered GaN(0001) surface: a) n-type; b) p-type, both obtained from  $(1 \times 1)$  slab. The electronic temperature was 1000K. Reproduced Fig. 2 from Ref. 84 [84].

Similar data are obtained for the case of Fermi level close to VBM, presented in Fig. 14. The results were obtained for GaN(0001) surface fully covered by H atoms in the on top positions [84]. This creates Ga-H bonding state of the energy close, but below VBM. The state has  $n_e = 1 \frac{3}{4}$  electrons, one from H and 3/4 from Ga broken bond, i.e. it is not fully occupied. Therefore the state is pinning Fermi level at the surface. In the case of p-type the pinning is

close to Fermi level in the bulk so that no band bending occurs. In the case of n-type band bending is again close to bandgap, i.e.  $E_g \sim 3.47 \text{ eV}$ . Again band bending extends much wider than the estimate. This may be attributed to several factors, such as charge carrier density lower than estimated, or nonlinear effects.

In general, the majority of the simulations use undoped slabs, thus the screening is much less effective. Therefore in the most cases, the potential profiles are linear which is related to the absence of the bulk charge and the difference in the energy of the states pinning Fermi level at both surfaces [17]. Such situation is typical, and was shown in Fig. 2 (a) and (b) and also in Fig 3 (c). In other cases, such as Fig. 2 (c) and Fig 3 (a) and (b), the profile is nonlinear which is related to the penetration of Fermi level in the bands and existence of the band charge. In case of Fig. 3 (c) the Fermi level is in the conduction band in more than half of the slab thickness that leads to downward band bending close to Ga(0001) surface. In case of Fig. 3 (a) Fermi level penetrates into valence band so that the holes are present close to  $GaN(000\bar{1})$  surface. The band bending indicates presence of positive charge in the bulk. In case of Fig. 3 (b) this is the opposite, the negative charge is present in the bulk. Generally, these cases correspond to the presence of mobile charge and the screening of the charge occupying surface states.

An interesting application of these methods was presented recently by publication of ab initio investigations of two-dimensional electron (2DEG) at AlN/GaN heterointerface within more complex structures being basis of high electron mobility transistors (HEMTs) [85]. GaN based HEMTs are important devices for future high frequency applications [86]. Due to spontaneous and piezoelectric polarization the 2DEG emerge at the GaN/AlN interfaces without additional doping thus allowing these devices to operate at high frequency. The critical parameter is high electron mobility which could be attained with relatively high density of the gas. This is attained at the GaN/AlN interface close to the surface. The developed method were recently used in ab initio investigation. The results of ab initio calculations of such system are presented in Fig. 15 (a).

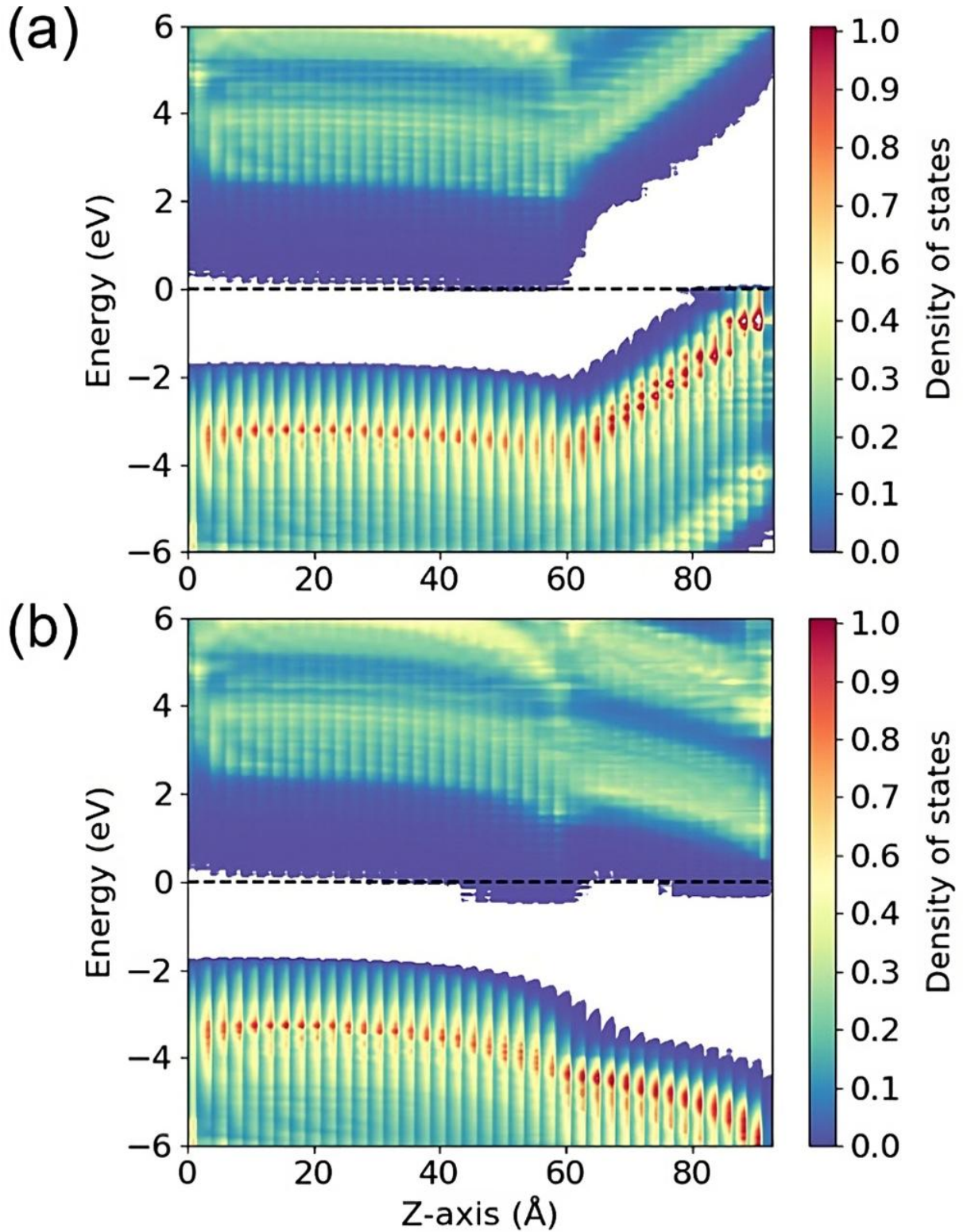


Fig. 15 . Spatially projected DOS profiles for the different pseudohydrogen atoms used to passivate the both nitrogen-side of GaN and aluminum-side of AlN surfaces of GaN/AlN slab: (a)  $Z_N = 0.733$  and  $Z_{Al} = 1.260$ , (b)  $Z_N = 0.733$  and  $Z_{Al} = 1.380$ . Reproduced from Fig 3 of Ref. 85 [85].

The obtained slab profile indicate intersection of the conduction band minimum and Fermi level on the GaN side of AlN/GaN interface indication the possible presence of 2DEG at the interface. This was in fact shown by the charge profiles presented in Fig. 16.

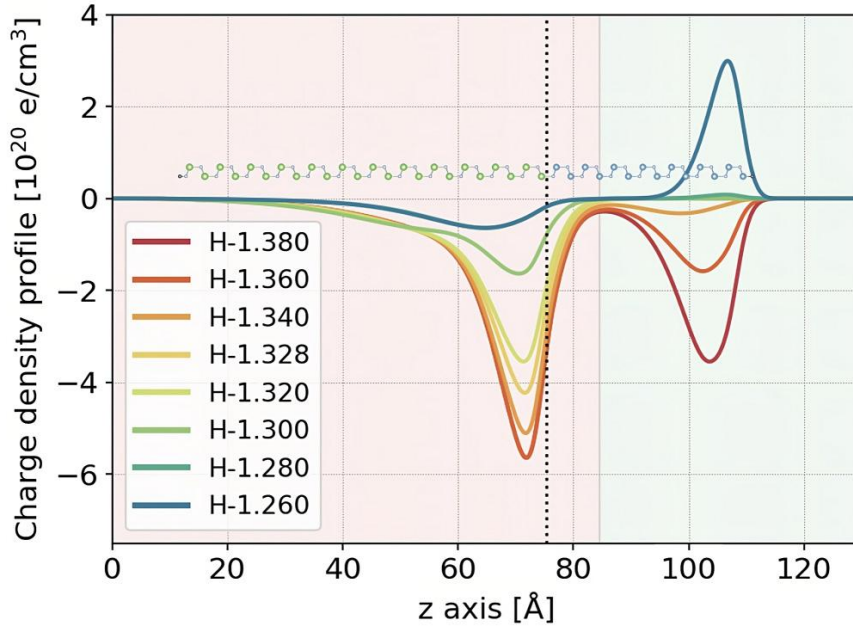


Fig. 16. Charge density profiles of 2DEG obtained along z-axis of the AlN/GaN slab obtained for different values of hydrogen pseudoatoms at AlN surface. The first peak is located at GaN/AlN interface, the second is at AlN surface. Reproduced for Fig. 4 of Ref 85 [85].

In real devices an additional oxide passivation layer is deposited above AlN layer. Typically this layer is obtained by the deposition of  $\text{Al}_2\text{O}_3$  as the most natural choice. Therefore such triple GaN/AlN/ $\text{Al}_2\text{O}_3$  structure was also investigated in Ref 85a. The results are presented in Fig 17.

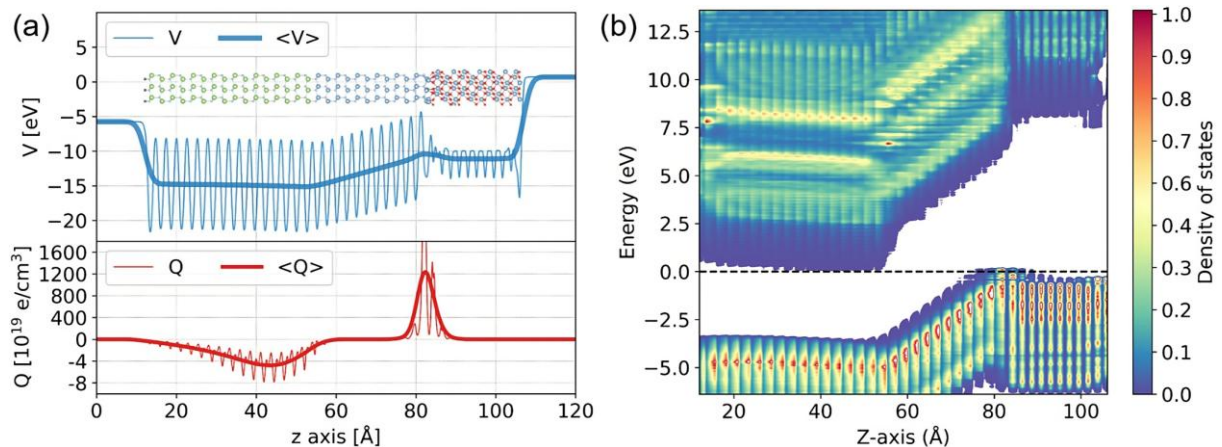


Fig. 17. Electric properties of GaN/AlN/Al<sub>2</sub>O<sub>3</sub> structure: (a) Electric potential profiles (b) band diagram. Reproduced Fig 3 from Ref. 85 [85].

Summarizing this part it is worth to stress out that the *ab initio* calculations are capable to catch the characteristic features of the doping in the bulk of the solids and its consequences to the surface internal dipole layer. It is possible to simulate the mobile charge at the surface and the screening of the surface charge in the interior. This is due to the presence of the mobile charge so that the Fermi level penetrates the bands close to the surface. Precise account of screening is possible in case of very heavy doping, of order of  $n = p \cong 10^{20} \div 10^{21} \text{ cm}^{-3}$ . For lower doping the other effective mass approaches could be used [4,5].

## VI. Charge role in surface reconstruction

Reconstruction of semiconductor surface is one of the most prominent features of the semiconductor surfaces that differs them from the surfaces of the other substances. In the case of the surfaces of other type substances, the phenomenon of reduction of translational symmetry is diminished and relatively rarely observed. Nevertheless in such cases a small displacement is sufficient to remove symmetry, therefore the small amplitude reconstructions are observed for surfaces of other crystals. The reconstructions that could drastically change the properties of the surfaces, and are large in magnitude are mainly observed in the case of semiconductor surfaces. Therefore, the main efforts of investigation of the reconstructions were directed towards investigation of reconstructions of semiconductor surfaces. They are intensively investigated for many years so that large number of the various patterns was identified [3, 87, 88].

In these investigations several principal rules, governing the reconstruction selection, were identified. These rules in general indicate the transformation to semiconducting (insulator) surface by:

- (i) atomic relaxation that leads to lower total energy of the system by separation of the empty and occupied states,
- (ii) creation of new bonds,
- (iii) relaxation according to the electron counting rule (ECR).

Generally, these arguments are well based, as the transformations (i-iii) lead to the modification of the overlap of the quantum states by the atomic motion so that the occupied states have their energies lowered and the empty increased. As the occupied states are the only ones that

contribute to the total energy of the system, the total energy value is decreased, i.e. more stable structure is attained.

ECR was proposed first by Chadi for the tight-binding analysis of As-rich reconstruction of GaAs surfaces [89] and then applied by Pashley in the interpretation of Transmission Electron Microscopic (TEM) images of GaAs(0001) – (2 x 4) surface [90]. The rule is essentially a simple calculation of electron occupation of the surface states, assuming the fractional charge contribution from broken bond state derived from chemical valence concept [89-91]. Thus, the fractional charge contribution from Ga broken bond is  $q_{Ga} = 3/4$ . Similarly, the fractional charge contributions from N and Si broken bonds are  $q_N = 5/4$  and  $q_{Si} = 1$ , respectively. The contribution from the other elements from the same row in Periodic Table is identical. ECR calculation is proceeded as follows: assume that the total number of valence electron is:  $Q = \sum_i q_i$  and the number of the quantum states below the supposed Fermi energy is:  $N = \sum_j n_j$ . Then the occupation of all states is  $f = Q/N$ . The following results can be obtained:

- i)  $f = 2$ . The Fermi level is located above the higher energy of all included states, and below the energy of the first higher energy quantum state not included. Naturally each state is double spin degenerated. In case spin degeneration is removed, the  $f$  value should be changed to 1.
- ii)  $f > 2$ . The number of the states is not sufficient. The additional states should be added to until the condition  $f \leq 2$  is attained. In the case the condition is attained assume that the lower energy states have occupation  $f = 2$ , subtract the charge and the value. The ratio of the residue of the charge and the number of states gives the fractional charge of the highest energy state.
- iii)  $f < 2$ . The highest energy state or states are fractionally occupied. Then the highest states should be removed and the calculation repeated, to obtain the fractional occupation according to (ii).

In fact ECR procedure is equivalent to the well-known treatment of HOMO and LUMO orbitals in quantum chemistry [92]. In fact ECR calculation is a very simple version of the determination of the occupation of the one-electron states in DFT procedure. In the latter it is assumed that the occupation of the one-electron states is determined by Fermi-Dirac (F-D) statistics, i.e. the occupation fraction is real number obtained from F-D distribution at the selected temperature. ECR mimics this calculation in a drastically simplified way. In fact the surface states are taken into account only, those degenerated with valence band (VB) and conduction band (CB), are

assumed to be occupied or empty, respectively. The important addendum is the assumption that these in the bandgap (i.e. broken bond states) are fractionally occupied. The latter is correct in the case when these surface states are located far away from the band states in energy scale. Thus ECR could be applied in case of bandgap surface states that are located deep in the bandgap. Nevertheless, in the difference to the Fermi-Dirac occupation numbers, ECR has the advantage to be informative, intuitively appealing when addressed to small number of states. Therefore it was applied and in large number of *ab initio* simulations [46-53]. Afterwards it was extended (EECR) to use in the adsorption at semiconductor surfaces [85].

ECR provides basically correct guidance for the treatment of the structures of semiconductor surfaces. The minimal energy criterion is generally applicable to any systems in equilibrium. The deviation stems from the fact that such simple formulation does not take into account all contribution to the energy [93]. This formulation is not sufficiently elaborate to describe such different phenomena as those existing in semiconductor surfaces [3]. Even those that are limited to pure elemental semiconductor are not within the scope of the application of ECR.

Stoichiometric gallium nitride Ga-terminated GaN(0001) surface originally was identified as reconstruction-free [48]. This finding was confirmed by a number of other reports [47-51]. In addition, the Fermi level was determined to be pinned at the surface Ga broken bond, about 0.5 eV below conduction band minimum (CBM) [47-51]. As a rule these calculations employed small ( $2 \times 2$ ) slabs. Later investigation discovered ( $2 \times 1$ ) row structure [94,95]. It was discovered that the difference between these two structures were very small and that the unreconstructed surface was due to persistent metastability.

Recently more detailed investigations of the stoichiometric GaN(0001) surface were undertaken using larger different size slabs, including ( $4 \times 4$ ), ( $6 \times 4$ ) and ( $8 \times 4$ ) [96]. It was shown that reconstruction of GaN(0001) leads to division of the top Ga atom surface later into  $sp^3$  and  $sp^2$  coordinated Ga atoms. That leads to the division of the Ga-broken bond band into two separate subbands as shown in Fig. 18.

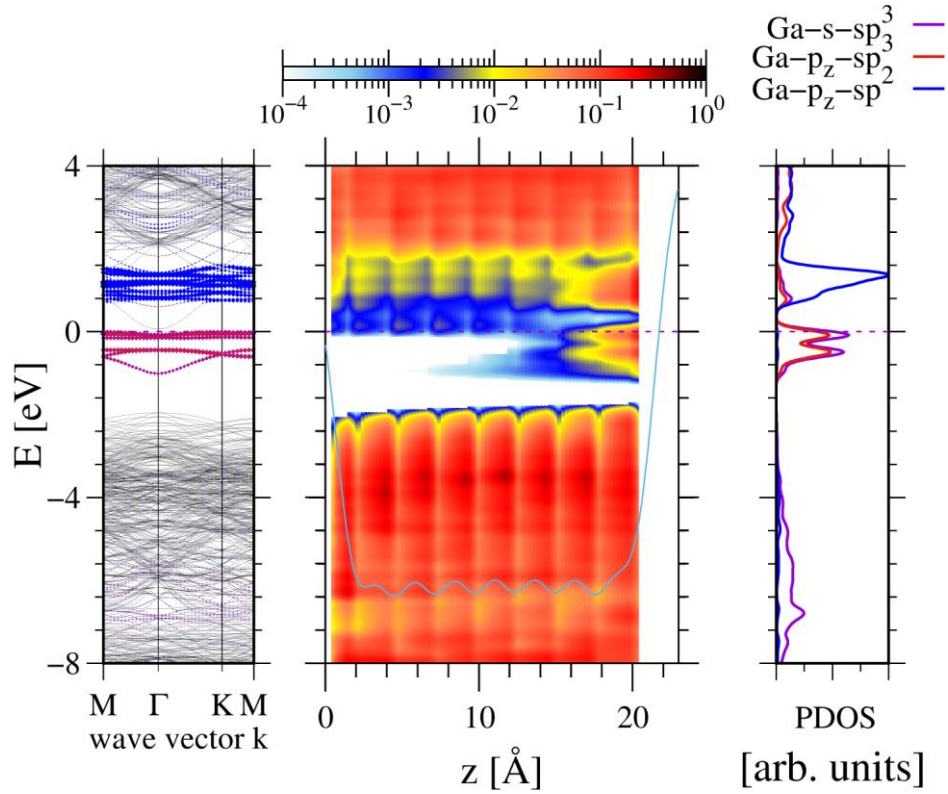


Fig. 18. Electronic properties of  $(4 \times 4)$  8 double Ga-N atomic layers (DALs) thick slab, representing stoichiometric Ga-terminated GaN(0001) surface: left – band diagram in momentum space, center - energy bands in real space, plotted along c-axis, right - partial density of states (PDOS) plotted for the top layer Ga atoms. The blue and magenta color represent surface layer Ga atoms:  $Ga4sp^3$  hybridized and  $Ga4p_z$  orbital states -in conjunction to  $Ga4sp^2$  hybridized states, respectively. Reproduced from Fig. 1 Ref. 84 [84].

The first is created by the gallium  $sp^2$  hybridized orbitals, the second with  $p_s$  states of  $sp^2$  hybridized topmost Ga atoms. The existence of such separation is confirmed by the plots of GaN slabs in Fig. 19.

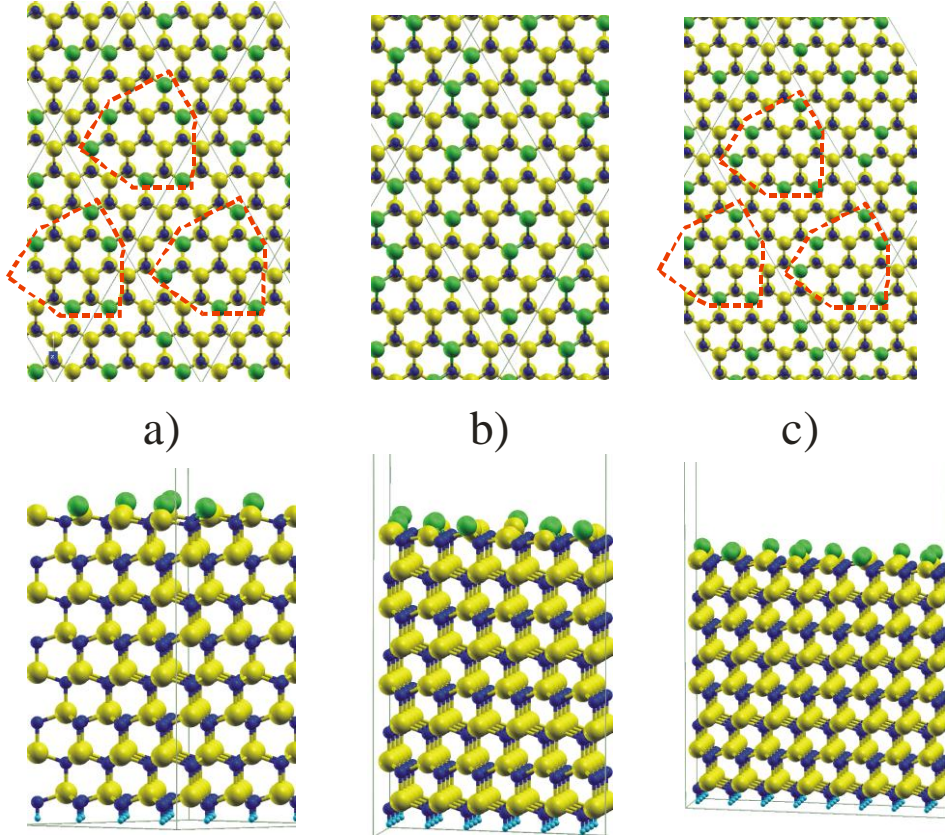


Fig. 19. Gallium nitride 8 Ga-N double atomic layer (DALs) thick slabs representing Ga-terminated GaN(0001) surface: a)  $(4 \times 4)$  slab, b)  $(6 \times 4)$  slab, c)  $(8 \times 4)$  slab. The upper and lower rows present the top and side view, respectively. The balls represent the following atoms: blue – nitrogen, yellow – gallium, green – surface layer gallium ( $sp^3$ ) hybridized, cyan – hydrogen termination pseudoatoms. The red color broken lines mark the basic units of  $(4 \times 4)$  reconstruction pattern. Reproduced from Fig. 2 of Ref 96 [96].

As it is shown a fraction of topmost atoms are located in the plane of nitrogen layer atoms, clearly indicating  $sp^2$  reconstruction. In this figures the  $(4 \times 4)$  reconstruction unit was identified. In fact this size was determined by ECR charge balance as follows. All Ga-N bonds are occupied therefore the excess charge for surface Ga top layer atom broken bond (i.e. vertical) is  $(3/4)$  electron (elementary charge) for single Ga topmost atom. The ECR based electron charge balance thus assumes occupation by 2 electrons the vertical bond state in  $sp^3$  configuration, i.e. a fraction of  $(1-x)$  sites, and 0 electrons in  $p_z$  orbital in  $sp^2$  hybridized atom, i.e. a fraction of  $x$  sites:

$$(1 - x) \times 2 + 0 \times x = \frac{3}{4} \quad (2)$$

From this relation it follows that the fraction of  $sp^2$  hybridized Ga atoms is:  $x = \frac{5}{8}$ . The remaining fraction  $1 - x = \frac{3}{8}$  Ga atoms is  $sp^3$  hybridized. In fact, in  $(4 \times 4)$  slab 10 Ga atoms should be located in the N atom plane while the remaining 6 Ga atoms are predicted to be located in the higher, lattice compatible positions. The calculated distribution of Ga atoms in the topmost plane remains in a perfect agreement with this prediction. Similarly, in the case of  $(6 \times 4)$  slab 15 and 9 Ga atoms are in the predicted position in a full agreement with the ECR argument. And finally, in the case of  $(8 \times 4)$  slab, 20 and 12 Ga atoms are in  $sp^2$  and  $sp^3$  hybridization, respectively. In summary, the *ab initio* results fully confirms prediction based on ECR analysis, therefore the atoms are hybridized due to the electron redistribution. In the case of  $(4 \times 4)$  and  $(8 \times 4)$  slabs, the emerging  $(4 \times 4)$  reconstruction is compatible with the slab periodicity. In case of  $(6 \times 4)$  it is not, therefore this reconstruction is not observed. Thus successful simulations of the surface reconstruction requires proper choice of the simulation slab. For large size surface  $(4 \times 4)$  reconstruction based on electron redistribution is energetically stable configuration of GaN(0001) stoichiometric surface. This identification was confirmed by the simulations of Mg and Si doped slabs where the fraction of the  $sp^3$  and  $sp^2$  hybridized Ga topmost atoms was changed.

The driving force of the above reconstruction is the difference of the energy of  $Ga - s$  and  $Ga - p$  orbitals. Therefore this reconstruction cannot occur for surfaces of typical III-V semiconductors such as GaAs(111). In case of the nitrides, Ga terminated surfaces can undergo this reconstruction such as investigated GaN(0001). On the contrary, nitrogen terminated surfaces will not undergo this reconstruction at N-terminated  $GaN(000\bar{1})$  surface [12, 51]. Due to large difference in the energies of nitrogen  $s$  and  $p$  orbitals, the bonding of the solid does not involve  $sp^3$  hybridization of nitrogen, therefore such reconstruction is not observed.

In conclusion it is demonstrated that these results prove the charge balance control of the energy optimization of semiconductor surfaces via reconstruction. This mechanism was proved in case of simple  $sp^3$  to  $sp^2$  bonding transition. More elaborate bonding, such as bridge formation, etc. need elucidation by the investigation of the charge contribution to the energy optimization in the future.

## VII. Charge role in adsorption

### 1. Basic description

During adsorption of any species, the positively charged nucleus and negatively charged electrons are attached to the surface. In most cases when no charged species are present, e.g. in

exclusion of the plasma processes, the attached adsorbate is electrically neutral. Thus, the existence of the external and internal dipole layers does not affect the adsorbate as the interactions between the field and the positive and negative charge cancel out. Nevertheless, there are other charge related contributions that are not balanced perfectly [97, 98].

Adsorption at semiconductor surfaces generally leads to creation of the new covalent bonds between adsorbate and the surface. Thus, the quantum states are modified, so that their energy is lower. Additionally some of the states in the adsorbate, are added. In the process the number of the electrons is also increased. Naturally some states with energy higher than Fermi level are also created but these do not contribute to the system energy. The important ones are only those that are located below Fermi level. Thus the contribution to the energy change of the system during adsorption stems from the two basically different factors [97 - 99]:

- i) the change of the energy of the states occupied by the electrons,
- ii) the change of the number of the electrons in the system.

Since the number of new added electrons and the number of the newly added states could be different, the second effect may involve the change of the occupation of the surface states by their shift to lower or to the higher energy states. Both directions are possible, depending on the number of electrons and the number of the new states created. These additional electron transitions, between the surface states are different from the bond creation, as the effect involves electrons that are located on the surface states both before and after adsorption, therefore the phenomenon was named intra-surface state electron transition [99].

This so called intra-surface electron transition contribution depends on the position of Fermi level. These states, located close to Fermi energy, donate or accept electrons generating additional contribution to the adsorption energy. This effect may exist in adsorption at any surface causing the shift of Fermi level by the coverage increase until the maximum possible value is reached. There exist two different scenarios:

- i) there is no gap in the density of states (DOS) in energy range between the initial and final position of the Fermi level
- ii) there exist DOS gaps, one or more, in the above range.

The initial and final positions of the Fermi level is taken as the Fermi energy at the surface in total absence or close to or at the full coverage of the adsorbate. Thus in some cases the Fermi level may be selected for the coverage not equal but very close to zero or unity.

In the absence of the gap the change of the adsorption energy in function of the coverage is continuous. Thus the adsorption energy change related to the electron transition could be accommodated as the part of the bonding energy. This is the case of metal surfaces and also for

some cases at the surfaces of semiconductors or insulators. The gap case is different, because in the full coverage range, there exist critical coverage ( $\theta = \theta_{cr}$ ) at which the fraction of the surface states is occupied and the remaining ones are empty (at  $T = 0 K$ ). At this coverage the adsorption energy may undergo the finite jump to the new value as the electron transition contribution changes in jump-like manner. This phenomenon could be observed only for nonmetallic surfaces, i.e. for semiconductors and insulators.

In order to determine this possibility, the application of the procedure denoted as extended electron counting rule (EECR) was proposed in Ref. 100 [100]. First, the possibility of Fermi level jump across any energy gap should be determined. In order to do so the adsorption process has to be considered using smallest periodic surface unit at which the single adsorbate may be attached. The unit has to be defined in such a way that the entire surface is a direct sum of such units. Thus the surface coverage is zero or full. The EECR procedure is used to determine the Fermi level position for jump across the gap at fractional coverage from the analysis of the surface states. In this analysis all available additional information could be used, including the projected density of states (PDOS) and Crystal Orbital Hamilton Population (COHP) data [99, 100].

Technically the EECR calculation is used to determine the average fraction of the units with the adsorbate attached  $g$  ( $0 \leq g \leq 1$ ). Assume that the number of the topmost surface atoms (adsorption sites) in the unit is  $z$ . Thus the unit may be a single site in the case of the adsorption in the on-top position ( $z = 1$ ), a pair of sites in the case of the bridge configuration ( $z = 2$ ), three sites in the case of H3 or T4 positions ( $z = 3$ ), or even larger. The coverage  $\theta$  is defined as the ratio of the adsorbates (molecules or atoms) to the number of the topmost sites in the unit i.e.  $\theta = g/z$ . Assume that the surface electron charge in the unit before adsorption event (i.e. for the coverage  $\theta$  equal to zero) is  $Q_i = \sum_i q$  where the occupation of the broken bond surface states is calculated using ECR prescription described above. The electron charge contributed by the adsorbate is  $Q_a = \sum_a q_a$  where  $q_a$  are the number of the electrons in the atom  $a$  (index  $a$  runs over all atoms in the adsorbate). In the fractional occupation  $g$  there exist the surface states that were present before and after adsorption. Still they can be occupied due to position of Fermi level after adsorption. The number of such states is  $N_f$ . The number of occupied states due to the attached adsorbate is  $N_a$ . Then extended electron counting rule (EECR) determines the critical fraction  $g_{cr}$  of the units attached at which all states below Fermi level are occupied. The EECR charge balance is obtained from the electron charge (number) conservation equation:

$$Q_i + g_{cr} Q_a = N_a g_{cr} + (1 - g_{cr}) N_f \quad (3a)$$

This is calculated as follows: on the left is the charge in the system before adsorption  $Q_i$ . This is charge of the unit including the fractionally occupied states in accordance to ECR for broken bonds. The second contribution is the charge added by the adsorbate which is proportional to the critical occupation and the charge of the adsorbate, i.e.  $g_{cr} Q_a$ . On the right hand this charge is distributed into the states of the covered part which is again proportional to critical occupation, i.e.  $N_a g_{cr}$ . The second term is number of the states that are occupied by the electrons in the not covered fraction of the surface i.e.  $(1 - g_{cr}) N_f$ . This balance is used to achieve the full and zero occupation below above Fermi energy, respectively. Thus it is determine at which occupation the Fermi level jumps from the occupied to the empty states. In the double spin degenerate case, i.e. the factor  $f = 2$  is used for the calculation of the number of states  $N_f$  and  $N_a$  (those numbers are calculated after the adsorption). From this relation the critical fraction and the critical coverage may be obtained

$$g_{cr} = z\theta_{cr} = \frac{Q_i - N_f}{(N_a - N_f) - Q_a} \quad (3b)$$

Alternatively, this relation could be formulated as a calculation of the covered fraction of the units by consideration of the number of electrons donated and accepted:

- i) in the case of the donation of electrons from the surface state initially occupied ( $Q_i > N_f$ ), i.e. when the Fermi level goes down. The number of the donated electrons from the surface states in the unit is:  $Q_i - N_f$  as the initial number of the electrons is  $Q_i$  and the number of occupied states after (in ECR all states are occupied or empty) is  $N_f$ . The number of accepted electrons at the final state is  $[(N_a - N_f) - Q_a]$  because  $(N_a - N_f)$  is the number of the electron increase in the final state from which the number of the electrons contributed by the adsorbate, i.e.  $Q_a$ , should be subtracted.
- ii) in case of the acceptance of electrons at the initial state, i.e. initially empty ( $Q_i < N_f$ ), i.e. when the Fermi level goes up. The number of accepted electrons is  $N_f - Q_i$  as the number of electrons in final state is  $N_f$  and this number in initial state is  $Q_i$ . The number of donated electrons from the final state is  $Q_a -$

$(N_a - N_f)$  as  $(N_a - N_o)$  is the number of the electron decrease (due to  $N_a > N_o$ ) in the final states for which the number of electrons contributed by the adsorbate i.e.  $Q_a$  should be added.

Thus a fraction of units  $g_{cr}$  is occupied as determined from the number of available electrons.

Several examples will be discussed here to demonstrate EECR calculation of the charge. First - the case of hydrogen adsorption on-top ( $z = 1$ ) of the topmost Ga atom of GaN (0001) surface (Figs 13 and 14). In this case the initial charge is  $3/4$  electrons associated with Ga broken bond, i.e.  $Q_i = 3/4$ . These broken bond states are located in the vicinity of CBM (Fig. 13). Hydrogen brings one electron i.e.  $Q_a = 1$ . In the final state Ga-H state is at VBM, therefore  $N_a = 2$ . After adsorption the broken Ga bond state is above Fermi level thus it is empty, i.e.  $N_f = 0$  (Fig. 14). From this data it follows from Eq. 2b that  $g_{cr} = \theta_{cr-H} = 3/4$ .

The alternative determination based on argument (i) is as follows: broken bond state has  $3/4$  electrons initially ( $Q_i = 3/4$ ), and zero in the final state ( $N_f = 0$ ). The adsorption of hydrogen brings one electron ( $Q_a = 1$ ), thus in the final state we have from the adsorption  $1 \frac{3}{4}$  electrons, i.e.  $1/4$  electron is missing. This has to be borrowed from Ga broken bond states that is higher in energy. In fact single Ga broken bond state provides  $3/4$  electrons i.e. sufficient to occupy fully 3 Ga-H states. Therefore the ratio of covered to empty sites is  $3 : 1$ , for three covered sites we have on site empty, and accordingly the critical coverage is  $\theta_{H-cr} = 3/4$ .

The second example is the mixed  $\text{NH}_2\text{-NH}_3$  coverage where GaN(0001) surface is covered by mixture of  $\text{NH}_2$  radicals ( $\theta_{\text{NH}_2} = 0.75 \text{ ML}$ ) and  $\text{NH}_3$  admolecules ( $\theta_{\text{NH}_3} = 0.25 \text{ ML}$ ) [55] presented in Fig. 20. The EECR condition can be determined as follows: the coverage is full, i.e. all sites are covered either by  $\text{NH}_2$  radicals or by  $\text{NH}_3$  molecules. Therefore the change from  $\text{NH}_2$  to  $\text{NH}_3$  configuration may be treated as an attachment of H atom. The surface unit can be selected including single Ga surface atom site, i.e.  $z = 1$ . Thus the initial configuration consists of Ga broken bond with attached  $\text{NH}_2$  radical. All  $\text{NH}_2$  states are degenerated with the valence band: Ga-N states are located deep while N broken bond is at VBM. This confirms the location of the Fermi level at the midgap and the absence of the field inside the slab. Moreover the projected density of states (PDOS) and Crystal Orbital Hamilton Population (COHP) diagrams confirms that nitrogen and hydrogen s and p overlapped states are located in the valence band.

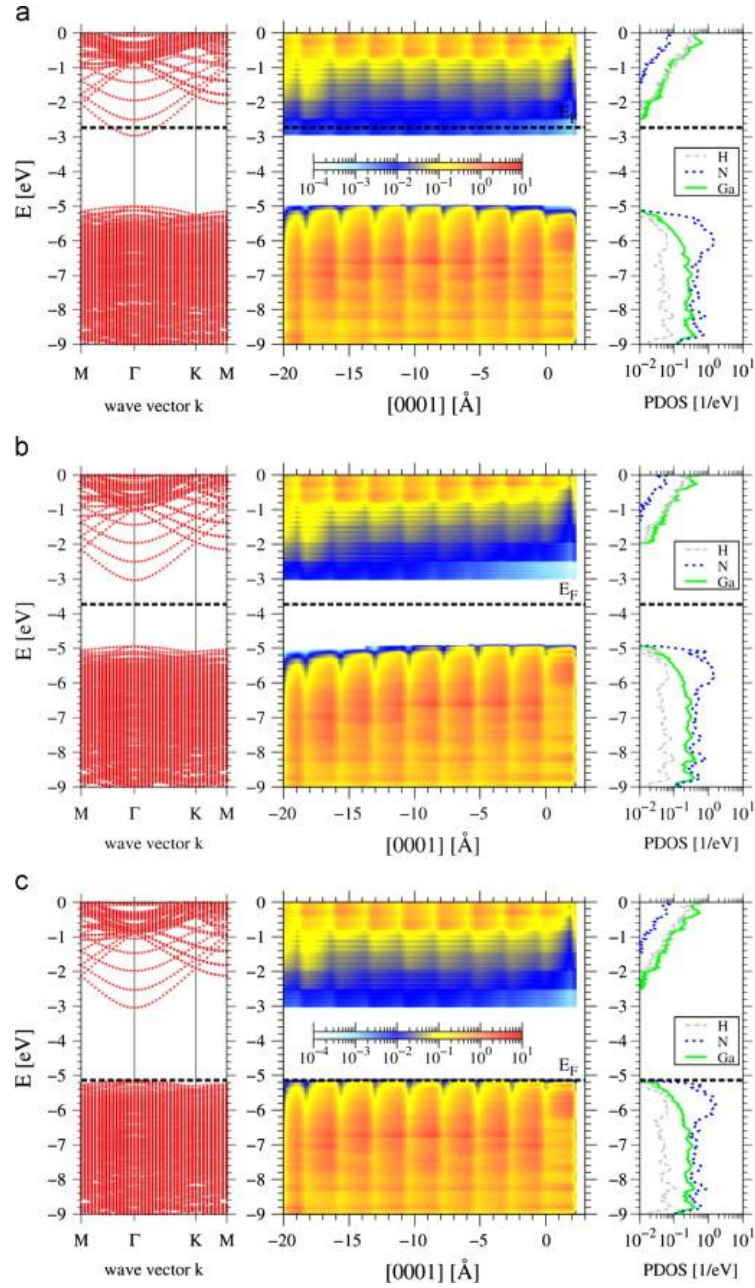


Fig. 20. Electronic properties of the (4×4) 8 GaN DALs slab representing GaN(0001) surface covered with 0.25 NH<sub>3</sub> admolecules and 0.75 NH<sub>2</sub> radicals. Left – the band diagram of the slab; middle – DOS projected on the atom quantum states (PDOS), showing the spatial variation of the valence and conduction bands in the slab; right – DOS of the topmost Ga atoms and NH<sub>3</sub>/NH<sub>2</sub> admolecules. The states density scale (logarithmic) is included in the diagrams. Top, middle and bottom panels represent *n*-type, semi-insulating and *p*-type material respectively, simulated by charge background procedure implemented in SIESTA package. Reproduced Fig. 3 from Ref. 99 [99].

This remains in full agreement with the data presented in Fig. 20. More interesting are the nitrogen  $p$  states of  $\text{NH}_2$  radicals without overlap. As indicated by COHP diagram these states are located at the top of valence band, thus they are also occupied. Therefore the occupation is full but  $3/4$  electrons are borrowed from valence band. Accordingly the initial charge is  $Q_i = 3/4 + 7$  in which  $3/4$  in Ga-broken bond contribution and 7 stems from 5 electrons in nitrogen and 2 electrons from two hydrogen atoms. After adsorption the number of the states is  $N_f = 8$ . Thus all  $\text{NH}_3$  states are occupied and  $1/4$  electrons is shifted to conduction band as there is no states in the gap. The adsorbate, i.e. hydrogen atom charge is  $Q_a = 1$ . From Eq 3b it follows that  $g_{cr-H} = \theta_{cr-H} = \theta_{cr-NH_3} = 1/4$ . Thus the critical coverage is the mixture of  $\text{NH}_2$  radicals ( $\theta_{NH_2-cr} = 0.75 ML$ ) and  $\text{NH}_3$  admolecules ( $\theta_{NH_3-cr} = 0.25 ML$ ).

It is worth to note that EECR critical state does not correspond to any energetically preferable state of the surface, it is merely the coverage at which the Fermi level is liberated, i.e. located in the gap between one pinning state and the other. As such it is mere termination of the coverage range in which the jump of the Fermi level corresponds to the jump in adsorption energy. As argued above, this change usually corresponds to the absence of the internal dipole layer because the Fermi level is governed by its position in the bulk, i.e. no surface-internal charge is present. The example of the absence of the electric field in the slab is presented in Fig. 20.

It is therefore expected that in the vicinity of the EECR state the adsorption energy depends on the doping in the bulk. The band profiles presented in Fig. 20 confirm this prediction, the bands are flat and the Fermi level is located in CB, VB and in the midgap for n-type, p-type and semi-insulating bulk GaN, respectively. As it was claimed, the adsorption energy should be approximately constant for wide range of the coverage (it may depend on adsorbate-adsorbate interaction only) and undergo considerable jump at EECR state where the Fermi level is liberated to be shifted to the other pinning state. This was best shown in the case of hydrogen adsorption at GaN(0001) surface. In this case molecular hydrogen is dissociated during adsorption and the resulting hydrogen atoms are located in the on-top positions. Hydrogen is exemplary case because it is small, so the quantum overlap is extremely small so that these atoms are essentially noninteracting [100]. The surface unit consist of single Ga site, to which H atom is attached. The Ga broken bond state is located 0.5 eV below CBM, therefore it is empty, i.e.  $n_i = 0$ , it is fractionally charged by  $3/4$  electron thus  $q_i = 3/4$ . Ga-H two spin states are located at VBM, therefore it is occupied thus  $n_f = 2$ . Hydrogen brings single electron therefore  $q_a = 1$ . From Eq. 2a the EECR critical hydrogen coverage is  $\theta_{H-cr} = 3/4$ . At this

coverage Fermi level is free, for  $\theta < \theta_{H-cr}$  Fermi level is pinned by Ga-broken bond state below CBM, for  $\theta > \theta_{H-cr}$  it is pinned by G-H state at VBM. Therefore it is expected that the adsorption energy have a jump as presented in Fig. 15. The adsorption energy was obtained from *ab initio* calculations, according to the formula:

$$\Delta E_{DFT}^{ads-GaN}(H) = E_{DFT}^{tot}(slab + H) - E_{DFT}^{tot}(slab) - E_{DFT}^{tot}(H) \quad (4)$$

and plotted in Fig 15 for entire range hydrogen coverage ( $0 \leq \theta_H \leq 1$ ). The adsorption energies were calculated for the atomic hydrogen adsorption [ $H(v) \rightarrow H(s)$ ] and the molecular adsorption [ $H_2(v) \rightarrow 2H(s)$ ] are [100]:

$$\Delta E_{DFT}^{ads-GaN}(H) = \begin{cases} -3.40 \text{ eV} & \theta_H < 0.75 \text{ ML} \\ -1.10 \text{ eV} & \theta_H > 0.75 \text{ ML} \end{cases} \quad (5a)$$

and

$$\Delta E_{DFT}^{ads-GaN}(H_2) = \begin{cases} -2.24 \text{ eV} & \theta_H < 0.75 \text{ ML} \\ 2.36 \text{ eV} & \theta_H > 0.75 \text{ ML} \end{cases} \quad (5b)$$

The jump by about 2.30eV is due to electron transfer from Ga broken bond to H bonding state located below VBM, present and absent for low and high coverage, respectively. The energy difference, obtained for dissociative adsorption of molecular hydrogen and the adsorption of atomic hydrogen is in accordance with the molecular hydrogen dissociation energy  $E_{DFT}^{diss}(H_2) = 4.56 \text{ eV}$ . This calculated value is slightly different from the experimental value  $E_{exp}^{diss}(H_2) = 4.58 \text{ eV}$  [102]. As it is shown in Fig. 21 the adsorption energy is constant with the random variation below 0.1 eV.

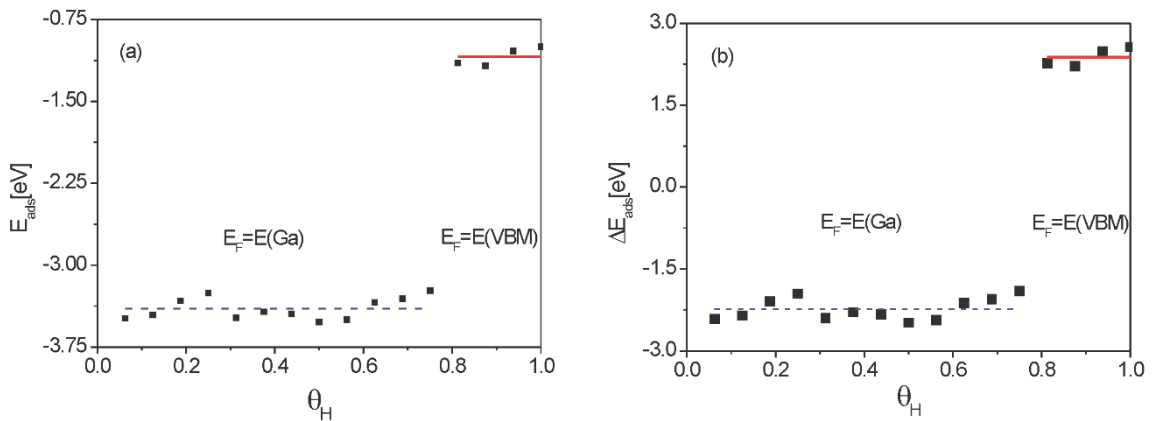


Fig. 21. Atomic (a - Eq. 3a) and molecular (b - Eq. 3b) hydrogen adsorption energy in function of hydrogen coverage of the GaN(0001) surface (black squares), calculated using 4 x 4 slab. The horizontal lines represent coverage independent energy values for low and high coverage regime, denoted by dashed blue and solid red lines respectively. Reproduced Fig. 8 from Ref. 100 [100].

Additional effect is observed for the above presented case of NH<sub>2</sub>/NH<sub>3</sub> coverage of GaN(0001) surface [100]. The band structure of the surface covered by  $\theta_{NH_2-cr} = 3/4$  and  $\theta_{NH_3-cr} = 1/4$  is presented in Figs 20. As it was shown in Fig. 20, n-type, SI and p-type doped crystals has the Fermi level descending from CBM, midgap to VBM. The NH<sub>2</sub> to NH<sub>3</sub> conversion is essentially an attachment of a single hydrogen atom. The adsorption energy presented in Fig. 21 shows the energy change during attachment of H<sub>2</sub> molecule at (4 × 4) i.e. 16 site slab. The adsorption for the case of finite state above critical value, i.e.  $\theta > \theta_{cr-NH_3} = 1/4$  leads to the shift of electrons to the other states, i.e. above Fermi energy. As it is shown in Fig. 22, the reduction of the energy gain occurs exactly at  $\theta = \theta_{cr-NH_3} = 1/4$  for n-type as these electrons are shifted up very high. Subsequently, this reduction is observed for SI and p-type as in these cases these electrons are located first in the partially empty VB states. Further increase of the coverage leads to the energy gain until energy gain finally becomes negative due to electron transfer over the gallium nitride bandgap. This effect is second confirmation of the electron character of the observed effect of adsorption energy change.

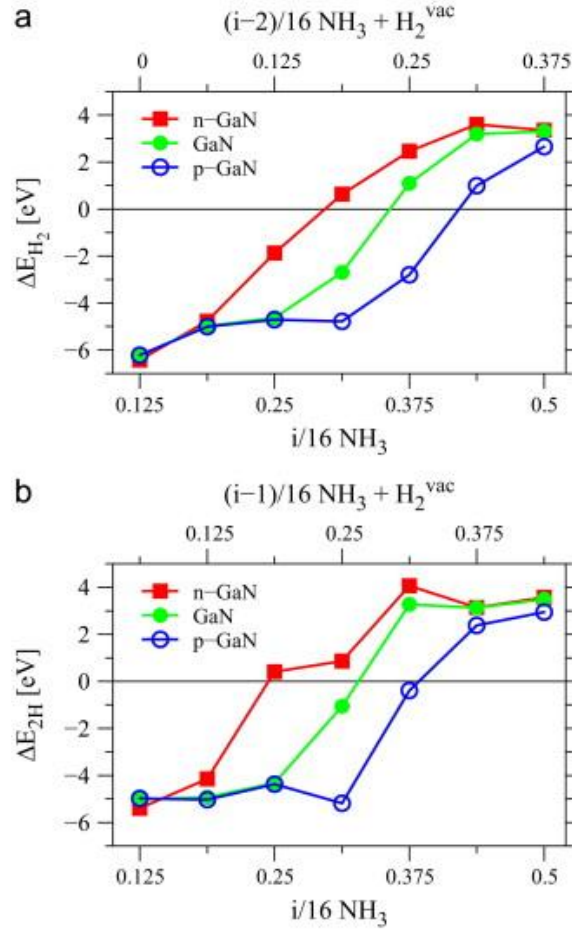


Fig. 22. Energy changes during adsorption/desorption of  $H_2$  molecule on GaN(0001) surface covered with various  $NH_3/NH_2$  mixture. The data are obtained for  $n$ -,  $p$ -type and semi-insulating bulk. The negative value of energy means that the surface configuration indicated on the bottom horizontal axis has a lower energy than the configuration marked on the upper axis. Reproduced Fig. 4 from Ref. 99 [99].

It is worth to stress out that the adsorption energy jump related to intra-surface electron transfer exerts drastic influence on the thermodynamic properties of the two-phase semiconductor-vapor systems. From Van t'Hoff relation it follows that the equilibrium pressure of the adsorbate  $p$  depends exponentially on the evaporation energy  $\Delta H$ , i.e.  $p \approx \exp\left(-\frac{\Delta H}{kT}\right)$ . In addition to *ab initio* calculated energy difference the evaporation energy  $\Delta H$  can additionally change due to thermal contribution to the enthalpy, i.e.  $\Delta H(T) = \Delta H(T_0) + \int_{T_0}^T \Delta C(T) dT$ . The thermal contribution to this difference may be calculated assuming that:

- i) for the vapor phase, the thermal contributions stem from the translational, rotational and vibrational degrees of freedom [103-107],

- ii) for the adsorbate the thermal contribution to enthalpy, entropy and free energy arises from the lattice vibrations only [106].

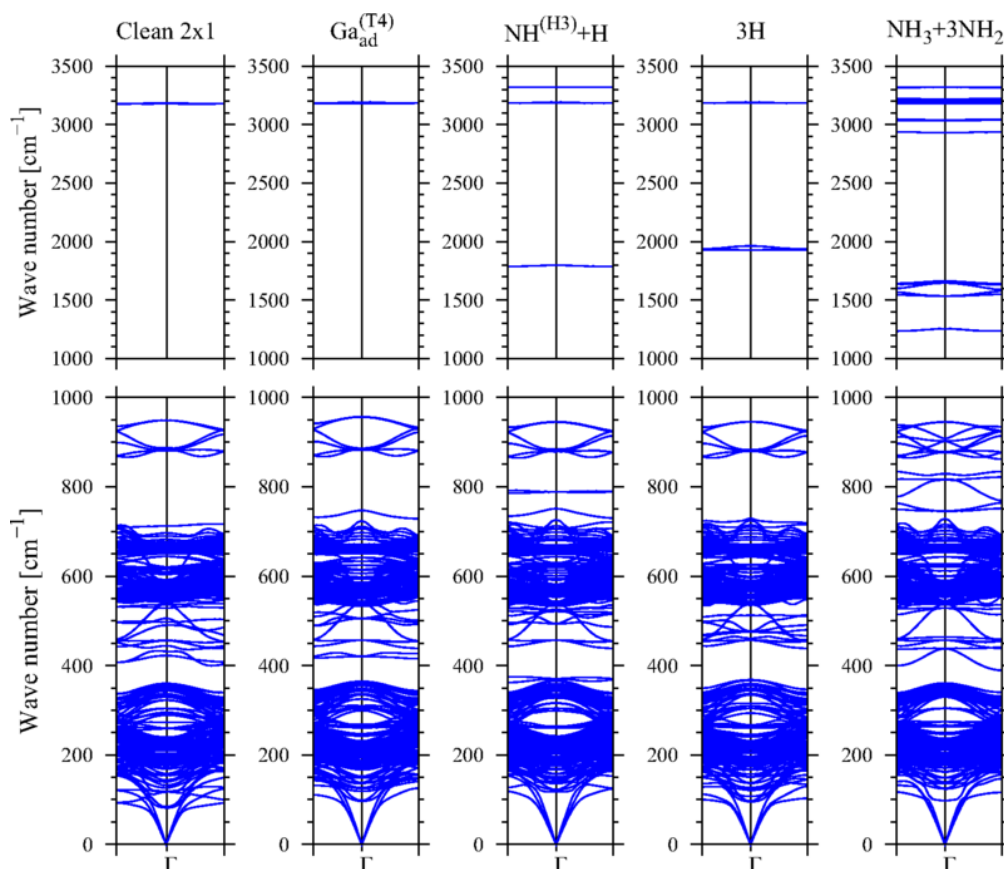


Fig. 23. Phonon dispersion relations of (2 x 2) slab representing GaN(0001) surface: lower row – full slab spectra, upper row – only spectra associated with different adsorbate: from the left: none, Ga adatom, NH-radical in H3 position plus H adatom, 3 H adatoms, NH<sub>3</sub> admolecule and 3 NH<sub>2</sub> radicals. In addition, the modes associated with pseudo-hydrogen termination atoms at the opposite surface are shown (approximately 3200  $cm^{-1}$ ). The bands in the range between 850  $cm^{-1}$  and 950  $cm^{-1}$  are related to N atom close to the termination. Reproduced Fig. 3 from Ref. 106 [106].

The adsorbate part was treated in a simplified way employing the vibrational degrees of freedom only (ii). This is in some sense reduction of the more general approach (i) used for the derivation of the data shown in the thermochemical tables for the molecules and atoms. Since the adsorbates are located in the lattice sites, only the vibrational calculations were applied [87]. In this case, the adsorbate contribution is defined as the difference between the vibrational spectrum of the slab with and without adsorbate. The example of such calculation results is presented in Fig. 23 for the case of GaN(0001) surface with several adsorbates. The results

show additional modes associated with the several adsorbates. In addition, by direct summation the zero point energy may be calculated as difference of the energies of the ground quantum states of the adsorbed atoms and the molecule in the vapor:  $\Delta E_{sv}^{ZPE} = 2E_s^{ZPE}(H) - E_v^{ZPE}(H_2)$

From these spectra the standard thermodynamic formulae may be used to derive thermodynamic quantities by direct summation [106-108]

$$E^{vib}(x) = k_B T \sum_j \frac{x_j}{\exp(x_j) - 1} \quad (6a)$$

$$C^{vib}(x) = k_B \sum_j \frac{x_j^2 \exp(x_j)}{[\exp(x_j) - 1]^2} \quad (6b)$$

$$S^{vib}(x) = k_B \sum_j \frac{x_j}{\exp(x_j) - 1} - \ln[1 - \exp(-x_j)] \quad (6c)$$

$$F^{vib}(x) = k_B T \sum_j \ln[1 - \exp(x_j)] \quad (6d)$$

where  $x_j \equiv \frac{\hbar \omega_j}{k_B T}$  and  $\omega_j$  is phonon frequency of a j-th phonon mode. From these formulae the temperature dependent free energy vibrational contribution  $\Delta F^{vib}(T)$  and zero point energy contribution was  $\Delta E^{ZPE}$  were calculated for several adsorbates at GaN(0001) surface [108]. The results are shown in Fig. 24.

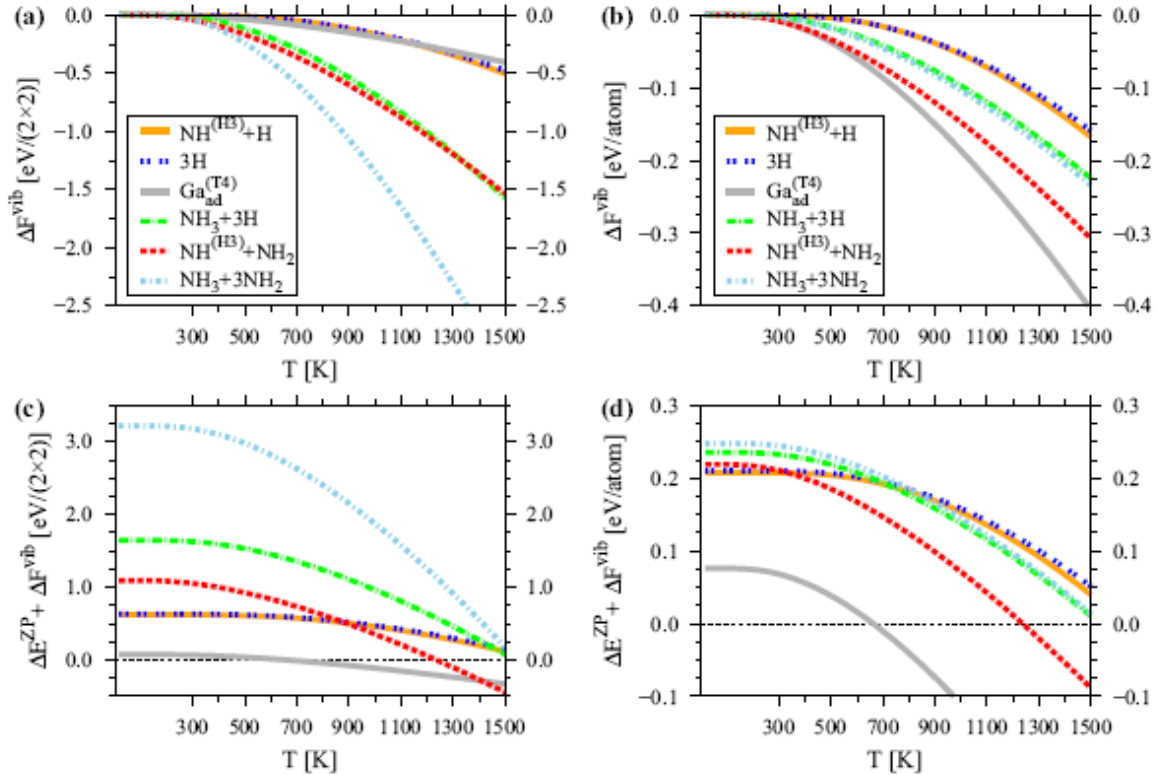


Fig 24. Changes in the vibrational free energy versus temperature for the GaN(0001) surface covered with different adsorbates, determined in relation to clean surface with  $2 \times 1$  reconstruction; (a), (b)  $\Delta F^{vib}(T)$  dependence; (c), (d)  $\Delta F^{vib}(T)$  dependence including zero-point  $\Delta E^{ZPE}$  offset . Graphs (a) and (c) show energies of the entire  $2 \times 2$  surface cell, while graphs (b) and (d) show the average energy per atom. Fig. 4 from Ref 106 [106].

A simplified treatment may be alternatively used, based on Debye theory in which the acoustic phonon frequencies are approximated by linear dependence on the wavevector. Accordingly, the maximum phonon energy, known as the Debye energy, and its equivalents: the Debye frequency and the Debye temperature, are related as follows:  $E_D = \hbar\omega_D = k_B\theta_D$ . Using this simplified representation the complex summation can be replaced by integration [108]:

$$E^{vib}(T) = 9k_B T \left(\frac{T}{\theta_D}\right)^3 \int_0^{\theta_D/T} \frac{x^3 dx}{\exp(x)-1} \quad (7a)$$

$$C^{vib}(T) = 9k_B \left(\frac{T}{\theta_D}\right)^2 \int_0^{\theta_D/T} \frac{x^4 \exp(x) dx}{[\exp(x)-1]^2} \quad (7b)$$

$$S^{vib}(T) = 9k_B \left(\frac{T}{\theta_D}\right)^3 \int_0^{\theta_D/T} \left\{ \frac{x}{\exp(x)-1} - \ln[1 - \exp(-x)] \right\} x^2 dx \quad (7c)$$

$$F^{vib}(T) = 9k_B T \left(\frac{T}{\theta_D}\right)^3 \int_0^{\theta_D/T} x^2 \ln[1 - \exp(-x)] dx \quad (7d)$$

In the case of hydrogen adsorbed at GaN(0001) surface, the Debye formulation provided satisfactory approximation to exact summation [108]. This formulation show that the interaction between the adsorbate and the substrate may be complex, quite different from simple increase of the number of the degrees of freedom and emergence of additional frequencies. The interaction may affect the elastic lattice properties so that the specific heat change may be negative at low temperature due to the lower excitement of large number of lattice vibrations that can offset the increase of the number of degrees of freedom during adsorption. Generally, this is reflected in the coverage dependence of the effective Debye temperature, which for complex adsorbate may be substantial. Thus in the case of Al adsorption at AlN(0001) surface [109] it is

$$\theta_D(\theta_{Al}) \cong \begin{cases} 1002.4 - 1254.5\theta_{Al} + 745.1\theta_{Al}^2 & \theta_{Al} \leq 1 \\ 493 & 1 < \theta_{Al} \leq 2 \end{cases} \quad (8)$$

which reflects the dramatic reduction of the stiffness for higher Al coverage, e.g.  $T_D(\theta_{Al} = 0.1) = 875 \text{ K}$  which is reduced to  $T_D(\theta_{Al} = 0.75) = 550 \text{ K}$  [109]. Naturally, zero point energy is also coverage dependent:

$$E_{Al}^{ZPE}(\theta_{Al}) \cong 0.097 - 0.101\theta_{Al} + 0.06\theta_{Al}^2 \quad (9)$$

That complicates use of simplified formulation. It is worth to note that the presence of the adsorbate may lead to the increase but also to decrease of the heat capacity. This is shown for the case of Al adsorption on AlN(000-1) surface presented in Fig. 26.

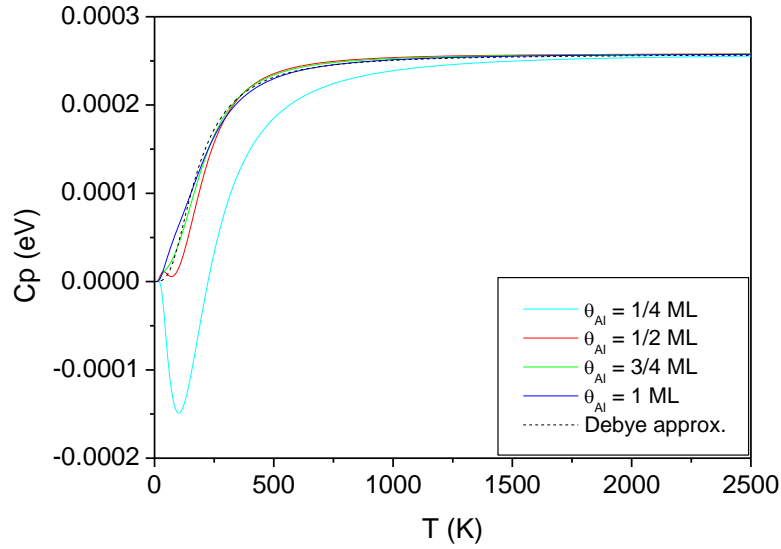


Fig. 25. Temperature dependence of the specific heat related to Al adatoms, attached to  $4 \times 4$  slab representing AlN(0001) surface, obtained from phonon frequency summation (solid lines). For the comparison, the specific heat obtained for the Debye temperature  $\theta_D = 740 \text{ K}$  is plotted using broken line. Reproduced Fig. 13 from Ref 109 [109].

The differential specific heat was calculated as the difference of the surface as specific coverage and the clean surface. This value becomes negative for low Al coverage at low temperature. Since the obtained increase of the heat difference due to attachment of Al adatoms is compensated by the negative contribution related to the adsorption that stiffen the lattice, so that the overall contribution is negative. This is observed for low temperature only, for higher temperature all degrees are excited so the increment of the specific heat is positive.

The thermodynamic quantities of the vapor phase were calculated according to the formulation (i) and tabulated for large number of substances that may be used for derivation of effective formulae for enthalpy, entropy and free energy. These tables provide thermodynamic data for all elements and compound in two basic states of matter: vapor at normal pressure  $p = 1\text{ bar}$  and the condensed phase (solid/liquid) up to 3000 K. Therefore it is sufficient to obtain sufficiently precise data which could be used for the vapor phase contributions.

Accordingly the full determination of the equilibrium is possible. This was formulated first for 3-d transitions by Jackson and Walsh [110] and later independently for surface adsorption (2-d) by Kempisty et al. [107]. Remarkably, the results formulated as solid/surface-vapor chemical potential difference  $\Delta\mu_{sv}$ , were identical. Here we present chemical potential difference (which is zero at equilibrium) formulae for dissociative adsorption of molecular hydrogen ( $\text{H}_2$ ) at GaN(0001) gallium terminated gallium nitride surface [107]:

$$\begin{aligned} \Delta\mu_{sv}(p, T) = \mu_{H(s)}(T, x) - \frac{1}{2}\mu_{H_2(v)} = \Delta H_{dis}^{DFT}(0) + \Delta G_{ads} + \Delta H_{therm} + \Delta G_{S-therm} + \\ \Delta G_{pres} + \Delta G_{conc}(T, \theta_N) = \Delta H_{ads}^{DFT} - T_o\Delta s_{sv} + \int_0^{T_o}(C_s - C_v)dT - \int_{T_o}^T(s_s - s_v)dT + \\ \int_{p_o}^p(v_s - v_v)dp + k_B T \ln\left(\frac{\theta_N}{1 - \theta_N}\right) = 0 \end{aligned} \quad (10)$$

where the surface-vapor chemical potential difference  $\Delta\mu_{sv}$  is expressed as sum of:

- i) enthalpy change at adsorption  $\Delta H_{ads}^{DFT} = \Delta E_{DFT}^{ads-GaN}(H_2) + \Delta E_{sv}^{ZPE}$ , taken as the sum of adsorption energy and zero point energy difference. The former is obtained from *ab initio* calculations, and given by Eq. 4. Note that this quantity undergoes jump at  $\theta_H = \theta_{H-cr} = 0.75\text{ ML}$ . The latter is given as  $\Delta E_{sv}^{ZPE} = 2E_s^{ZPE}(H) - E_v^{ZPE}(H_2)$ . This value was obtained from *ab initio* phonon calculations  $\Delta E_{sv}^{ZPE} = -0.21\text{ eV}$  [106] and is much smaller than the enthalpy change.
- ii) the free energy  $\Delta G_{ads} = -T_o\Delta s_{sv}$  related to the entropy change at adsorption that could be obtained as the difference of entropies of nitrogen at the surface and in the vapor  $\Delta s_{sv} = 2s_s - s_v$ , where solid phase entropy is due to phonon contribution only as solid phase entropy is zero thus free energy contribution is therefore  $\Delta G_{ads} = 0.633\text{ eV}$  [107].
- iii) the thermal enthalpy change  $\Delta H_{therm} = 2h_s(T_o) - h_v(T_o) = \int_0^{T_o}(2C_s - C_v)dT$  in which the enthalpy of the adsorbate is  $h_s(T_o) = 1.71 \times 10^{-4}\text{ eV}$  and  $h_v(T_o) =$

$8.99 \times 10^{-2} \text{ eV}$  that gives  $\Delta H_{therm} = -0.051 \text{ eV}$  [107]. This component is relatively small.

- iv) the thermal entropy change  $\Delta G_{S-therm} = \int_{T_0}^T (2s_s - s_v) dT = [2[\mu_{H-s}(T) - \mu_{N-s}(T_0)] - \mu_{H_2}(T) - \mu_{H_2}(T_0)]$  which could be obtained from free energy dependence of ideal H<sub>2</sub> vapor at 1 bar, given as [111]:

$$\mu_{H_2}(T) = -1.22 \times 10^{-3}T - 0.26 \times 10^{-6}T^2 + 2.4 \times 10^{-11}T^3 \quad (10)$$

while the chemical nitrogen chemical potential of nitrogen at the surface could be approximated to Debye thermal dependence as

$$\mu_{H-s}(T) = 7.56 \times 10^{-6}T - 2.38 \times 10^{-7}T^2 + 3.26 \times 10^{-11}T^3 \quad (11)$$

which combined  $\Delta G_{S-therm}(T) = 2\mu_{H-s}(T) - \mu_{H_2}(T)$  to give

$$\mu_{H_2}(T) - 2\mu_{H-s}(T) = -1.23 \times 10^{-3}T - 2.82 \times 10^{-7}T^2 + 1.54 \times 10^{-11}T^3 \quad (12)$$

that determines this value at any T. At  $T = 1300 \text{ K}$  this contribution is

$$G_{S-therm}(1300 \text{ K}) = -1.497 \text{ eV}.$$

- v) pressure dependent term can be used in ideal gas approximations, as the typical growth nitride vapor growth conditions correspond to high temperature and relatively low pressure :  $\Delta G_{pres} = k_B T \ln(p_{N_2}/p_o)$  where  $p_o = 1 \text{ bar}$ .
- vi) the configuration term  $\Delta G_{conc}(T, \theta_N) = k_B T \ln(\theta_N / (1 - \theta_N))$ . The term is responsible for Langmuir singularity at  $\theta_N = 1$ , therefore in the vicinity of the full coverage can attain very high values.

In total, several terms contribute similar values. The pressure dependent term can be used for the determination of the equilibrium pressure of hydrogen at GaN surface at any temperature according to the formula [107]:

$$\frac{p}{p_o} = \left(\frac{\theta_H}{1-\theta_H}\right)^2 \exp\left\{\frac{-[\Delta H_{vap} + \Delta H_{therm} + \Delta G_{S-vap} + \Delta G_{S-therm}]}{k_B T}\right\} \quad (14)$$

The results of these calculations are given at Fig. 26.

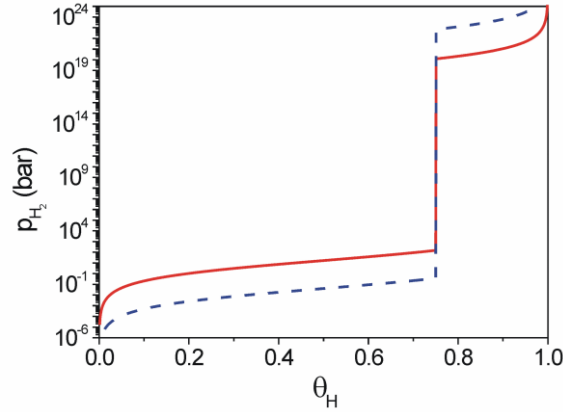


Fig. 26. Equilibrium pressure of molecular hydrogen at GaN(0001) in function of hydrogen coverage. The two lines: dashed blue and solid red correspond to 1000K and 1300K, respectively. Reproduced Fig. 2 from Ref 107 [107].

From these data it follows that the equilibrium pressure of the vapor strongly depends on the temperature which is related to the thermal contribution to the chemical potential difference (ii-v). Nevertheless the most important is jump-like change at the critical coverage  $\theta_H = \theta_{H-cr} = 0.75 ML$  where the pressure change is by far the greatest. Additionally, at both ends, i.e.  $\theta_H = 0$  and  $\theta_H = 1 ML$ , the entropy contribution diverges asymptotically and is visible in Fig. 26. In summary, the charge related term is the most important contribution affecting equilibrium between molecular hydrogen and GaN(0001) surface. In the following we discuss the vapor-solid equilibria historically showing that this phenomenon was identified in many systems thus changing the physics of these systems.

## 2. Historical resume and material review

Historically, the contribution of intra-surface electron transfer was obtained first in the paper devoted to determination of the adsorption energy of hydrogen at GaN(0001) surface, published in 2012 [101]. Specifically, the adsorption energy of single hydrogen atom at the surface was about 3.4 eV for hydrogen coverage below 0.75 monolayer ( $\theta_H < 0.75 ML$ ), and was reduced to 1.4 eV for higher coverage ( $\theta_H = 0.75 ML$ ) [82]. The first diagram showing this adsorption energy change is reproduced in Fig. 27. In the following years far more precise and extensive calculations of hydrogen adsorption was published proving that the energy gain follows Eq. 4a and Eq. 4b for atomic and molecular hydrogen, respectively [101]. It was shown that far away from the critical coverage, i.e.  $\theta_H = 0.75 ML$ , adsorption energy is essentially constant, independent on the doping, i.e. H adatoms effectively do not interact with the

neighbors. In the close vicinity of critical coverage, i.e. for Fermi level not pinned at the surface, the adsorption energy depends on the doping in the bulk, finally confirming electron transfer contribution.

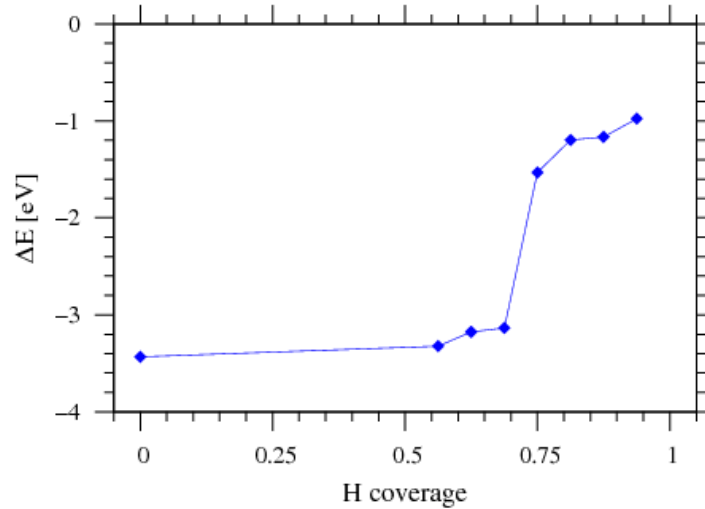


Fig. 27. Adsorption energy of single hydrogen atom, at differently covered GaN(0001) surface, obtained using 4 x 4 supercells. Reproduced Fig. 5 from Ref. 101 [101].

Somewhat later, phonon related contribution was introduced, so that free energy of the hydrogen adsorbate was temperature dependent [106]. Afterwards, the full contribution to chemical potential of both adsorbate and the vapor was determined allowing to obtain complete equilibrium [107]. Therefore hydrogen vapor adsorption on the Ga terminated GaN(0001) surface is fully determined in terms of the surface coverage, temperature and the pressure of the vapor.

Several month after the first publication of hydrogen adsorption energy dependence on the coverage [101], Chen and Kuo published investigation of wetting of GaN(0001) surface [95]. Actually, they calculated the energy change during adsorption of water molecule at the surface in the three different forms:

- i) molecular,
- ii) fully dissociated water,
- iii) molecular hydrogen plus O adatom.

They observed some changes of the adsorption energy during adsorption of four water molecules. These changes were relatively small and of different nature: generally smaller for the set of four molecules. No clear identification of the profound difference was identified. The authors speculated that this was due to reconstruction contribution, which they discussed earlier.

This identification as related to reconstruction contribution and the magnitude of the effect is different from later confirmed contribution from the charge transfer. Thus the clear identification of the effect was not obtained. Afterwards the reconstruction hypothesis turned out to be incorrect.

Molecular hydrogen adsorption on the opposite, N-terminated GaN (000-1) surface was also investigated showing that hydrogen adsorption process is dissociative and barrierless again [112]. Hydrogen atom is adsorbed in the on-top position, therefore the EECR unit have single N topmost atom ( $z = 1$ ). Their fractional charge is  $q_i = 5/4$  thus  $Q_i = q_i = 5/4$ . As it was shown N-terminated surface is different from Ga-terminated because N-broken bond states energies are located close to VBM [51]. Thus the Fermi level is pinned there at clean GaN(000-1) surface. The number of the states before and after the adsorption is identical  $N_a = N_f = 2$ . Thus from Eq. 2b we obtain  $g_{cr} = \theta_{cr} = \frac{3}{4}$ . In other words, addition of hydrogen charge  $Q_a = 1$  creates a surplus of  $1/4$  electron which is donated to the other N-broken bond state that are not saturated. As the N-broken bond state can accept  $3/4$  electron, the three H-adsorbed sites are needed for full saturation of single N-broken bond so that the critical condition for filling all broken states is at  $\theta_H = \theta_{H-cr} = 0.75 ML$  [112]. Thus the energy change in adsorption of hydrogen molecule at fractionally H-covered GaN(000-1) surface is:

$$\Delta E_{DFT}^{ads-GaN}(H_2) = \begin{cases} -7.04 eV & \theta_H < 0.75 ML \\ -1.60 eV & \theta_H > 0.75 ML \end{cases} \quad (15)$$

The jump is considerable as for high coverage the  $1/2$  electron is shifted to conduction band across the bandgap. These data were used to estimate hydrogen equilibrium pressure at the benchmark temperature  $T = 1300 K$  via simple van t'Hoff approach to be  $p \cong 10^{-24} bar$  and  $p \cong 1 bar$  for  $\theta_H < 0.75 ML$  and  $\theta_H > 0.75 ML$ , respectively. Thus GaN(000-1) surface adsorbs molecular hydrogen rapidly which can lead to the decomposition via desorption of ammonia. The high coverage of hydrogen are therefore not accessible for experimental investigation of hydrogen at GaN(000-1) surface, unless ammonia ambient is used. Until present no further theoretical investigations of this process has been made. Nevertheless, these scarce data confirm decisive role charge transfer contribution in this process.

Epitaxial processes widely employed for creation of nitride device structures use either plasma activated nitrogen [113,114] or ammonia [115-117]. The growth is conducted almost exclusively on GaN(0001) surface by metal organic vapor phase epitaxy (MOVPE) as the layers

grown on this surface have superior optical properties, useful for optoelectronic devices. Therefore adsorption of ammonia at this surface is of considerable interest and was investigated by many researchers. The early stage of these investigations was summarized by Van de Walle and Neugebauer in their Letter [118]. They presented phase diagram for GaN(0001) surface in which the nitrogen-hydrogen rich region of the surface can be divided into:

- i) hydrogen covered at  $\theta_H = 0.75 ML$
- ii) mixed  $HN_3 - NH_2$  covered at  $\theta_{NH_3} = 0.25 ML$  and at  $\theta_{NH_2} = 0.75 ML$
- iii) mixed  $HN_3 - H$  covered at  $\theta_{NH_3} = 0.25 ML$  and at  $\theta_H = 0.75 ML$ .

The remaining part of the diagram correspond to Ga-rich diagram which is not relevant to ammonia adsorption. This diagram was obtained using  $(2 \times 2)$  slab, therefore these data indicate basic features only. In fact these values correspond to critical coverages at which the Fermi level becomes free as it was proved above for the case of hydrogen ( $\theta_{H-cr} = 0.75 ML$ ) and mixture of  $NH_2$  radicals ( $\theta_{NH_2-cr} = 0.75 ML$ ) and  $NH_3$  admolecules ( $\theta_{NH_3-cr} = 0.25 ML$ ). As it will be shown below, from the point of the charge  $NH_2$  radicals and equivalent to H adatoms, therefore the mixture ( $\theta_{H-cr} = 0.75 ML$ ) and  $NH_3$  admolecules ( $\theta_{NH_3-cr} = 0.25 ML$ ) is also critical. In accordance to the above described arguments, the coverages indicated in the phase diagram are therefore the points in which the change of the electron transfer occurs causes jump-like change of the adsorption energies.

The investigations in the following prove that the data presented in Ref. 118 are basically correct but simplified the issue overly. In fact they correspond to relatively high pressure of ammonia and hydrogen in the vapor. Several years later the detailed investigations started from ammonia adsorption at clean GaN(0001) surface. Since ammonia decomposition leads to hydrogen release, the incorporation of hydrogen coverage into  $NH_3$  investigations was indispensable. It was shown that two different adsorption scenarios are possible: ammonia can be adsorbed molecularly with the energy  $\Delta E_{DFT}^{ads-mol}(NH_3) = 2.0 eV$  or dissociatively with  $\Delta E_{DFT}^{ads-mol}(NH_3) = 2.6 eV$  for hydrogen coverage  $\theta_H < 0.75 ML$  [100]. For higher coverage, the molecular adsorption energy remain unchanged while the dissociative adsorption energy becomes negative [119]. As shown in Fig. 21, all states of  $NH_3$  admolecule are degenerate with valence band so they are occupied. Ammonia molecular adsorption is neutral as it brings 8 electrons to occupy all states. Therefore 3/4 electron is shifted into conduction band. Thus no EERC condition is possible and the adsorption energy is reduced by the electron transfer for any hydrogen coverage. The dissociative adsorption is creates  $NH_2$  admolecule and H adatom. Both cases are equivalent, 1/4 electron is missing. Therefore the number of electrons

transferred from Ga broken bonds state is doubled, and accordingly this creates substantial contribution to the adsorption energy. The energy difference at the critical coverage  $\theta_{cr-H} = 3/4$  is close to 5 eV [119].

More detailed investigations revealed complex pattern of ammonia dissociative adsorption, especially to low surface coverage [84, 94]. Several configurations are possible:

- i) NH radical in H3 position
- ii) NH radical on-top
- iii) NH<sub>2</sub> radical – bridge
- iv) NH<sub>2</sub> radical – on top

According to the data in Ref 11., all states of these radicals are degenerate with valence band [119]. In case of the on-top position the unit is single site ( $z = 1$ ). Thus the charge is  $Q_i = 3/4$ . In the case of the NH radical, the adsorbate charge is  $Q_a = 6$ . Number of initial occupied states after adsorption is  $N_f = 0$ , configuration number of states after adsorption  $N_a = 8$ . This leads to the NH critical coverage at coverage  $\theta_{cr-NH-top} = 3/8$ . And accordingly, the adsorption energy gain of dissociative adsorption of ammonia at  $\theta_{NH-top} < 0.375 ML$  is  $\Delta E_{NH-top}^{DFT} \cong 1.42 eV$ . For higher coverage this gain is negative.

In the case of NH radical located in the H3 position the unit contains 3 Ga sites, i.e. ( $z = 3$ ), so that the initial charge  $Q_i = 9/4$ . The adsorbate charge is  $Q_a = 6$ . The number of occupied initial states after adsorption is  $N_i = 0$ , configuration number of occupied states after adsorption  $N_a = 8$ . This leads to critical fraction  $g_{cr-NH-H3} = 9/8$ . Accordingly the critical coverage is  $\theta_{cr-NH-H3} = 3/8$ . Therefore this energy jump should be observed  $\theta_{NH-top} \cong 0.375 ML$ . This is in accordance of general result, the adsorption energy gain of dissociative adsorption of ammonia at  $\theta_{NH-top} < 0.375 ML$  is  $\Delta E_{NH-top}^{DFT} \cong 1.42 eV$ . For higher coverage this gain is negative.

In the case of NH<sub>2</sub> radical in the bridge position the unit contains 2 Ga sites, i.e. ( $z = 2$ ), so that the initial charge  $Q_i = 3/2$ . The adsorbate charge is  $Q_a = 7$ . The number of occupied initial states after adsorption is  $N_f = 0$ , configuration number of occupied states after adsorption is  $N_a = 8$ . This leads to critical fraction  $g_{cr-NH2-bridge} = 3/2$ . Accordingly the critical coverage is  $\theta_{cr-NH2-bridge} = 3/4$ . This is not possible as the top coverage is  $\theta_{cr-NH2-bridge} = 1/2$ .

Finally, the case of NH<sub>2</sub> radical in the on-top position ( $z = 1$ ), thus the initial charge is  $Q_i = 3/4$ , the adsorbate charge is  $Q_a = 7$ . The number of occupied initial states after

adsorption is  $N_f = 0$ , configuration number of occupied states after adsorption is  $N_a = 8$ . This leads to critical fraction  $g_{cr-NH_2-on-top} = 3/4$ . Accordingly the critical coverage is  $\theta_{cr-NH_2-on-top} = 3/4$ . Therefore this energy jump should be observed  $\theta_{NH_2-on-top} \cong 0.75 ML$ . No such investigation has been done because this configuration is unstable.

These investigations were finished before full thermodynamic procedure for determination of vapor-surface equilibria was formulated [107,110]. Therefore the thermal contribution was limited to the configurational entropy. Using this the estimate of the mixed hydrogen-ammonia pressure in equilibrium with the specified coverage of GaN(0001) was obtained [100]. The coverage by both type ammonia derived radicals: NH (on-top) and NH<sub>2</sub> (on-top and bridge) is limited to hydrogen pressure below  $p_{H_2}(min) = 10^{-5} bar$  and ammonia pressure below  $p_{NH_3}(min) = 10^{-2} bar$ . These conditions cannot be achieved separately in ammonia growth of GaN due to thermal decomposition of ammonia, therefore this suggest that the standard coverage of GaN(0001) surface is full NH<sub>2</sub> – NH<sub>3</sub> mixed coverage. The relative ratio of the radicals and the molecule depends on the ammonia to hydrogen pressure ratio. It has to be stressed out that this is rough estimate, precise determination of the coverage at given temperature-pressures conditions requires a number of simulations in the future. These investigations should include phonon simulations which are extremely demanding numerically. On the other hand, the complex atomic structure of the adsorbate indicate on much larger phonon contribution to free energy which will affect the equilibrium much more than in the case of hydrogen. Thus one can expect that the phonon contribution is comparable to the adsorption energy. Therefore the obtained equilibria may be modified considerably. Since MOCVE and HVPE methods are very important technologically, these calculations are needed in the nearest possible future.

An important example of the influence of the electronic charge on the results of the MOVPE growth of nitrides is well known problem of the growth of GaInN necessary for visible range active LED's and LDs [120-122]. The growth is conducted at high V-III ratio, of about  $p_{NH_3}/p_{Ga} = 4000$  for GaN and  $p_{NH_3}/p_{In} = 10000$  for InGaN. In addition, incorporation of indium into the nitride layers is totally blocked by minuscule presence of hydrogen in the vapor. Thus in InGaN epitaxy molecular nitrogen is used as group III metals carrier gas and the ammonia is the second main component. The typical pressure ratio of the ammonia and the carrier gas is  $p_{NH_3}/p_{H_2} = p_{NH_3}/p_{N_2} = 1$ . Nitrogen is essentially inert and therefore the vapor consists of the two active components: ammonia and molecular hydrogen, which is generated due to ammonia thermal decomposition. The total vapor pressures used in the MOVPE

processes is in the ( $0.1 \text{ bar} \div 1 \text{ bar}$ ) range. Thus the ammonia partial pressures are in the same range. In case of use of nitrogen carrier gas, hydrogen pressures is small fraction of this value.

In the *ab initio* calculations it was assumed that the mixed  $NH_2 - NH_3$  coverage of GaN(0001) surface is full, i.e. all topmost Ga atoms have their broken bonds saturated either by  $NH_2$  radicals or  $NH_3$  ad molecules located in the on-top positions. The electronic properties of such system were presented above in Fig. 28 [120]. All states of the adsorbates, including unsaturated N state in  $NH_2$  radical are degenerate with valence band. In these simulations ( $4 \times 4$ ) slab was used in which the  $NH_2 - NH_3$  ratio was changed by addition of single hydrogen so that the ammonia ad molecules coverage was ( $\theta_{NH_3} = 0, 1/16, \text{ up to } 5/16$ ), thus for the coverage range ( $\theta_{NH_3} \leq 0.25 \text{ ML}$ ) an accordingly ( $\theta_{NH_2} \geq 0.75 \text{ ML}$ ). In all cases ( $\theta_{NH_3} < 1/4$ ), the Fermi level is located at VBM. For higher  $NH_3$  coverage ( $\theta_{NH_3} = 1/4$ ) Fermi level is free in the gap and for higher coverage, e.g. for coverage ( $\theta_{NH_3} = 5/16$ ), is in the conduction band.

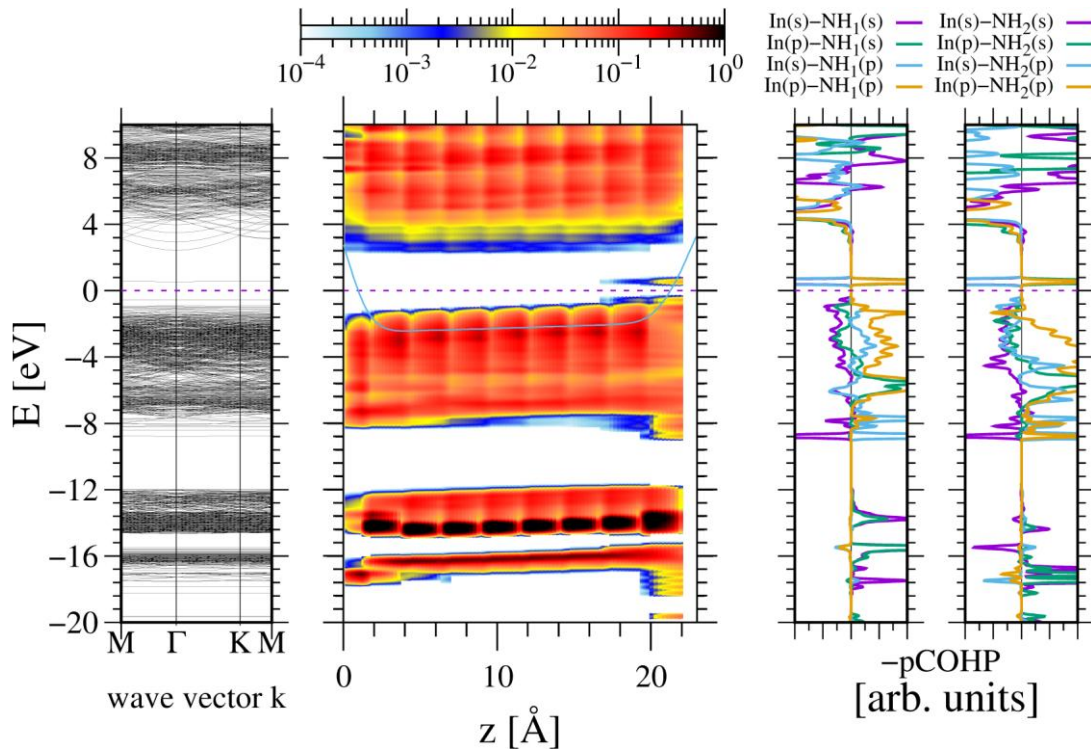


Fig. 28. Electronic properties of  $4 \times 4$  slab representing single In adatom at fully  $NH_2$  covered GaN(0001) surface. The panels from the left present: electron energy in momentum space (band diagram); electron energy in real space, plotted in the direction perpendicular to the surface; Crystal Orbital Hamilton Population (COHP) [67,68] of In and N atoms with  $NH$ ,  $NH_2$  radicals.

The surface is located at the right hand edge of real space diagram. Reproduced from Fig. 3 Ref. 120 [120].

Indium carrier trimethylindium (TMI) is highly unstable at temperature  $T > 600\text{ }^{\circ}\text{C}$ . Therefore in the typical GaInN growth conditions at the temperature  $T \cong 800\text{ }^{\circ}\text{C}$  it is decomposed and single In atom is adsorbed. The stable configuration of In adatom and the  $\text{NH}_3/\text{NH}_2$  coverage depends on the coverage ratio. In case of the low  $\text{NH}_3$  coverage ( $\theta_{\text{NH}_3} \leq 1/16$ ) In adatom is located in the vicinity of the symmetrical H3 site, bonded to two NH and one  $\text{NH}_2$  radicals. Thus one  $\text{NH}_2$  neighbor remains intact while the two others loose one H atom each, i.e. they are converted into NH radicals. In the consequence the two more distant  $\text{NH}_2$  radicals are converted into  $\text{NH}_3$  admolecules. Thus the In adatoms is shifted away from  $\text{NH}_3$  admolecules that indicates on a strong repulsion.

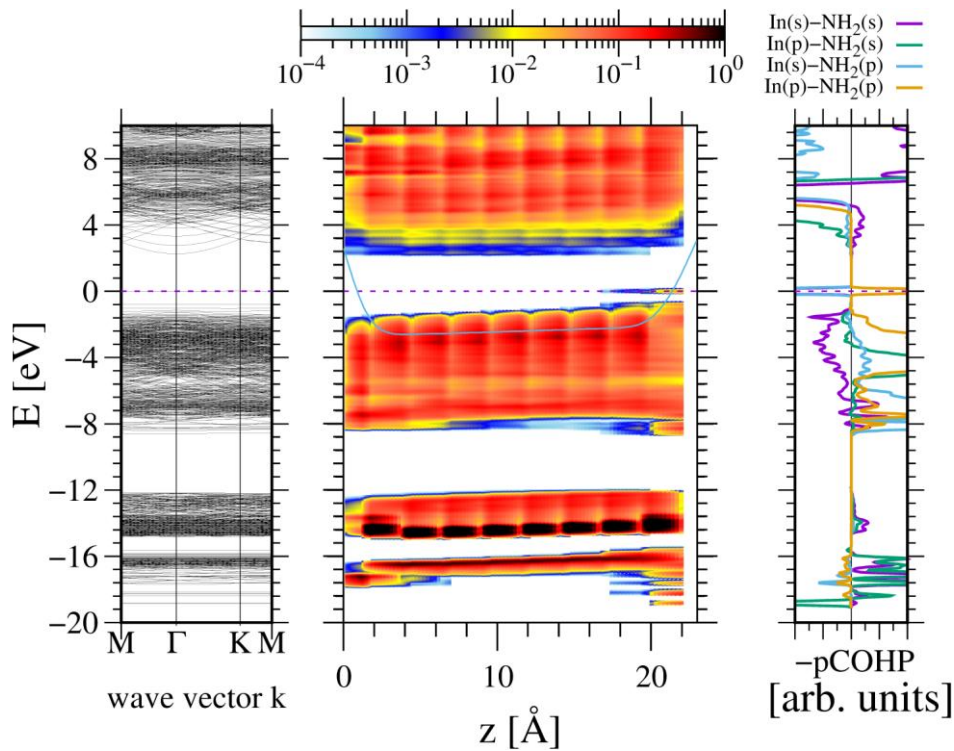


Fig. 29. Electronic properties of  $4 \times 4$  slab representing In adatom at GaN(0001) surface covered by 14  $\text{NH}_2$  radicals and 2  $\text{NH}_3$  molecules ( $x = 1/8$ ). The panels from the left present: electron energy in momentum space (band diagram); electron energy in real space, plotted in the direction perpendicular to the surface; COHP of In and N atoms belonging to  $\text{NH}_2$  radicals. No  $\text{NH}_3$  are present in close vicinity so this overlap is missing. The surface is located at the right hand edge of real space diagram. Reproduced from Fig. 4 Ref. 120 [120].

Since the system considered is changed by the relative  $NH_3/NH_2$  occupation, it is necessary to use entire slab as EECR unit, i.e. 16 surface sites. The initial charge of the unit depends on the number ammonia admolecules. In the case of full  $NH_2$  coverage, the initial charge is of 16 radicals ( $q_{NH_2} = 7$ ) and broken Ga bonds ( $q_{Ga-br} = 3/4$ ) that gives in total  $Q_i = 124$ . We have to account presence of single In atom that adds the adsorbate charge by  $q_{In} = 3$  to  $Q_i = 124$ . Replacement of single  $NH_2$  radical by  $NH_3$  admolecule, i.e. coverage change by  $\theta_{NH_3} = 1/16$ , is equivalent of adsorption of single hydrogen atom with the charge  $Q_a = 1$ . All states of radicals and admolecules are occupied that adds 8 states for each. In summary the number of original states that are occupied by adsorption is  $N_f = 16 \times 8 = 128$ . The EECR rule gives the following  $g_{cr} = 1$ . Thus the fully  $NH_2$  covered slab with attached single In admolecule will have Fermi level at VBM. Accordingly, attachment of single  $NH_3$  admolecule leads to EECR condition with all states filled. This is in accordance with the band diagram plotted in Fig. 23 where the Fermi level is located in the gap between VBM and In antibonding states.

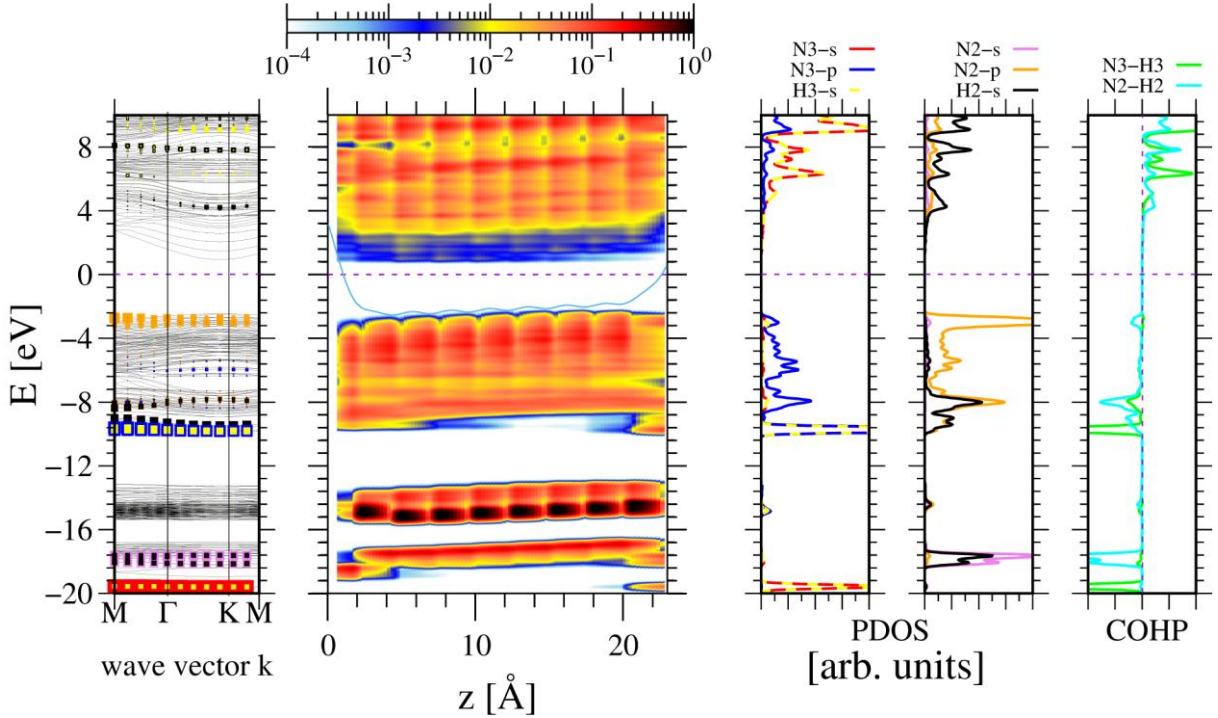


Fig. 30. Electronic properties of the  $(2 \times 2)$  8 GaN DALs slab, covered by single  $NH_3$  admolecule and three  $NH_2$  radicals representing GaN(0001) surface with  $\theta_{NH_3} = 0.25 ML$  and  $\theta_{NH_2} = 0.75 ML$  coverage. Two left panels - the band diagrams of the slab in momentum and real space respectively. Right panels – the first two present density of states (DOS) projected on the atom quantum  $s$  and  $p$  states of the nitrogen atom in  $NH_3$  admolecule and  $NH_2$  radical

respectively. The rightmost panel present Crystal Orbital Hamilton Population (COHP) of nitrogen and hydrogen atoms in the admolecule and the radicals, respectively [67,68]. The color codes in PDOS and momentum diagrams are identical. Reproduced Fig. 3 from Ref. 120 [120]

Additional hydrogen , i.e.  $\theta_{NH_3} = 1/8$  leads to Fermi level pinned at the latter state as shown in Fig. 31.

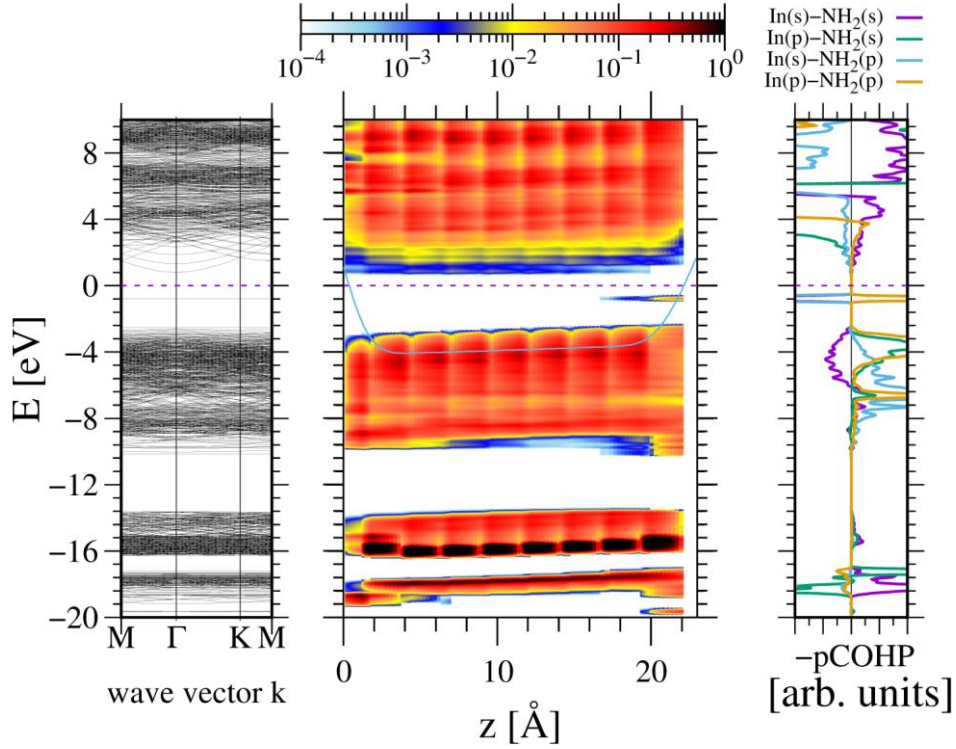


Fig 31. Electronic properties of  $4 \times 4$  slab representing In adatom at GaN(0001) surface covered by 13  $NH_2$  radicals and 3  $NH_3$  molecules ( $x = 3/16$ ). The panels are identical to those in Fig 30. Reproduced from Fig. 4 Ref. 120 [120].

In the higher  $NH_3$  coverage ( $\theta_{NH_3} = 1/8$ ) up to ( $\theta_{NH_3} = 1/4$ ) In adatom is located in T4 site, surrounded by  $NH_2$  radicals only. No  $NH_3$  admolecules are present within the neighbors. For the case  $\theta_{NH_3} = 3/16$  the second EECR condition is fulfilled, the Fermi level is located between In- $NH_2$  antibonding states and conduction band minimum (CBM). After consecutive hydrogen addition, i.e. for  $\theta_{NH_3} = 1/4$  Fermi level is shifted up to CBM. Drastically different case is observed for the highest simulated coverage i.e. ( $\theta_{NH_3} = 5/16$ ).

The atom is located close to the  $NH_3$  admolecule and connected to two or  $NH_2$  radicals. Fermi level is located again in CBM.

Adsorption energy of indium is therefore dependent on GaN(0001) surface coverage. The contribution is important as the number of electrons shifted may reach three. The adsorption energy in function of the coverage is presented in Fig 32. Note that in fact this relation is jump-like but due to limited size of the slab these jumps were not obtained.

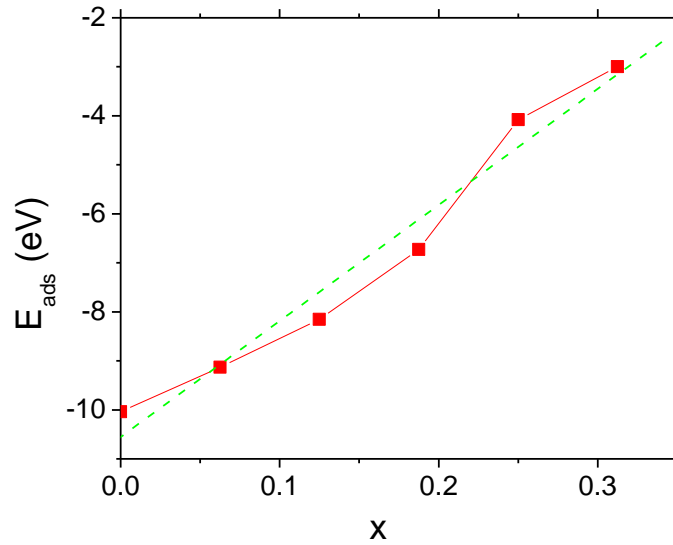


Fig. 32. Indium adsorption energy in function of the  $NH_3$  molecules ( $n_{NH_3}$ ) to  $NH_2$  radicals ( $n_{NH_2}$ ) ratio ( $x$ ), simulated using  $4 \times 4$  slab. All sites of GaN(0001) surface are occupied by  $NH_3$  molecules or by  $NH_2$  radicals. Green dashed line represent the linear approximation in Eq. 15. Reproduced from Fig 8 Ref 120 [120].

These data were approximated by the following expression

$$E_{ads}^{DFT}(x) = -10.55 + 23.68 x \quad (16)$$

where the energy is expressed in eV. The difference between n- and p-type bulk is negligible. As it is shown, the dependence is steep, thus the energy gain is small for higher ammonia coverage. The thermodynamics of In adsorption was also investigated, showing drastic reduction of the probability of In adsorption for increased hydrogen pressure. This is confirmed by MOVPE growth experiments where slight presence of hydrogen blocks incorporation of In in the growth layers [123 - 125]. Moreover, this effect was used in the technology as the growth

of In-free GaN does not require termination of In flow. Much faster is addition of hydrogen in the flow which leads to growth of GaN layers [125 - 128].

In the recent years an important part of the nitride investigations were redirected towards the shorter wavelength devices, active in UV range [129-132]. That entails growth of Al-rich structures and AlN substrates. AlGaN layers crack under tensile strain when grown on GaN substrates, therefore growth of high quality AlN single crystals is indispensable [133-135]. The most promising method is physical vapor transport growth from Al and N<sub>2</sub> [135]. These crystals are grown on polar AlN surfaces: Al-terminated AlN(0001) and N-terminated AlN(000-1). Therefore adsorption of both Al and N<sub>2</sub> was investigated by *at initio* methods [136-139]. It is important that these processes are hydrogen-free.

Adsorption of nitrogen at AlN(0001) surface was investigated first [136]. It was shown that bare AlN surface has no reconstruction with partially filled Al-broken bond state located below CBM. Molecular nitrogen is adsorbed dissociatively without any energy barrier at clean AlN(0001) surface in H3 position, still by very complex path as shown in Fig. 33.

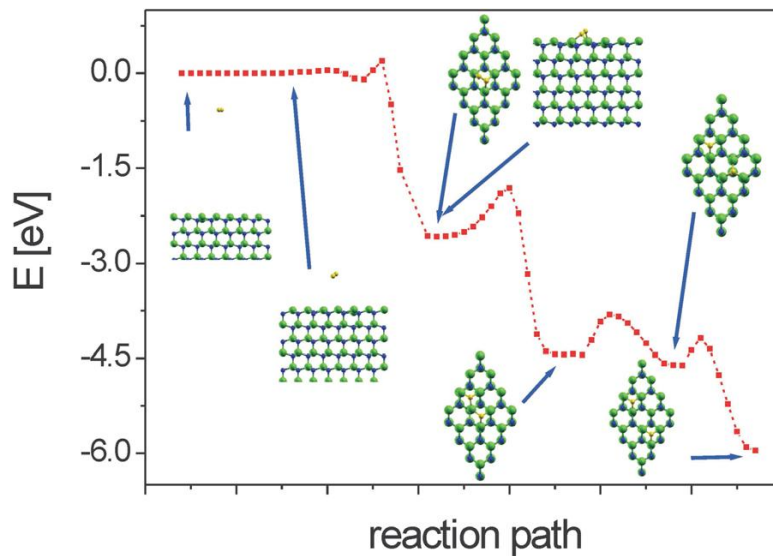


Fig. 33. N<sub>2</sub>-AlN(0001) clean surface slab interaction energy in function of the molecule reaction path. The configuration of the molecule is presented in the inserted diagrams. The molecule undergoes dissociation before reaching the minimum energy point. The energy level is set to zero for asymptotically far distance. Reproduced from Fig. 8 Ref 136 [136].

The adsorbed nitrogen atom *N<sub>s</sub>* state is located deep in the valence band while *N<sub>p</sub>* states are located in the bandgap, below Al-broken bond state. Thus at low coverage these states are occupied by electrons drawn from Al-broken bond state. The EECR unit may encompass three Al sites, i.e. ( $z = 3$ ). The Al broken bond charge is  $q_{Al-br} = 3/4$  thus initial electron charge

of the unit is  $Q_i = 9/4$ . Adsorbed N atoms brings 5 electrons, i.e.  $Q_a = 5$ . The number of the initial states that are occupied after adsorption is  $N_f = 0$ . The number of occupied states after adsorption is  $N_a = 0$ . Therefore the EECR condition is  $g_N = 3/4$  from which the critical N coverage is  $\theta_{N-cr} = 1/4$ . The *ab initio* data confirm this prediction, at  $\theta_{N-cr} = 1/4$  Fermi level is at the top of the highest energy N state [136]. Accordingly, the adsorption energy of molecular nitrogen has a jump at this coverage as shown in Fig. 34.

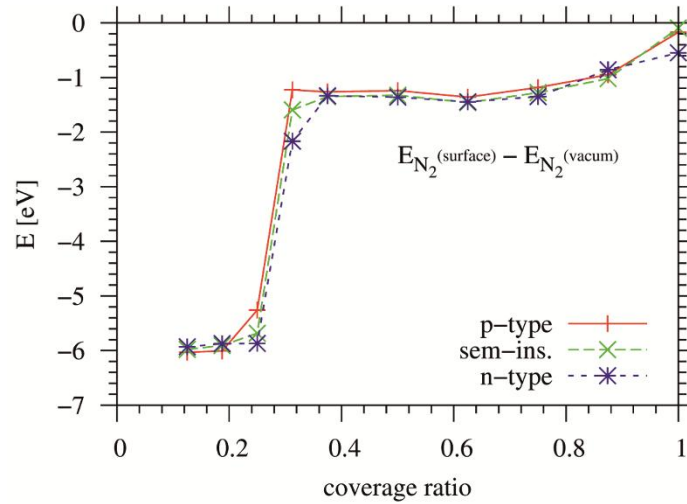


Fig. 34. Adsorption energy of  $N_2$  molecule in function of N adatom coverage ratio, calculated using an energetically stable configuration: for  $\theta_N < 0.25 ML$  - dissociative process leading to concentration of separate N atoms in H3 position, for  $\theta_N > 0.25 ML$  - the excess nitrogen is in the form of  $N_2$  ad molecule in a skewed-vertical position located on top of an Al surface atom. The colors present data for a slab representing the following dominant doping in the bulk: *p*-type, *semi-insulating*, and *n*-type. Carrier concentration was set to  $2.4 \times 10^{20} \text{ cm}^{-3}$ .

Reproduced from Fig. 9 Ref 136 [136].

The obtained adsorption energy change for  $N_2$  molecule could be summarized as follows:

$$\Delta E_{DFT}^{ads-AlN}(N_2) = \begin{cases} -6.0 \text{ eV} & \theta_N < 0.25 ML \\ -1.0 \text{ eV} & \theta_N > 0.25 ML \end{cases} \quad (17)$$

For  $\theta_N < 0.25 ML$  the adsorption is dissociative, for the remaining part the adsorption has no electron transfer contribution which lowers the energy gain is 5.6 eV which is much below the nitrogen molecule dissociation energy. Therefore for  $\theta_N > 0.25 ML$  adsorption is molecular with the energy gain equal to 1.0 eV. Thus the drastic difference in the adsorption type and the energy is related to electron transfer. From that the equilibrium pressure of nitrogen was estimated,

without full thermodynamic analysis. The result the saturation nitrogen pressure below 0.01 bar for the nitrogen coverage below critical ( $\theta_N < 0.25 ML$ ) at PVT AlN growth temperature  $T = 2300 K$ . For molecular adsorption ( $\theta_N > 0.25 ML$ ) the required nitrogen pressure is prohibitively high, of order of  $10^5$  bar.

Molecular nitrogen adsorption at the opposite N-terminated AlN(000-1) surface is drastically different [137]. Clean N-terminated AlN(000-1) surface has no reconstruction. Molecular nitrogen interact with the surface by weak Van der Waals forced typical for closed shell systems. Therefore it is adsorbed molecularly without localization with the energy gain of about  $\Delta E_{DFT}^{ads-AlN}(N_2) = 1.0 eV$ . In case of Al covered surface molecular nitrogen is dissociated with the energy gain given by the relation (in eV):

$$\Delta E_{DFT}^{ads-AlN}(N_2, \theta_N) = 2\Delta E_{DFT}^{ads-AlN}(N, \theta_N) - \Delta E_{DFT}^{diss}(N_2) = -8.32 + 4.88 \theta_N \quad (18)$$

which reflects transformation of the metallic surface into semiconducting, gradual downward motion of the Fermi level and reduction of the electron transfer contribution to adsorbed N adatom. Single N adatom has 8 atomic states while the number of the electron is  $N_e = 7\frac{1}{4}$  thus  $\frac{3}{4}$  electron is transferred from top energy states of Al coverage. Therefore the change of the adsorption energy is considerable. The thermodynamics of nitrogen adsorption was formulated based on vibrational energy contribution to the chemical potential of adsorbed nitrogen at high temperatures. The results show considerable variation of the pressure for limited coverage which remains in agreement for propensity of creation of metallic Al inclusions during growth.

The complementary process of Al adsorption at principal AlN surfaces was also investigated [109, 138]. Al is adsorbed at Al-terminated AlN(0001) surface without any energy barrier. The adsorption energy depends on the Al coverage in the following way:

$$\Delta E_{DFT}^{ads-AlN}(Al) = \begin{cases} -5.06 + 0.02 \theta_{Al} & \theta_{Al} < 1 \\ -6.02 - 8.35 (\theta_{Al} - 1) + 47.45 (\theta_{Al} - 1)^2 & 1 \leq \theta_{Al} \leq 1.2 \\ -3.43 - 1.64(\theta_{Al} - 1) & \theta_{Al} > 1.25 \end{cases} \quad (19)$$

The energy gain has maximum of about 6.1 eV for  $\theta_{Al} = 1.1$ . Thus the contracted layer model formulated for Ga coverage of GaN(0001) surface is applicable also for AlN(0001) surface [109]. No direct confirmation of the role of electron transfer was found. Thus this process is similar to the typical adsorption processes at metal surfaces.

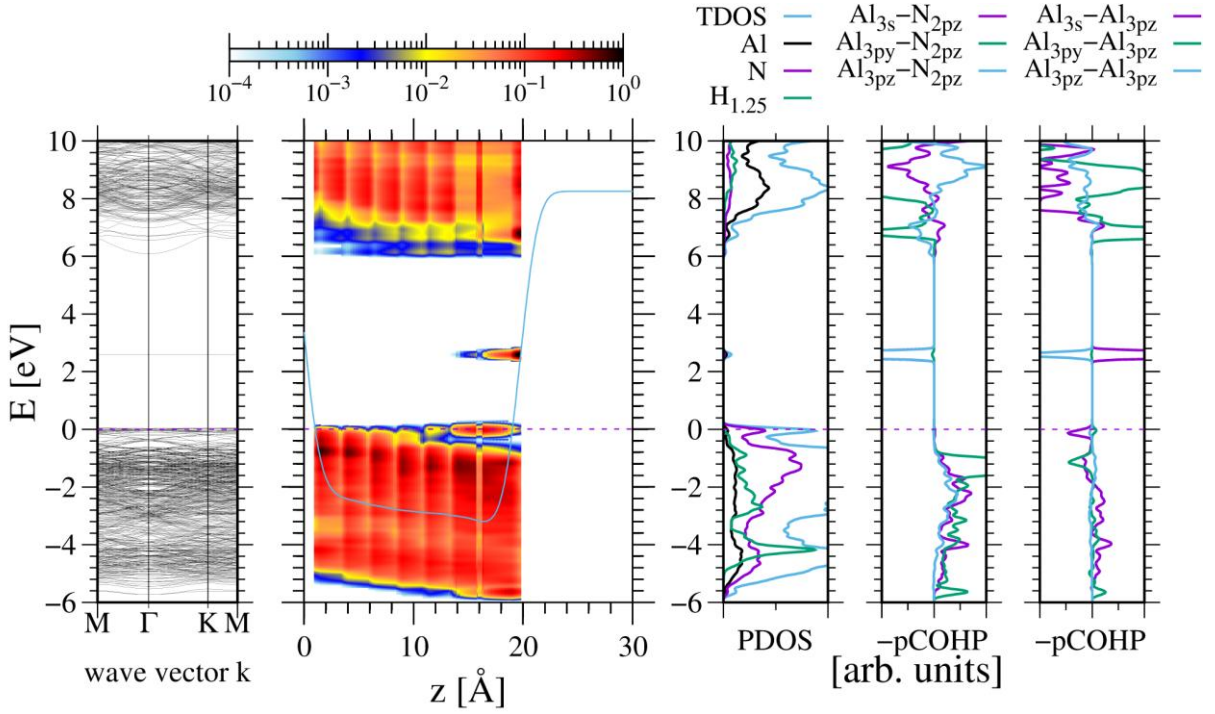


Fig. 35. Electronic properties of 4 x 4 AlN slab with single Al adatom, representing AlN(000-1) surface with  $\theta_{Al} = 0.0625 ML$  coverage. The panels from the left present: electron energy in momentum space (band diagram); electron energy in real space (obtained by projection of the density of states of each atom on the atomic eigenstates and associated with position of the atom), plotted in the direction perpendicular to the surface; total density of states (DOS), projection of the minus crystal orbital Hamilton population (-pCOHP) [54,55] of Al adatom and neighboring N and Al surface atoms, respectively. The surface is located at the right hand edge of real space diagram, close to  $20\text{\AA}$ . Reproduced from Ref. 138 [138].

Different, complex picture was obtained in investigations of adsorption of Al at the opposite, N-terminated AlN(000-1) surface [138]. The electron contribution plays important role in the adsorption. As it is shown in Fig. 35, Al atoms creates bonding states with three topmost N atoms thus the unit has three sites ( $z = 3$ ). The  $Al3s$ ,  $Al3p_x$  (and equivalently  $Al3p_y$ ) and  $Al3p_z$  overlaps with nitrogen atom  $N2p_z$  state create bonding states. The first three are degenerate with VB thus they are occupied but  $Al3p_z-N2p_z$  state is located in the bandgap, thus it is empty. Therefore 6 Al states are occupied ( $N_a = 6$ ). Al atom contributes three electrons, hence  $Q_a = 3$ . The number of electrons in each N surface atoms is  $q_N = 5/4$  which gives  $Q_i = 15/4$ . Nitrogen states and full after adsorption  $N_f = 6$ . Therefore EECR critical fraction for occupation of 6 states is  $g_{Al-cr} = 3/4$  and accordingly, the critical Al coverage is  $\theta_{Al-cr} =$

1/4. Naturally Al adsorption creates surplus of 3/4 electrons which is shifted to other N-broken bond states which are located close to VBM. At the critical coverage this charge is sufficient to fill single N atom broken bond state to 2 electrons. Thus both Al states and N broken bond states are occupied and the further increase of Al coverage leads to electron transfer to higher energy states. This is considerable energy cost therefore for the coverage above critical  $\theta > \theta_{Al-cr} = 1/4$  the Al adsorption energy should be lower. The Al adsorption energy in function of Al coverage is presented in Fig. 36.

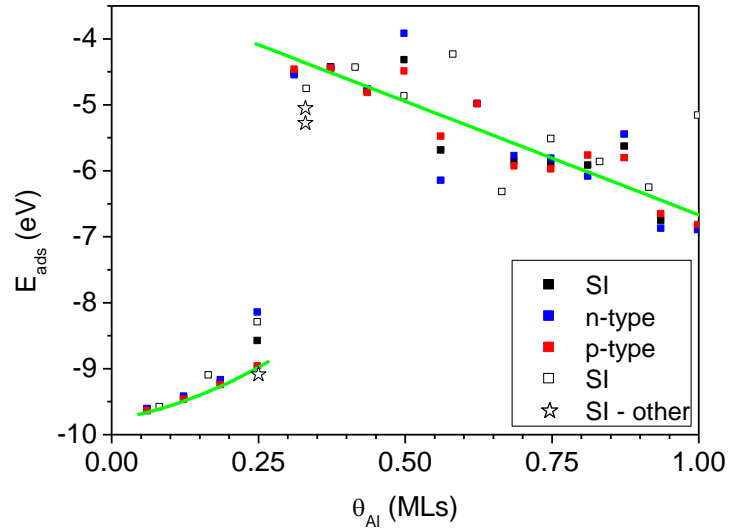


Fig 36. Adsorption energy of Al atom at AlN(0001) surface, in function of Al coverage. Full squares represent data obtained using  $4 \times 4$  slab, empty squares -  $2\sqrt{3} \times 2\sqrt{3}$  slab, empty stars – additional configurations in  $2\sqrt{3} \times 2\sqrt{3}$  slab. The coverage on the horizontal axis refers to the value after the process. Green dashed line presents polynomial approximation to ab initio data. Reproduced from Fig. 3 Ref 138 [138].

The obtained energy may be approximated by the formula:

$$E_{ads}(Al) = \begin{cases} -9.776 + 1.470 \theta_{Al} + 6.856 \theta_{Al}^2 & \theta_{Al} < \frac{1}{4} \\ -4.089 - 3.438 \times \left( \theta_{Al} - \frac{1}{4} \right) & \theta_{Al} \geq \frac{1}{4} \end{cases} \quad (20)$$

As predicted at the critical coverage adsorption energy has the jump by about 3.5 eV. The high coverage dependence is due to transition of the surface to metallic state and closing the gap. The full thermodynamic analysis was made to obtain extremely low pressure values for coverage below critical. The second stability region corresponds to coverage close to full, which

is stable at somewhat higher but still also relatively low Al pressure. Thus N-terminated surface has strong tendency to attain metallic state.

These investigations were concentrated predominantly into investigations of nitride semiconductor surfaces. This was related to rapid development of nitride based optoelectronic devices mostly light emitting diodes (LEDs) and laser diodes. This was fortunate because GaN and AlN have wide bandgaps. This is essential because the gas pressure is required to reveal electron transfer contribution during adsorption as a result of the jump-like change of Fermi energy. The other widegap semiconductor, outside nitride family, suitable for these investigations, is silicon carbide SiC [139]. Clean Si-terminated SiC(0001) surface has Fermi level pinned by broken bond state located 0.8 eV below CBM. Si atom is adsorbed in H3 site, saturating three broken bonds of Si topmost atoms ( $z = 3$ ). The four bonds are created, thus 8 states are occupied ( $N_a = 8$ ). Si topmost atom contributes one electron, thus for three atoms  $Q_i = 3$ . Si adsorbed atom has four electrons therefore  $Q_a = 4$ . Si broken bond states are empty after adsorption thus  $N_f = 0$ . Therefore EECR critical fraction for occupation of 6 states is  $g_{Si-cr} = 3/4$  and accordingly, the critical Si coverage is  $\theta_{Si-cr} = 1/4$ . The Si adsorption energy is plotted in Fig. 37. As it is shown at the coverage in the neighborhood of the critical value, Si adsorption energy is reduced.

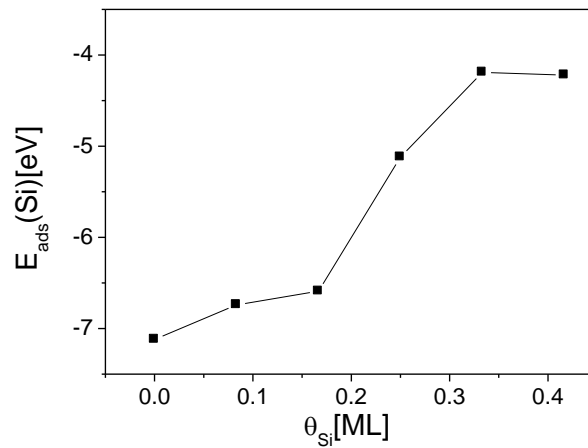


Fig. 37. Adsorption energy of Si adatoms located in H3 sites at the SiC(0001) surface simulated using  $(2\sqrt{3} \times 2\sqrt{3})$  slab. The coverage is defined as the ratio of the Si adatoms before adsorption to the number of the Si topmost atoms in the SiC lattice. Thus in case of finite coverage this points should be shifted to the right to the neighboring value. Reproduced from Fig. 10 Ref 139 [139].

As it is shown again, Si adsorption is reduced by the fact that for the coverage above critical  $\theta_{Si} > \theta_{Si-cr} = 1/4$  one electron should be shifted to higher energy state. The causes adsorption energy in the neighborhood of the critical value. This behavior indicates that the process is more complex and that needs further investigations.

Fairly recently, more extensive simulations of the interactions between polar GaN surfaces and mixed  $NH_3/H_2$  vapor [140]. They confirmed dependence on the adsorption energy on the Fermi level pinning at the surface. They identified three different adsorption regimes for adsorption of gallium on both Ga- and N-terminated surfaces. As shown in Fig 38, the adsorption energies varies considerably.

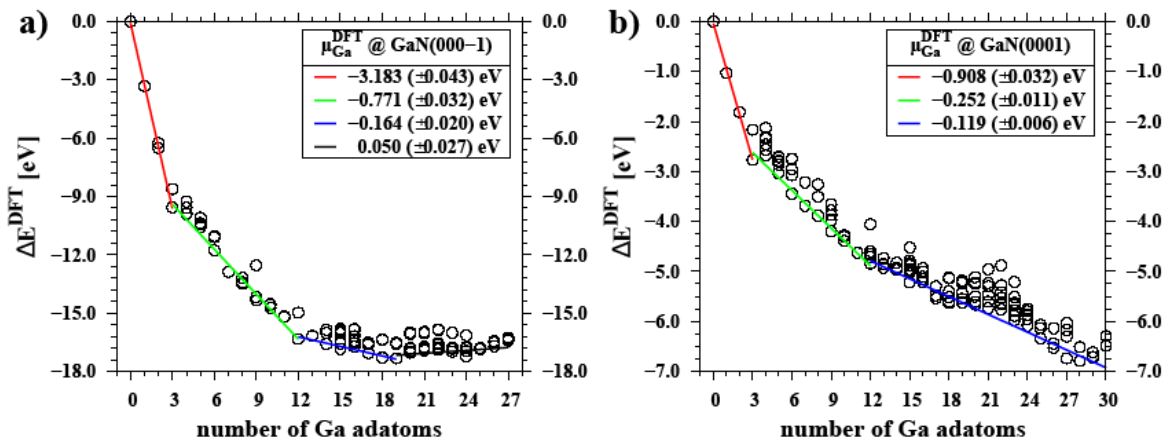


Fig. 38. Change of DFT total energy as a function of the number of Ga adatoms on polar GaN surfaces, (a) GaN(000-1), (b) GaN(0001). The reference level is the sum of energies of the clean surface and the corresponding number of Ga atoms bound in the crystal. All data points (circles) represent energies obtained from DFT calculations for different adatom distributions on the surface. Linear relationships were fitted to the points with the lowest energies. In summary, these reviews of adsorption processes show that the above listed cases show jump-like change of the adsorption energy at the critical coverage for many systems. In some cases this process is gradual and in these cases the other factors may be invoked. In case of jump-like changes such additional factor were not found thus we could conclude that the effect has been proven. Reproduced from Fig. 3 of Ref 140 [140].

The data on these diagrams corresponds to the surface free energy change calculated as the difference between the surface with Ga adatom attached and the surface and G atom separate

in function of the attached atom. It is shown that the dependence is linear in three separate parts. The slope of these lines defines the adsorption energy at these coverages.

Using these data the authors were able to determine the chemical potential surface of Ga adatom at both surfaces. These data were projected on the MOVPE and HVPE growth conditions allowing to determine the basic thermodynamic state of the surfaces during growth of GaN layers by these methods.

### VIII. Charge role in diffusion

Surface diffusion is related to the surface mobility of localized species, i.e. effectively the jumps between the minimal energy positions at the surface. In consequence this is simulated using NEB procedure most frequently [141,142]. This approach leads to a single value of diffusion energy barrier, obtained as the energy difference between the activated complex and the initial value [143]. It is widely used in many cases relevant to surface diffusion [144].

Recently it was recognized that the phenomenon has to be investigated with explicit incorporation of the quantum effects in bonding and statistics [11,12]. Several possible scenarios were formulated, depending on the bonding type and statistics, basically dependent on the Fermi level. These cases are presented in Fig. 39. As it is shown the diffusion barrier may be affected by the initial energy by: (i) standard bonding picture (Fig 39(a)), (ii) bonding by resonant states (Fig 38(b)), (iii) statistics influence via change of the activated complex quantum states close to Fermi energy level, (iv) electron transfer to other state pinning the Fermi level in case for the activated complex quantum states attaining the energy above Fermi energy and in consequence empty.

As an exemplary case for the investigation of the diffusion mechanism was selected the case of diffusion of nitrogen adatoms at Ga-terminated GaN(0001) surface. This case is important also from technological point of view as one of the growth methods of nitride structures used in the devices in plasma-activated molecular beam epitaxy (PA-MBE) [113,114]. The layers are grown in metal-rich conditions thus it is assumed that a metal layer covers the surface. Accordingly the diffusion model was initially proposed in which the nitrogen atom diffuses underneath, known as “new diffusion channel” [145]. First, the energy barrier for diffusion of N adatom at clean GaN(0001) surface was found to be  $\Delta E_{bar} = 1.3 \text{ eV}$  [126]. This was corrected later to a higher value  $\Delta E_{bar} \geq 1.5 \text{ eV}$  [145]. In the case of GaN(0001) surface fully covered by indium adlayer, this barrier was dramatically lower  $\Delta E_{bar} = 0.5 \text{ eV}$ . High barrier for clean GaN(0001) surface was attributed to breaking of two Ga-N bonds which was supposed

to cost about 3.0 eV while in case of indium coverage creation of strong In-N bond compensates this effect. It was concluded that in case of gallium coverage this effect is similar which leads to emergence of fast diffusion channel. Afterwards this effect was used in interpretation of PA-MBE growth experiments [114, 148].

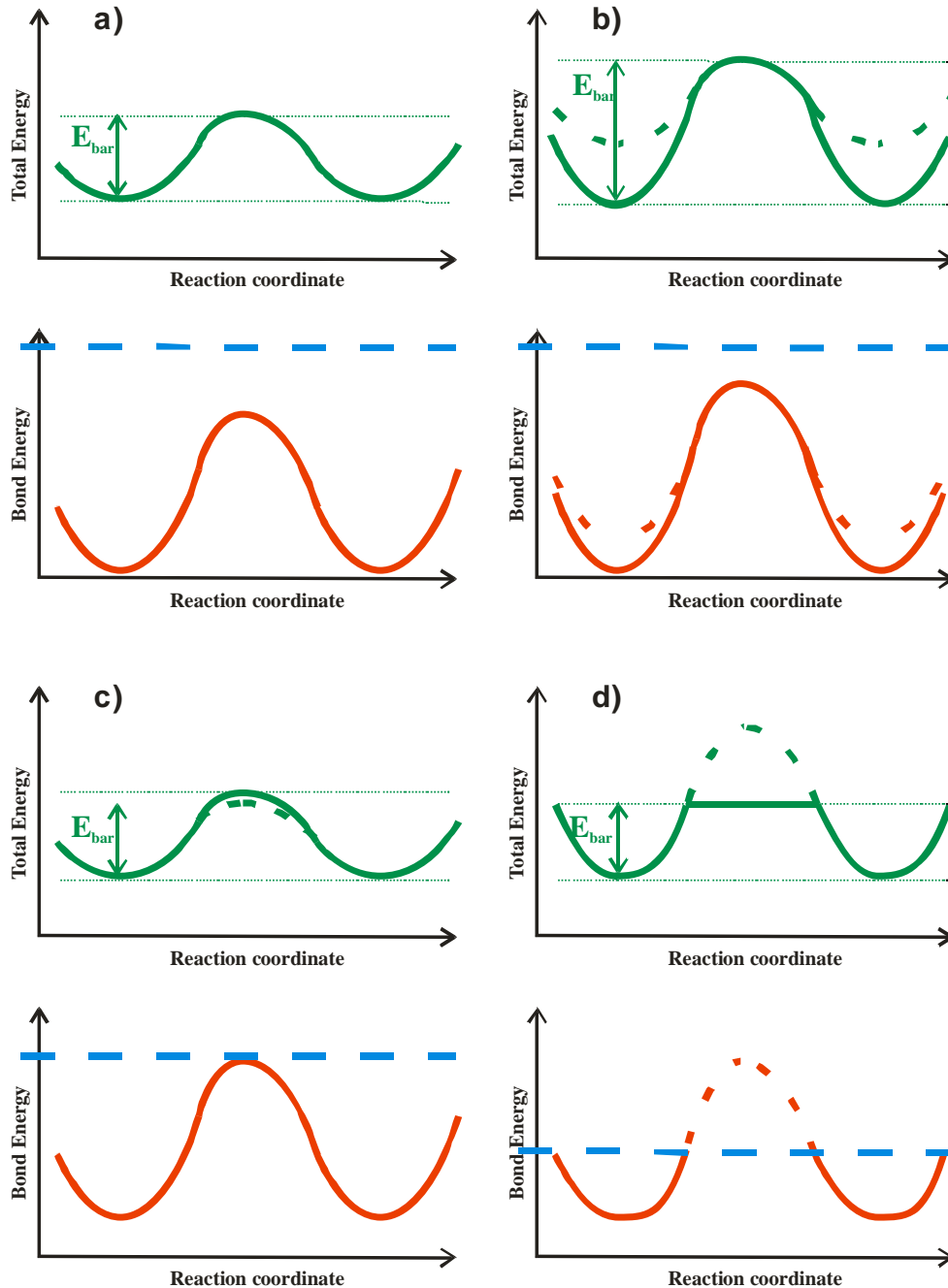


Fig. 39. The factors affecting the effective barrier for diffusion via modification of the energy of the quantum states (red line) and the resulting total energy change (green line) in the course of the jump between two sites: a) standard case: the energy of quantum state remains far below Fermi energy, b) the energy and the occupation of quantum states, standard and resonant in initial state is changed affecting the barrier c) the energy of quantum states

approaches the Fermi energy – the barrier affected via occupation of the states, d) the energy of quantum states extends over the Fermi energy – the energy of the barrier is determined by the Fermi level. The energy of quantum state pinning the Fermi energy (and the Fermi energy itself) is denoted by blue line. Reproduced from Fig. 1 Ref 12 [12].

Therefore the case of N adatom diffusion at GaN(0001) surface under various Ga coverage was investigated again [12]. It was shown that for low Ga coverage N adatom diffusion path begins at the lowest energy point at H3 site via saddle point in bridge configuration to T4 site and repeated again in the inverse order in the symmetric part. The N adatom energy change was investigated along the NEB surface diffusion path. The results of these investigations for the fractional coverage of GaN(0001) surface by Ga adatoms are plotted in Fig.40.

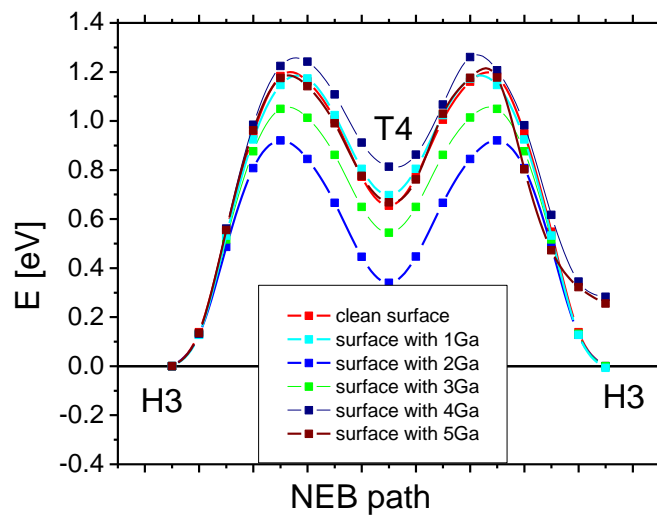


Fig 40. System energy change during motion of the nitrogen adatom along the jump path over GaN(0001) surface partially covered with Ga adatoms. The number of Ga atoms refer to  $(2\sqrt{3} \times 2\sqrt{3})$  slab representing GaN(0001) surface, thus a single Ga adatom refer to  $1/12 ML$  Ga coverage. The “clean” surface corresponds to the absence of Ga adatoms, i.e. with N adatom present. Reproduced from Fig. 5 Ref 14 [14].

As it is shown the diffusion energy barrier for clean GaN(0001) surface is  $\Delta E_{bar} = 1.18 eV$  which is in good agreement with the results in Ref. 145 and basically also with Ref 146. The barrier was determined using refer to  $(2\sqrt{3} \times 2\sqrt{3})$  slab representing GaN(0001) surface, thus

the coverage change was  $(1/12) ML$  [14]. The lowest barrier obtained was  $\Delta E_{bar} = 0.92 eV$  for  $(1/6)ML$  Ga coverage. For higher coverage the barrier was increased again.

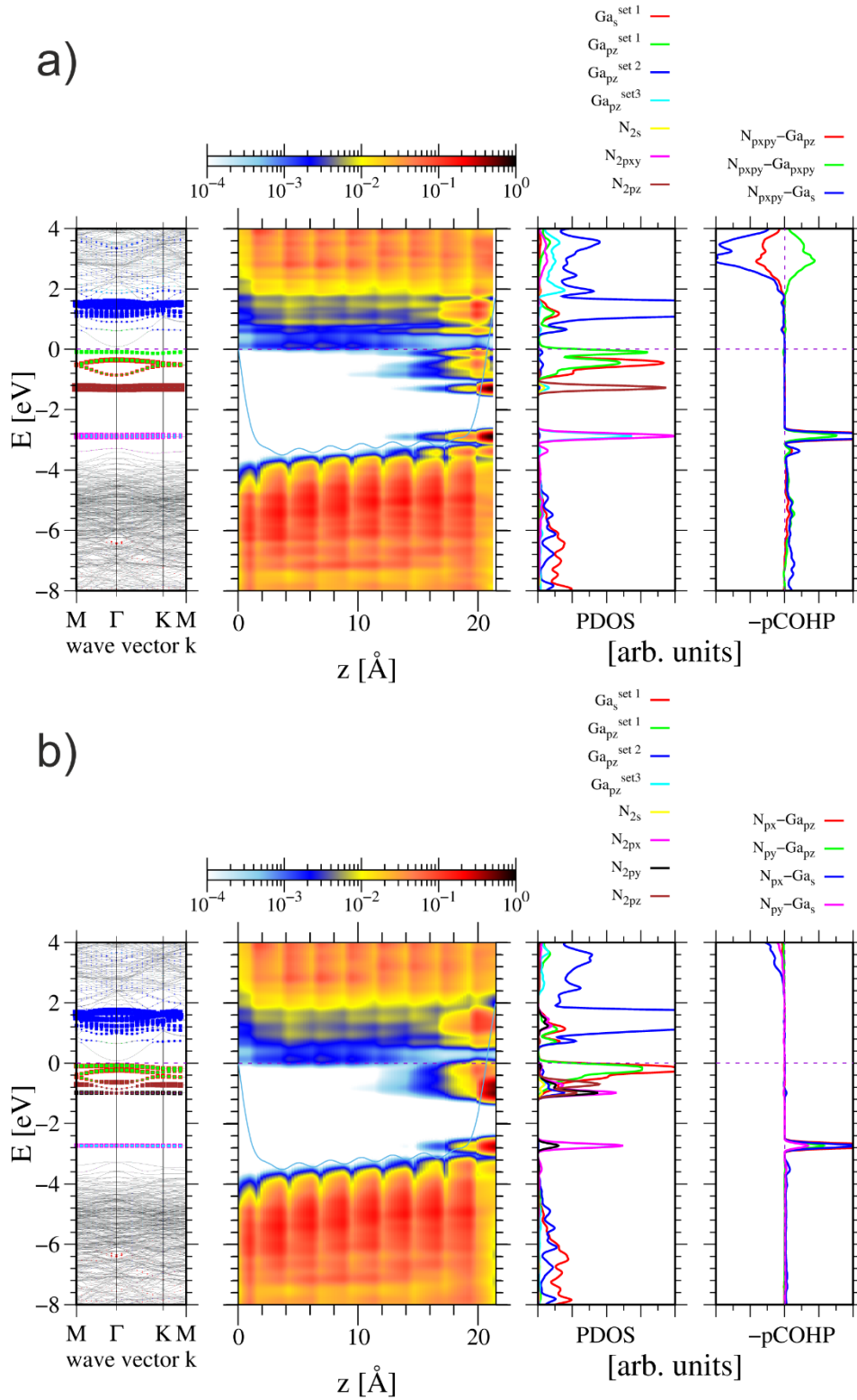


Fig 41. Energies of the quantum states of the  $(2\sqrt{3} \times 2\sqrt{3})$  slab representing clean GaN(0001) surface with single N adatom located in: (a) – H3 site, (b) MAX - max energy position. The

panels represents, from the left: energy of the quantum states in the momentum and the position space, projected density of states (PDOS) of the top Ga atoms and N adatom, and the rightmost panel - Crystal Orbital Hamilton Population (COHP) of the nearest atoms [54, 55]. Thus the COHP data correspond to N adatom and the closest topmost Ga atoms. The Fermi energy is set to zero. COHP positive values correspond to the bonding overlap. Reproduced from Fig. 7 Ref 14 [14].

Therefore the detailed studies of the bonding properties for the path were undertaken. As it is shown in Fig. 40 the bonding of N adatom in H3 site is related to the existence of the three resonating bonds discussed earlier. They are located 2.4 eV below Fermi level which is pinned by broken bond  $sp^3$  hybridized state of top layer Ga atoms. Thus they are fully occupied, due to their resonating character with the probability  $P = 2/3$ . In addition the fourth N bond is broken having its energy about 0.5 eV below Fermi energy and is also occupied. In the bridge configuration one of these bond is broken with the energy located 0.68 eV below the Fermi levels. Therefore it is still occupied. The barrier energy difference between H3 and bridge configuration is related to the change of the energy of fully occupied state. No N state is empty which is related to generally low energy of the nitrogen atom quantum states.

The increase of Ga coverage to  $(1/6) ML$  leads to the change of the Fermi level pinning as these top layer Ga atoms have Ga adatom attached. Some other still preserve  $sp^2 - p_z$  configuration in which  $p_z$  state is empty. The Fermi level is pinned to bonding  $|Ga_{4p_z}\rangle - |Ga_{sp^3}\rangle$  states and therefore lower. Therefore the broken bond nitrogen state has changed its occupation which leads to the energy barrier decrease to  $\Delta E_{bar} = 0.92 eV$  for  $(1/6)ML$ .

The energy barrier for full Ga coverage (13 adatoms for  $(2\sqrt{3} \times 2\sqrt{3})$  slab) was also investigated. As it was shown, minimal energy N adatom position is changed to the on-top. This has important consequences to general understanding of atomic GaN growth mechanism in MBE. In fact the on-top position is required to build a new crystalline layer of GaN. The N adatom is bonded to the three Ga atoms: one from top layer of GaN lattice and the two from adlayer. The other two Ga neighbors belong to the Ga adlayer. The quantum states created by overlap between  $|N_{2p}\rangle$  and  $|Ga_{sp^3}\rangle$  hybridized states are identified at  $E_1 = -7.97 eV$  and  $E_2 = -7.68 eV$ . These states and their overlaps are clearly identified in Fig. 41 (a) and Fig. 41 (b).

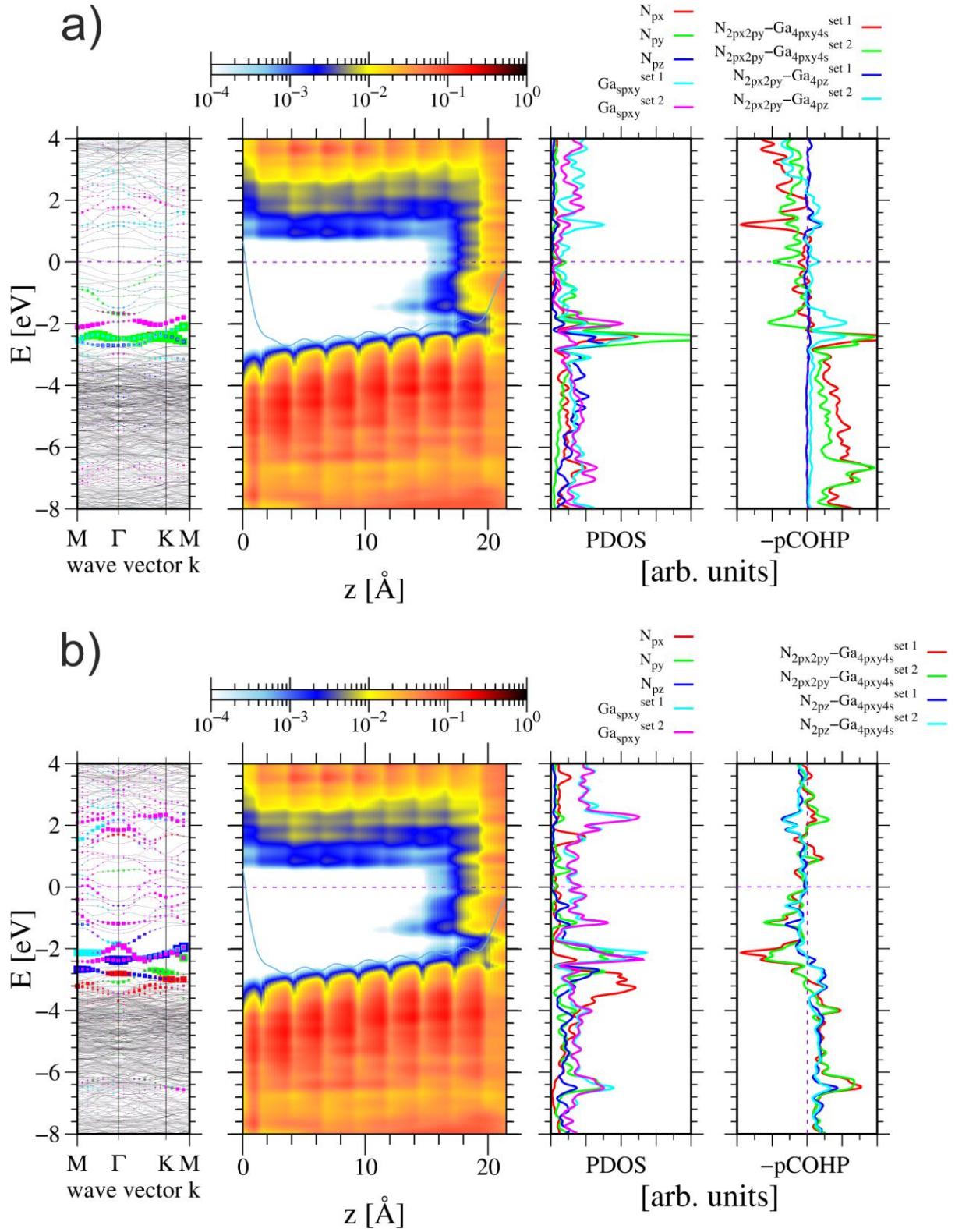


Fig 42. Energies of the quantum states of the  $(2\sqrt{3} \times 2\sqrt{3})$  slab representing GaN(0001) surface fully covered by Ga adatoms, a single N adatom located in: (a) – on-top, (b) max energy position (H3). The symbols are analogous to Fig. 28. Reproduced from Fig. 14 Ref 14 [14].

The motion along the diffusional path leads to the energy maximum which is located at H3 site. In this case the path avoids the bridge location so the overlap is different from the earlier results. Due to the coverage by excess of Ga adatoms, no nitrogen broken bond states are created. In fact the N adatom creates full bonding with the Ga neighbors. Nevertheless, the energies of these states change considerably to  $E_1 = -7.54 \text{ eV}$  and  $E_2 = -7.33 \text{ eV}$ . Thus the energy change is substantial at  $\Delta E_1 = 0.43 \text{ eV}$  and  $E_2 = 0.35 \text{ eV}$ . The change of the energy of the extended state cannot be assessed. Nevertheless, since these changes involve 4 electrons, they fully explain the existence of the barrier  $\Delta E_{bar} = 1.23 \text{ eV}$ . Thus such barrier is associated with the change of the energy of the quantum states. The energy profile is presented in Fig 43.

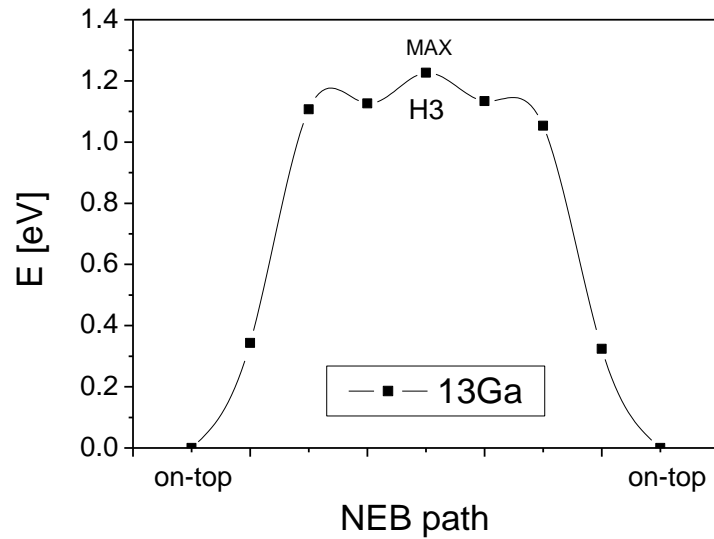


Fig 43. System energy change during motion of the nitrogen adatom along the jump path over GaN(0001) surface fully covered by Ga adatoms. The number of Ga atoms refer (13) to  $(2\sqrt{3} \times 2\sqrt{3})$  slab representing GaN(0001) surface, thus it is excess of Ga single layer coverage  $\theta_{Ga} = (13/12) ML$ . Reproduced from Fig. 12 Ref. 14 [14].

From these data it follows that the energy barrier for full Ga coverage is  $\Delta E_{bar} = 1.23 \text{ eV}$ . Thus it is higher than to  $\Delta E_{bar} = 0.92 \text{ eV}$  for  $(1/6)ML$  Ga fractional coverage. Therefore the existence of the diffusion channel for gallium coverage was not confirmed. It has to be added that the low energy barrier is related to relatively low energy of the broken bond state of N adatoms. The entire picture is therefore related to quantum statistics and quantum bonding affecting the properties of N adatom.

## IX. Summary

This review summarizes the *ab initio* investigations of the charge influence on properties of semiconductor surfaces due to quantum effects in the recent period. These results are summarized by presenting the state of art before these investigations took place, the results reported in this review and the state of art after these investigations were accomplished. The results reported may be divided into the methodology and the physics.

Summarizing, the state of the art before this research was made may be presented as follows (10):

1. The surface dipole charge leads to emergence of the potential coupling of the slab copies via PBC which can be counterbalanced by introduction of the compensating opposite dipole in the vacuum between the slab copies.
2. Separation of the real and termination surface by several atomic layers leads to the asymptotic behavior in which these surfaces are quantum independent so that the system properties obtained are independent of the number of the layers in the slab for relatively limited slab thickness.
3. Surface states band diagram can be obtained by direct projection of all states in the slab on the plane of the momentum parallel to the surface.
4. Adsorption energy of the adsorbate is obtained by direct calculation of the energy difference between the total energy values of the far distance position of the adsorbate and the adsorbate attached at the surface.
5. Adsorption energy is the inherent value of the adsorbate and the surface bonding, that could be affected by adsorbate-adsorbate interactions only. In the case of absence of these interactions adsorption energy is described by a single value of the energy gain in the process.
6. Reconstruction is related to the minimization energy of the surface. The reconstruction period is intrinsic property of the surface, not related to the charge balance.
7. ECR analysis can be successfully used to the charge distribution and the determination of the Fermi level at the surface.
8. Gallium nitride and other wurtzite nitride semiconductors are bonded by the overlap of  $sp^3$  hybridized orbitals that leads to emergence of the valence and conduction bands separated by the bandgap.
9. Thermalization of the adsorbate is relatively minor issue in adsorption in which the dissipation of the excess kinetic energy proceeds via motion of “hot” atoms along the surface.

10. Diffusion energy barrier is a single value, independent on Fermi level and the quantum statical properties of the bonding.

The results obtained in the reported period may be summarized as follows (16):

1. The existence of the dipole in the surface slab was confirmed and thus justifying the incorporation of the opposite, compensating dipole to the slab models as physically sound approach. The only problem that may arise is the precision of the calculated dipole. The alternate method, known as Laplace correction, that could zero the electric field in the space between slab copies by addition of the solution of Laplace equation to electric potential may possibly lead to better precision.

2. The system consisting of the two presumably isolated subsystems such as the slab and the species at far distance may possibly have two different Fermi energy levels. The standard *ab initio* procedures use single Fermi energy and accordingly distribute the electrons among the quantum states using their energies equally of both subsystems. This may lead to charging the slab and the adsorbate (opposite charge). In this case the energy of the system composed of two parts is different from the energy calculated separately for both parts that affects the obtained adsorption energy values.

3. Asymptotic far distance behavior of the wavefunction of any finite system is exponential with no cutoff value. The separation of the real and termination surface leads to mere decrease of the overlap magnitude of their wavefunctions not to complete isolation. Therefore in asymptotic regime the wavefunction overlap could be reduced only. Thus separation of the two surfaces of the slab (real and termination) is not complete.

4. The electric potential and the semiconductor bands are controlled by the charge distribution in the slab. In the case of Fermi level pinning and the presence of the net charge on the surface states, the profile has the slope. In the presence of the net bulk charge within the slab the potential profile has additional parabolic component. Thus the best way of the analysis is to use real space electric potential and band distribution. The nonzero electric field slab solution reflects real semiconductor surface in which the internal surface charge layer exists.

5. In most cases the Fermi level is pinned at the real surface of the slab. Therefore the potential profile has the slope, and accordingly the bands also. Thus the effective bandgap obtained by direct projection is smaller than the bandgap calculated for the bulk material. Therefore projection type presentation of the quantum states at the surface is burdened by the field related errors.

6. The long range variation of the potential may be obtained by appropriate averaging procedures. The resulting variation in the space is in the agreement with the spatial variation of the bands.
7. Reconstruction is correctly recognized as minimization energy process. In addition however, the reconstructed surface patterns and periodicity stems from the charge balance within the surface states so it could be determined from ECR.
8. ECR analysis may be extended to the charge of the adsorbate and the occupation of the new and old states. Thus ECR may be extended to EECR.
9. Adsorption leads to emergence and disappearance of the new quantum states which are occupied by the electron of the slab and the adsorbate. This may lead to total occupation of some states and the drastic change of the adsorption energy value at some coverage. At this point Fermi level is not pinned by surface states and changes freely. This is followed by drastic changes of the equilibrium pressures at some specific conditions. Accordingly crystal growth is conducted at the conditions at which the Fermi level is not pinned.
10. Entropy contribution may play important role in the thermodynamic properties of the adsorption.
11. Gallium nitride bonding occurs via creation of two separate subbands: the upper due to overlap of the  $sp^3$  hybridized gallium states and nitrogen  $p$  states, the lower due to overlap of gallium  $d$  states and nitrogen  $s$  states. Wurtzite tetrahedral symmetry of the lattice is stable due to resonant states of nitrogen bonding where four nitrogen states are bonding to the gallium neighbors according to resonant states created from three nitrogen  $p$  orbitals and occupied with fractional probability.
12. Thermalization of the adsorbate occurs via tunneling of electrons from adsorbate to the solid in external dipole charge electric field. In the following positively charged adsorbate is decelerated by this field losing the excess kinetic energy.
13. Diffusion energy barrier may be affected by the change of the energy of the bonding states that may be close or even crossed Fermi level. This may affect the energy barrier drastically.
14. Diffusion energy barrier may be affected by the quantum statistics influence on the initial states either via resonant state or due to Fermi energy change.

The present state of art is different from the previous state. The main changes are (11):

1. Coulomb interaction of the separate subsystems, both the slab copies and the slab and a far distant adsorbate are described using electric potential distribution showing its possible consequences to surface modelling.
2. Asymptotic exponential behavior of the wavefunction is elucidated with its particular consequences to slab models.
3. The existence of internal charge dipole layer and its role in the ab initio representation of the wavefunctions is demonstrated, with the emphasis on the electric potential profile and the charge distribution close to the surface.
4. The electric field at the is usually present for Fermi level pinned at the surface. Therefore it is present in the slab simulation, even if the Fermi level is not pinned at the termination surface. Thus projection of the band states across the slab leads to artificially small bandgap.
5. The charge role in the clean and adsorbate covered surfaces with direct application of EECR in explanation of the selection of the structure and periodicity of the reconstructed surfaces.
6. The role of charge balance in adsorption: discovery of the adsorption energy jump at the coverage corresponding to Fermi level free.
7. The role of the jump-like change of the adsorption energy gain in thermodynamics of the adsorbate: special role of the case of surface state having Fermi level not pinned as corresponding to vast, dominant portion of thermodynamic states of the vapor in equilibria with the adsorbate covered surfaces. This is the opposite effects observed for surface diagrams: the fraction of the surface with Fermi level pinned is extended in the coverage coordinate and reduced for equilibrium pressure coordinate. The opposite is for Fermi level free: it is contracted in coverage coordinate and extended in pressure coordinate.
8. The above connection has direct consequence for the growth that occurs predominantly for Fermi level free.
9. The role of external charge dipole layer in thermalization of the adsorbate via electron tunneling is formulated.
10. Introduction of the hypothesis of resonant bonding of nitrogen that is important both in the bulk nitrides and at some configuration of nitrogen as an adsorbate.
11. The important role of quantum effects in bonding and statistics in determination of surface diffusion barrier, both in the initial state and the activated energy complex.

In summary, the reported development have changed the scientific picture of the semiconductor surfaces in large extent. It has to be added that in total the progress is not

complete in any sense. The present state of art in the field requires research horizontally directed towards extension of the scope of the semiconductor systems and the surfaces. The finished examples constitute a tiny fraction of all cases that need investigation. Fortunately, the formulation of fundamentals was advanced which provides good starting point for application of massive calculation approach based on algorithms of artificial intelligence (AI).

The second research direction should be in depth, i.e. to proceed towards investigation of the completely new features of semiconductor surface systems. This include the surfaces with different structure and composition. This certainly will include, the vicinal surfaces, i.e. the surface structures with the parallel step sequences. In more distant perspective this will incorporate also the kink structures, i.e. the local jumps on the steps. In these cases the number of the assumption used in the presently used model has to be considerably modified. These approach require creative approach which cannot be solved by AI based methods. In fact these investigation of the steps were already started [149,150]. At this moment they used the old approach which has limited chance of success. Therefore considerable extension of these models are necessary in the future.

### **Acknowledgement**

The paper was critically read by Victor M. Bermudez for which the authors would express their gratitude, especially for the critical comments and the corrections to the text.

The calculations reported in this paper were performed using the computing facilities of the Interdisciplinary Centre for Mathematical and Computational Modelling of Warsaw University (ICM UW) under several grant over the reported period.

### **References**

- [1] C.P. Correia V. Bernardo, R. A. Marques Lameirinhas, J. P. de Melo Cunha, J. P. N. Torres, A revision of the semiconductor theory from history to applications. Disc. Appl. Sci. 6, 316 (2024). <https://doi.org/10.1007/s42452-024-06001-1>
- [2] L. Lukasiak, A. Jakubowski, History of Semiconductors. J. Telecommun. Inf. Technol. 1, 3 (2010).
- [3] W. Monch, *Semiconductor Surfaces and Interfaces*. Springer Berlin 1993.
- [4] L. Kronik, Y. Shapira, Surface photovoltage phenomena: theory, experiment and applications. Surf. Sci. Rep. 37, 1 (1999). [https://doi.org/10.1016/S0167-5729\(99\)00002-3](https://doi.org/10.1016/S0167-5729(99)00002-3)

- [5] L. Kronik, Y. Shapira, Surface photovoltage spectroscopy of semiconductor structures: at the crossroads of physics, chemistry and electrical engineering. *Surf. Interface Anal.* 31, 954 (2001). <https://doi.org/10.1002/sia.1132>
- [6] V. Bermudez, The fundamental surface science of gallium nitride. *Surf. Sci. Rep.* 72, 147 (2017). <http://dx.doi.org/10.1016/j.surfrep.2017.05.001>
- [7] C. Kittel, *Introduction to Solid State Physics* Wiley, N. York 1997 (7<sup>th</sup> ed.)
- [8] J. Gersten, *The physics and chemistry of materials*, Wiley, N. York 2001
- [9] N.D. Lang and W. Kohn, Theory of Metal Surfaces: Charge Density and Surface Energy. *Phys. Rev. B* 1, 4555 (1970). <https://doi.org/10.1103/PhysRevB.1.4555>
- [10] N.D. Lang and W. Kohn, Theory of Metal Surfaces: Work Function. *Phys. Rev. B* 3, 1215 (1973). <https://doi.org/10.1103/PhysRevB.3.1215>
- [11] M. Magnuson, F. Mattesini, C. Hoglund, J. Birch, L. Hultman, Electronic structure and bonding anisotropy investigation of wurtzite AlN, *Phys. Rev. B* 80, 155105 (2009). <https://doi.org/10.1103/PhysRevB.80.155105>
- [12] M. Magnuson, F. Mattesini, C. Hoglund, J. Birch, L. Hultman, Electronic structure of GaN and Ga investigated by soft x-ray spectroscopy and first-principles methods. *Phys. Rev. B* 82, 085125 (2010). <https://doi.org/10.1103/PhysRevB.81.085125>
- [13] M. Ptasinska, J. Sołtys, J. Piechota, S. Krukowski, Electronic properties on GaN(0001) surface – *ab initio* investigation. *Vacuum* 99, 166 (2013). <http://dx.doi.org/10.1016/j.vacuum.2013.05.006>
- [14] P. Strak, C. Sobczak, S. Krukowski. Quantum effects in surface diffusion: application to diffusion of nitrogen adatoms over GaN(0001) surface. [arXiv:2501.19079](https://arxiv.org/abs/2501.19079) <https://arxiv.org/abs/2501.19079>
- [15] J. Neugebauer, M. Scheffler, Adsorbate-substrate and adsorbate-adsorbate interactions of Na and K adlayers on Al(111). *Phys. Rev. B* 46, 16067 (1992). <https://doi.org/10.1103/PhysRevB.46.16067>
- [16] L. Bengtsson, Dipole correction for surface supercell calculations, *Phys. Rev. B* 59 12301 – 12304 (1999). <https://doi.org/10.1103/PhysRevB.59.12301>
- [17] S. Krukowski, P. Kempisty, P. Strak, Electrostatic condition for the termination of the opposite face of the slab in DFT simulations of semiconductor surfaces. *J. Appl. Phys.* 105, 113701 (2009). <http://dx.doi.org/10.1063/1.3130156>
- [18] P. Strak, P. Kempisty, K. Sakowski, J. Piechota, I. Grzegory, E. Monroy, A. Kaminska, S. Krukowski, Polarization spontaneous and piezo: fundamentals and their implementation in *ab initio* calculations. *Materials* – Accepted.

- [19] L.D. Landau, E. M. Lifshitz, *Electrodynamics of continuous media*, Pergamon Press, Londyn, 1960.
- [20] C. Wood, D. Jena, *Polarization Effects in Semiconductors*, Springer Berlin 2008
- [21] F. Bechstedt, U. Grossner, J. Furthmuller, Dynamics and polarization of group III nitride lattices: A first-principles study, *Phys. Rev. B* 62, 8003 (2000).  
<https://doi.org/10.1103/PhysRevB.62.8003>
- [22] E.T. Yu, X. Z. Dang, P.M. Asbeck, S. S. Lau, G. J. Sullivan, Spontaneous and piezoelectric polarization effects in III-V nitride heterostructures, *J. Vac. Sci. Technol. B* 17, 1742 (1999). <https://doi.org/10.1116/1.590818>
- [23] M. Feneberg, K. Thonke, Polarization fields of III-nitrides grown in different crystal orientations, *J. Phys. Condens. Matter* 19, 403201 (2007) .  
<https://doi.org/10.1088/0953-8984/19/40/403201>
- [24] J. Lahnemann, O. Brandt, U. Jahn, C. Pfüller, C. Roger, P. Dogan, F. Grosse, A. Belabbes, F. Bechstedt, A. Trampert, L. Gelhaar, Direct experimental determination of the spontaneous polarization of GaN, *Phys. Rev. B* 86, 081302(R) (2012).  
<https://doi.org/10.1103/PhysRevB.86.081302>
- [25] F. Bernardini, V. Fiorentini, and D. Vanderbilt, Spontaneous polarization-and piezoelectric constants of III-V nitrides, *Phys. Rev. B* 56 (2001) R10024.  
<https://doi.org/10.1103/PhysRevB.56.R10024>
- [26] V. Fiorentini, F. Bernardini, F. Della Sala, A. Di Carlo, and P. Lugli, *Phys. Rev. B* 60, 8849 (1999). <https://doi.org/10.1103/PhysRevB.60.8849>
- [27] P. Strak, P. Kempisty, K. Sakowski, A. Kaminska, D. Jankowski, K. P. Korona, K. Sobczak, J. Borysiuk, M. Beeler, E. Grzanka, E. Monroy, S. Krukowski, *Ab initio* and experimental studies of polarization and polarization related fields in nitrides and nitride structures, *AIP Adv.* 7, 015027 (2017). <https://dx.doi.org/10.1063/1.4974249>
- [28] C. E. Dreyer, A. Janotti, C. G. Van de Walle, D. Vanderbilt, Correct Implementation of Polarization Constant in Wurtzite Materials and Impact on III-Nitrides, *Phys. Rev. X* 6, 021038 (2016). <https://doi.org/10.1103/PhysRevX.6.021038>
- [29] S. Krukowski, P. Kempisty, P. Strak, Foundations of ab initio simulations of electric charges and fields at semiconductor surfaces within slab models. *J. Appl. Phys.* 114, 143705 (2013). <http://dx.doi.org/10.1063/1.4824800>

- [30] A. Yoshiasa, Y. Murai, O. Ohtaka, T. Katsura, Detailed Structures of Hexagonal Diamond (lonsdaleite) and Wurtzite-type BN, *Jpn. J. Appl. Phys.* 42, 1694 (2003).  
<https://doi.org/10.1143/JJAP.42.1694>
- [31] H. Angerer, D. Brunner, F. Freudenberg, O. Ambacher, M. Stutzmann, R. Höpler, T. Metzger, E. Born, G. Dollinger, A. Bergmaier, S. Karsch, H. -J. Korner. Determination of the Al Mole Fraction and the Band Gap Bowing of Epitaxial  $\text{Al}_x\text{Ga}_{1-x}\text{N}$  Films. *Appl. Phys. Lett.* 71, 1504 (1997). <https://doi.org/10.1063/1.119949>
- [32] M. Leszczynski, H. Teisseyre, T. Suski, I. Grzegory, M. Bockowski, J. Jun, S. Porowski, K. Pakula, J.M. Baranowski, C.T. Foxon, T.S. Cheng, Lattice parameters of gallium nitride, *Appl. Phys. Lett.* 69, 73 (1996). <https://doi.org/10.1063/1.118123>
- [33] W. Paszkowicz, J. Adamczyk, S. Krukowski, M. Leszczynski, S. Porowski, J. A. Sokołowski, M. Michalec, W. Lasocha, Lattice parameters, density and thermal expansion of InN microcrystals grown by the reaction of nitrogen plasma with liquid indium. *Phil. Mag. A* 79 1145 (1999). <https://doi.org/10.1080/01418619908210352>
- [34] Q. Zhang, Q. Li, W. Zhang, H. Zhang, F. Zheng, M. Zhang, P. Hu, M. Wang, Z. Tian, Y. Li, Y. Liu, F. Yun, Phase transition and bandgap engineering in  $\text{B}_{1-x}\text{Al}_x\text{N}$  alloys: DFT calculations and experiments, *Appl. Surf. Sci.* 575 (2022) 151641.  
<https://doi.org/10.1016/j.apsusc.2021.151641>
- [35] E. Silveira, J.A. Freitas, S. B. Schujman, L. J. Schowalter, AlN bandgap temperature dependence from its optical properties, *J. Cryst. Growth* 310, (2008) 4007.  
<https://doi.org/10.1016/j.jcrysgro.2008.06.015>
- [36] B. Monemar, J. P. Bergman, I. A. Buyanova, H. Amano, I. Akasaki, T. Detchprohm, K. Hiramatsu, N. Sawaki, The excitonic bandgap of GaN: Dependence on substrate, *Solid State Electron.* 41 (1997) 239. [https://doi.org/10.1016/S0038-1101\(96\)00208-0](https://doi.org/10.1016/S0038-1101(96)00208-0)
- [37] Y. C. Yeo, T. C. Chong, M.F. Li, Electronic band structures and effective-mass parameters of wurtzite GaN and InN, *J. Appl. Phys.* 83 (1997) 1429.  
<https://doi.org/10.1063/1.366847>

- [38] J. Wu, W. Walukiewicz, K. M. Yu, J. W. Ager, E. E. Haller, H. Lu, W. J. Schaff, Y. Saito, Y. Nanishi, Unusual properties of the fundamental band gap of InN, Appl. Phys. Lett. 80 (2002) 3967. <https://doi.org/10.1063/1.1482786>
- [39] T. Matsuoka, H. Okamoto, M. Nakao, H. Harima, E. Kurimoto, Optical bandgap of wurtzite InN, Appl. Phys. Lett. 81 (2002) 1246. <https://doi.org/10.1063/1.1499753>
- [40] J. Wu, W. Walukiewicz, Band gaps of InN and group III nitride alloys, Superlatt. Microstr. 34 (2003) 63. <https://doi.org/10.1016/j.spmi.2004.03.069>
- [41] P. Kempisty, S. Krukowski, On the nature of Surface States Stark Effect at clean GaN(0001) surface. J. Appl. Phys. 112, 113704 (2012). <https://doi.org/10.1063/1.4768256>
- [42] M. Revesz, I. Bertoti, G. Mink, I. Mayer, On the use of pseudo-atoms in cluster calculations for modeling of molecular fragments, solids and surfaces, J. Mol. Struct.-Theochem. 50, 335 (1988). [https://doi.org/10.1016/0166-1280\(88\)80500-1](https://doi.org/10.1016/0166-1280(88)80500-1)
- [43] N. N. Ilchenko, L. G. Gorb, V. V. Goncharuk, The application of “pseudoatoms” to quantum chemistry simulation of solid-surfaces with hypervalence coordination environment - $\alpha$ -Al<sub>2</sub>O<sub>3</sub>. J. Mol. Struct.-Theochem. 95, 17 (1992). [https://doi.org/10.1016/0166-1280\(92\)80020-M](https://doi.org/10.1016/0166-1280(92)80020-M)
- [44] S.H. Yoo, M. Todorova, D. Wickramaratne, L. Weston, C. G. Van de Walle, J. Neugebauer, Finite-size correction for slab supercell calculations of materials with spontaneous polarization, NPJ Comp. Mater. 7, 58 (2021). <https://doi.org/10.1038/s41524-021-00529-1>
- [45] J. E. Northrup, J. Neugebauer, Theory of GaN (10 $\bar{1}$ 0) and (11 $\bar{2}$ 0) surfaces. Phys. Rev. B 53, R10 477 (1995). <https://doi.org/10.1103/PhysRevB.53.R10477>
- [46] K. Rapcewicz, M. Buongiorno Nardelli, J. Bernholc, Theory of morphology of wurtzite GaN (0001) surfaces. Phys. Rev. B 56, R12 725 (1997). <https://doi.org/10.1103/PhysRevB.56.R12725>
- [47] F.-H. Wang, P. Kruger, J. Pollmann, Electronic structure of (1 × 1) GaN(0001) and GaN(000 $\bar{1}$ ) surfaces. Phys. Rev. B 64, 035305 (2001). <https://doi.org/10.1103/PhysRevB.64.035305>

- [48] A. L. Rosa, J. Neugebauer, First-principles calculations of the structural and electronic properties of clean GaN(0001) surfaces. *Phys. Rev. B.* 73, 205346 (2006).  
<https://doi.org/10.1103/PhysRevB.73.205346>
- [49] C. G. Van de Walle, D. Segev, Microscopic origin of surface states on nitride surfaces. *J. Appl. Phys.* 101, 081704 (2007). <https://doi.org/10.1063/1.2722731>
- [50] D. Segev, C. G. Van de Walle, Electronic structure of nitride surfaces. *J. Cryst. Growth* 300, 199 (2007). <https://doi.org/10.1016/j.jcrysgr.2006.11.039>
- [51] P. Strak, P. Kempisty, K. Sakowski, S. Krukowski, Ab initio determination of electron affinity of polar nitride surfaces, clean and under Cs coverage. *J. Vac. Sci. Technol. A* 35, 021406 (2017). <http://dx.doi.org/10.1116/1.4975332>
- [52] P. Kempisty, S. Krukowski, P. Strak, K. Sakowski, Ab initio studies of electronic properties of bare GaN(0001) surface. *J. Appl. Phys.* 106, 054901 (2009).  
<http://dx.doi.org/10.1063/1.3204965>
- [53] J. Soltys, J. Piechota, M. Lopuszynski, S. Krukowski, A comparative DFT Study of electronic properties of 2H-, 4H- and 6H-SiC(0001) and SiC(0001) clean surfaces. *N. J. Phys.* 12, 043204 (2010). <http://dx.doi.org/10.1088/1367-2630/12/4/043024>
- [54] P. Strak, P. Kempisty, M. Ptasinska, S. Krukowski, Principal physical properties of GaN/AlN multiquantum well (MQW) systems determined by density functional theory (DFT) calculations. *J. Appl. Phys.* 113, 193706 (2013).  
<http://dx.doi.org/10.1063/1.4805057>
- [55] P. Witczak, P. Kempisty, P. Strak, S. Krukowski, Ab initio study of Ga-GaN system: transition from adsorbed metal atoms to a metal-semiconductor junction. *J. Vac. Sci. Technol. A* 33, 061101 (2015). <http://dx.doi.org/10.1116/1.4927166>
- [56] J. Heyd, G. E. Scuseria, M. Ernzerhof, Hybrid functionals based on a screened Coulomb potential, *J. Chem. Phys.* 118, 8207 (2003).  
<https://doi.org/10.1063/1.1564060>
- [57] L. S. Pedroza, A. J. R. da Silva, K. Capelle, Gradient-dependent density functionals of the Perdew-Burke-Ernzerhof type for atoms, molecules, and solids, *Phys. Rev. B* 79, 201106(R) (2009). <https://doi.org/10.1103/PhysRevB.79.201106>
- [58] M. M. Odashima, K. Capelle, S. B. Trickey, Tightened Lieb-Oxford Bound for Systems of Fixed Particle Number, *J. Chem. Theory Comput.* 5, 798 (2009) .  
<https://doi.org/10.1021/ct8005634>

- [59] L.G. Ferreira, M. Marques, L.K. Teles, Approximation to density functional theory for the calculation of band gaps of semiconductors. *Phys. Rev. B* 78, 125116 (2008).  
<https://doi.org/10.1103/PhysRevB.78.125116>
- [60] M. Ribeiro, L.R.C. Fonseca, L.G. Ferreira, Accurate prediction of the Si/SiO<sub>2</sub> interface band offset using the self-consistent *ab initio* DFT/LDA-1/2 method. *Phys. Rev. B*, 79, 241312 (2009). <https://doi.org/10.1103/PhysRevB.79.241312>
- [61] W. Harrison, *Electronic Structure and the Properties of Solids* . Freeman San Francisco 1980
- [62] P. Y. Yu, M. Cardona, *Fundamentals of Semiconductors* Springer Heidelberg 2010
- [63] F. A. Kekule, Untersuchungen uber aromatische Verbindungen. *Liebigs Annalen der Chemie und Pharmacie* 137, 129 (1866). <https://doi.org/10.1002%2Fjlac.18661370202>  
(in German)
- [64] P. A. Schultz, R. P. Messmer, Are There  $\pi$  Bonds in Benzene? *Phys. Rev. Lett.* 58, 2416 (1987). <https://doi.org/10.1103/PhysRevLett.58.2416>
- [65] P. W. Anderson, The Resonating Bond State in LA<sub>2</sub>CuO<sub>4</sub> and Superconductivity. *Science* 235, 1196 (1987). <https://doi.org/10.1126/science.235.4793.1196>
- [66] C. Weber, *Variational Study of Strongly Correlated Electronic Models*. PhD thesis. EPFL Lausanne 2007.
- [67] R. Dronskowski, P. E. Bloechl, Crystal orbital Hamilton populations (COHP): energy-resolved visualization of chemical bonding in solids based on density-functional calculations. *J. Phys. Chem.* 97, 8617 (1993). <https://doi.org/10.1021/j100135a014>
- [68] V. L. Deringer, A. L. Tchougreeff, R. Dronskowski, Crystal Orbital Hamilton Population (COHP) Analysis as Projected from Plane-Wave Basis Sets. *J. Phys. Chem.* 115, 5461 (2011). <https://doi.org/10.1021/jp202489s>
- [69] M. C. Benjamin, C. Wang, R. F. Davis, J. Nemanich, Observation of negative electron affinity for heteroepitaxial AlN on SiC(0001). *Appl. Phys. Lett.* 64, 3288 (1994). <https://doi.org/10.1063/1.111312>
- [70] D. P. Malta, G. G. Fountain, J. B. Posthill, T. P. Humphreys, C. Pettenhofer, J. K. Markunas, *Mater. Res. Symp. Proc.* 468, 437 (1997)
- [71] V. M. Bermudez, T. M. Jung, K. Doverspike, A. E. Wickenden, The growth and properties of Al and AlN films on GaN(0001) – (1x1), *J. Appl. Phys.* 79, 110 (1996).  
<https://doi.org/10.1063/1.360917>

- [72] C. -I. Wu, A. Kahn, N. Taskar, D. Dorman, D. Gallagher, *GaN(0001) – (1 × 1) surfaces: Composition and electronic properties*. J. Appl. Phys. 83, 4249 (1998). <https://doi.org/10.1063/1.367182>
- [73] C. -I. Wu, A. Kahn, *Electronic states at aluminum nitride (0001) – 1 x 1 surfaces*, Appl. Phys. Lett. 74, 546 (1999). <https://doi.org/10.1063/1.123140>
- [74] V. M. Bermudez, C. -I. Wu, A. Kahn, *AlN films on GaN: sources of error in the photoemission measurements of electron affinity*. J. Appl. Phys. 89, 1991 (2001). <https://doi.org/10.1063/1.1333716>
- [75] P. Strak, K. Sakowski, P. Kempisty, S. Krukowski, *Dissipation of the excess energy of the adsorbate – thermalization via electron transfer*. Phys. Chem. Chem. Phys. 19, 9149 (2019). <https://doi.org/10.1039/c7cp00235a>
- [76] H. Brune, J. Wintterlin, R. J. Gehm, G. Ertl, *Surface migration of “hot” adatoms in the course of dissociative chemisorption of oxygen on Al(111)*. Phys. Rev. Lett. 68, 624 (1992). <https://doi.org/10.1103/PhysRevLett.68.624>
- [77] S. Schindke, S. Messerli, K. Morgenstern, J. Nieminen, W.-D. Schneider, *J. Chem. Phys.* 114, 4206 (2001). <https://doi.org/10.1063/1.1346687>
- [78] A. Gross, *Ab Initio Molecular Dynamics Study of Hot Atom Dynamics after Dissociative Adsorption of H<sub>2</sub> on Pd(100)*. Phys. Rev. Lett. 103, 246101 (2009). <https://doi.org/10.1103/PhysRevLett.103.246101>
- [79] W. W. Hayes, J. R. Manson, *Argon scattering from Ru(0001): Calculations and comparison with experiment*. Phys. Rev. B, 75, 113408 (2007). <https://doi.org/10.1103/PhysRevB.75.113408>
- [80] L. C. Ciacchi, M. C. Payne, *“Hot-Atom” O<sub>2</sub> Dissociation and Oxide Nucleation on Al(111)*. Phys. Rev. Lett. 92, 176104 (2004). <https://doi.org/10.1103/PhysRevLett.92.176104>
- [81] H. Siegle, G. Kaczmarczyk, L. Fillipidis, A. P. Litwinchuk, A. Hoffmann, C. Thomsen, *Zone-boundary phonons in hexagonal and cubic GaN*, Phys. Rev. B 55, 7000 (1997). <https://doi.org/10.1103/PhysRevB.55.7000>
- [82] A. K. Tiwari, S. Nave, B. Jackson, *Methane Dissociation on Ni(111): A New Understanding of the Lattice Effect*. Phys. Rev. Lett. 103, 253201 (2009). <https://doi.org/10.1103/PhysRevLett.103.253201>
- [83] J. Lindhard, *On the properties of gas of charged particles*. K. Dan. Vidensk. Selsk. Mat. Fys. Medd. 28, 57 (1954).

- [84] P. Kempisty, S. Krukowski, Adsorption of ammonia at GaN(0001) surface in the mixed ammonia/hydrogen ambient - a summary of ab initio data. *AIP Adv.* 4, 117109 (2014). <http://dx.doi.org/10.1063/1.4901922>
- [85] S. Zoino, L. Borowik, B. Mohamad, E. Nowak, P. Kempisty, Ab initio investigations of two-dimensional gas at interfaces in GaN/AlN and GaN/AlN/Al<sub>2</sub>O<sub>3</sub> heterostructures, *J. Appl. Phys.* 134, 155304 (2023). <https://doi.org/10.1063/5.0169332>
- [86] M. Menenghini, C. De Santi, I. Abid, M. Cioni, R. A. Khadar, L. Nela, N. Zagni, A. Chini, F. Mejoub, G. Menghesso, G. Verzellesi, E. Zenono, E. Matioli, GaN power devices: Physics, reliability and perspectives, *J. Appl. Phys.* 130, 181101 (2021). <https://doi.org/10.1063/5.0061354>
- [87] G. P. Srivastava, Theory of semiconductor surface reconstruction, *Rep. Prog. Phys.* 60, 561 (1997). <https://doi.org/10.1088/0034-4885/60/5/002>
- [88] H. Neddemeyer, Scanning tunneling microscopy of semiconductor surfaces. *Rep. Prog. Phys.* 59, 701 (1996). <https://doi.org/10.1088/0034-4885/59/6/001>
- [89] D. J. Chadi, Atomic structure of GaAs(100)-(2x1) and (2x4) reconstructed surfaces. *J. Vac. Sci. Technol. A* 5, 834 (1987). <https://doi.org/10.1116/1.574366>
- [90] M. D. Pashley. Electron counting model and its application to island structures on molecular-beam epitaxy grown GaAs(001) and ZnSe(001). *Phys. Rev. B* 40, 10481 - 10487 (1989). <https://doi.org/10.1103/PhysRevB.40.10481>
- [91] S.-H. Yoo, L. Lymperakis, J. Neugebauer, Efficient electronic passivation scheme for computing low-symmetry compound semiconductor surfaces in density-functional theory slab calculation. *Phys. Rev. Mater.* 5, 044605 (2021). <https://doi.org/10.1103/PhysRevMaterials.5.044605>
- [92] J. S. Griffith, L. E. Orgel, Ligand-field theory. *Q. Rev. Chem. Soc.* 11, 381 (1957). <https://doi.org/10.1039/QR9571100381>
- [93] N. A. Modine, E. Kaxiras. Theory of the (3 x 2) reconstruction of the GaAs(0001) surface. *Mater. Sci. Eng. B* 67, 1 (1999). [https://doi.org/10.1016/S0921-5107\(99\)00202-0](https://doi.org/10.1016/S0921-5107(99)00202-0)
- [94] P. Kempisty, P. Strak, S. Krukowski, Ab initio determination of atomic structure and energy of surface states of bare and hydrogen covered GaN (0001) surface - existence of the Surface States Stark Effect (SSSE). *Surf. Sci.* 605, 695 (2011). <http://dx.doi.org/10.1016/j.susc.2011.01.005>

- [95] Y.-W. Chen, J.-L. Kuo, Density functional study of the First Wetting Layer on the GaN (0001) surface. *J. Phys. Chem. C* 117, 8774 (2013).  
<https://doi.org/10.1021/jp312377t>
- [96] P. Strak, W. Miller, S. Krukowski, Charge-Controlled Energy Optimization of the Reconstruction of Semiconductor Surfaces:  $sp^3 - sp^2$  Transformation of Stoichiometric surface to  $(4 \times 4)$  Pattern, *Materials* 17, 2614 (2024).  
<https://doi.org/10.3390/ma17112614>
- [97] S. Krukowski, P. Kempisty, P. Strak, K. Sakowski, Fermi level pinning and the charge transfer contribution to the energy of adsorption at semiconducting surfaces. *J. Appl. Phys.* 115, 043529 (2014). <http://dx.doi.org/10.1063/1.4863338>
- [98] P. Kempisty, S. Krukowski, P. Strak, Fermi level influence on the adsorption at semiconductor surfaces - ab initio simulations. *J. Appl. Phys.* 114, 0637507 (2013).  
<http://dx.doi.org/10.1063/1.4817903>
- [99] P. Kempisty, P. Strak, K. Sakowski, S. Krukowski, General aspects of the vapor growth of semiconductor crystals - a study based on DFT simulations of the  $\text{NH}_3/\text{NH}_2$  covered GaN(0001) surface in hydrogen ambient, *J. Cryst. Growth* 390, 71 (2014).  
<http://dx.doi.org/10.1016/j.jcrysgro.2013.12.039>
- [100] P. Kempisty, P. Strak, K. Sakowski, S. Krukowski, Thermodynamics of GaN(s)- $\text{NH}_3(\text{v})+\text{N}_2(\text{v})+\text{H}_2(\text{v})$  system - electronic aspects of the processes at GaN(0001) Surface, *Surf. Sci.* 662, 12 (2017). <https://doi.org/10.1016/j.susc.2017.03.007>
- [101] P. Kempisty, S. Krukowski, Ab initio investigation of adsorption of atomic and molecular hydrogen at GaN(0001) surface. *J. Cryst. Growth* 358, 64 (2012).  
<http://dx.doi.org/10.1016/j.jcrysgro.2012.08.004>
- [102] M. Chase, C. Davies, J. Downey, D. Frurip, R. McDonald, A.N. Sverud, JANAF Thermochemical Tables. *J. Phys. Chem. Ref. Data Suppl.* 14 (1985) 1002.
- [103] W. P. Glushko (ed.) *Termodynamiczeskije swoistwa individualnykh wescstw*. Nauka, Moscow, 1978
- [104] I. Barin, *Thermochemical Data of Pure Substances*, VCH, Weinheim 1994.
- [105] NIST-JANAF Thermochemical Tables. NIST Standard Reference Database 13,  
<https://doi.org/10.18434/T42S31>
- [106] P. Kempisty, Y. Kangawa, Evolution of the free energy of the GaN(0001) surface based on first-principles phonon calculations. *Phys. Rev. B* 100, 085304 (2019).  
<https://doi.org/10.1103/PhysRevB.100.085304>

- [107] P. Kempisty, P. Strak, K. Sakowski, Y. Kangawa, S. Krukowski, Thermodynamic foundations of applications of ab initio methods for determination of the adsorbate equilibria: hydrogen at GaN(0001) surface. *Phys. Chem. Chem. Phys.* 19 (2017) 29676 – 29684. <http://dx.doi.org/10.1039/c7cp05214f>
- [108] J. Piechota, S. Krukowski, P. Sadovyi, B. Sadovyi, S. Porowski, I. Grzegory, Nitrogen Dissolution in liquid Ga and Fe: Comprehensive Ab initio Analysis. Relevance for Crystal Growth, *Materials* 14 (2021) 1306. <https://dx.doi.org/10.3390/ma14051306>
- [109] P. Strak, A. Ahmad, P. Kempisty, J. Piechota, K. Sakowski, G. Nowak, Y. Kangawa, J. Łażewski, Stanislaw Krukowski, Al coverage of AlN(0001) surface and Al vapor pressure – thermodynamic assessment based on *ab initio* calculations. *Comp. Mater. Sci.* 203 (2022) 111159. <https://doi.org/10.1016/j.commatsci.2021.111159>
- [110] A. J. Jackson, A. Walsh, Oxidation of GaN: An *ab initio* thermodynamic approach. *Phys. Rev. B* 88, 165201 (2013). <https://doi.org/10.1103/PhysRevB.88.165201>
- [111] S. Krukowski, P. Kempisty, A. Jalbout, Thermodynamic and kinetic approach in DFT studies of microscopic structure of GaN(0001) surface in ammonia-rich conditions. *J. Chem. Phys.* 129, 234705 (2008) . <http://dx.doi.org/10.1063/1.3037218>
- [112] M. Ptasinska, J. Piechota, S. Krukowski, Adsorption of Hydrogen at GaN(0001) surface – *Ab Initio* Study. *J. Phys. Chem. C.* 119, 11563 (2015). <http://dx.doi.org/10.1021/acs.jpcc.5b00836>
- [113] T. D. Moustakas, B. Paiella, Optoelectronic device physics and technology of nitride semiconductors from the UV to terahertz. *Rep. Prog. Phys.* 80, 106501 (2017). <https://doi.org/10.1088/1361-6633/aa7bb2>
- [114] C. Skierbiszewski, Z. R. Wasilewski, I. Grzegory, S. Porowski, Nitride-based laser diodes by plasma-assisted MBE- from violet to green emission. *J. Cryst. Growth* 311, 1632- 1639 (2008). <https://doi.org/10.1016/j.jcrysgro.2008.12.040>
- [115] T. Taki, M. Strassburg, Visible LEDs: More than Efficient Light. *ECS J. Solid State Sci. Technol.* 9, 015017 (2020). <https://www.doi.org/10.1149/2.0402001JSS>
- [116] M. Kneissl, T. Y. Seong, J. Han, H. Amano, The emergence and prospects of deep-ultraviolet light-emitting diode technologies. *Nature Photonics* 13, 233-244 (2019). <https://www.doi.org/10.1038/s41566-019-0359-9>
- [117] I. M. Watson, Metal organic vapour phase epitaxy of AlN, GaN, InN and their alloys: A key chemical technology for advanced device applications, *Coord. Chem. Rev.* 257 2120 (2013). <https://doi.org/10.1016/j.ccr.2012.10.020>

- [118] C. Van de Walle, J. Neugebauer, First-Principles Surface Phase Diagram for Hydrogen on GaN Surfaces. *Phys. Rev. Lett.* 88, 066103 (2002).  
<https://doi.org/10.1103/PhysRevLett.88.066103>
- [119] P. Kempisty, P. Strak, K. Sakowski, S. Krukowski, Adsorption of ammonia on hydrogen covered GaN(0001) surface – a Density Functional Theory study. *J. Cryst. Growth* 401, 514 (2014). <https://doi.org/10.1016/j.jcrysgro.2013.10.061>
- [120] P. Kempisty, A. Ahmad, P. Strak, K. Sakowski, A. Kafar, J. Piechota, and Stanislaw Krukowski, Incorporation of indium into GaN layers in the context of MOVPE thermodynamics and growth - *ab initio* studies, *Comp. Mater. Sci.* 230, 112489 (2023). <https://doi.org/10.1016/j.commatsci.2023.112489>
- [121] E. L. Piner, M. K. Behbehani, N. A. El-Masry, F. G. McIntosh, J. C. Roberts, K. S. Boutros, S. M. Bedair, Effect of hydrogen on the indium incorporation in InGaN epitaxial films, *Appl. Phys. Lett.* 70 (1997) 461-463.
- [122] F. Scholz, Metalorganic vapour phase epitaxy of GaN and GaInN/GaN heterostructures and quantum wells, *Prog. Cryst. Growth Charact. Mater.* 35 (1997) 243-262.
- [123] R. Czernecki, S. Kret, P. Kempisty, E. Grzanka, J. Plesiewicz, G. Targowski, S. Grzanka, M. Bilska, J. Smalc-Koziorowska, S. Krukowski, T. Suski, P. Perlin, M. Leszczynski, Influence of hydrogen and TMI<sub>n</sub> on indium incorporation in MOVPE growth of InGaN layers, *J. Cryst. Growth* 402 (2014) 330-336.
- [124] R. Czernecki, E. Grzanka, P. Strak, G. Targowski, S. Krukowski, P. Perlin, T. Suski, M. Leszczynski, Influence of hydrogen pre-growth flow on indium incorporation into InGaN layers, *J. Cryst. Growth* 464 (2017) 123-126.
- [125] R. Czernecki, E. Grzanka, J. Smalc-Koziorowska, S. Grzanka, D. Schiavon, G. Targowski, J. Plesiewicz, P. Prystawko, T. Suski, P. Perlin, M. Leszczynski, Effect of hydrogen during growth of quantum barriers on the properties of InGaN quantum wells, *J. Cryst. Growth* 414 (2015) 38-41.
- [126] Y. Zhu, T. Lu, X. Zhou, G. Zhao, H. Dong, Z. Jia, X. Liu, B. Xu, Effect of small flow hydrogen treatment at the upper well/barrier interface on the properties of InGaN/GaN multiple quantum wells, *Superlattices Microstruct.* 107 (2017) 293-298.
- [127] H.-L. Wang, X.-H. Zhang, H.-X. Wang, B. Li, C. Chen, Y.-X. Li, H. Yan, Z.-S. Wu, H. Jiang, Suppression of indium-composition fluctuations in InGaN epitaxial layers by periodically-pulsed mixture of N<sub>2</sub> and H<sub>2</sub> carrier gas, *Chin. Phys. B* 27 (2018) 127805.

- [128] H. Wang, Z. Lv, C. Chen, S. Zhang, Y. Guo, B. Li, Z. Wu, H. Jiang, Reduction of nonradiative recombination in InGaN epilayers grown with periodical dilute hydrogen carrier gas, *Appl. Surf. Sci.* 494 (2019) 285-292.
- [129] H. Hirayama, in: F. Roccaforte, M. Leszczynski (Eds.), *Nitride Semiconductor Technology. Power Electronics and Optoelectronic Devices*, Wiley-VCH, Weinheim, Germany, 2020,
- [130] F. Roccaforte, M. Leszczynski, *Introduction to Gallium Nitride Properties and Applications*, in: F. Roccaforte, M. Leszczynski (Eds.), *Nitride Semiconductor Technology. Power Electronics and Optoelectronic Devices*, Wiley-VCH, Weinheim, Germany, 2020, pp. 1 – 39.
- [131] D.B. Li, K. Jiang, X.J. Sun, C. L. Guo, AlGa<sub>N</sub> photonics: recent advances in materials and ultraviolet devices, *Adv Opt. Photon.* 10 (2018) 43-110.  
<https://doi.org/10.1364/AOP.10.000043>
- [132] C. K Tan, W. Sun, D. Borovac, N. Tansu, 2016. Large Optical Gain AlInN-Delta-GaN Quantum Well for Deep Ultraviolet Emitters. *Sci. Rep.* 6, 22983 .  
<https://doi.org/10.1038/srep22983>
- [133] H. Taketomi, Y. Aoki, Y. Takagi, A. Sugiyama, M. Kuwabara, H. Yoshida, 2016. Over 1 W record-peak-power operation of a 338 nm AlGa<sub>N</sub> multiple-quantum-well laser diode on a GaN substrate. *Jpn. J. Appl. Phys.* 55, 05FJ05.  
<https://doi.org/10.7567/JJAP.55.05FJ05>
- [134] A. Yadav, H. Hirayama, E.U. Rafailov, Light Emitting Diodes, in F. Roccaforte, M. Leszczynski (Eds) *Nitride Semiconductor Technology. Power Electronics and Optoelectronic Devices*, Wiley-VCH, Weinheim, Germany, 2020, pp. 253–299.
- [135] G. Selvaduray, L. Sheet, Aluminium nitride: review of synthesis methods. *Mater. Sci. Technol.* 9 (1993) 463-473. <https://doi.org/10.1179/mst.1993.9.6.463>
- [136] P. Strak, K. Sakowski, P. Kempisty, S. Krukowski, Structural and electronic properties of AlN(0001) surface under partial N coverage as determined by ab initio approach, *J. Appl. Phys.* 118, 095705 (2015). <http://dx.doi.org/10.1063/1.4929823>
- [137] P. Strak, K. Sakowski, J. Piechota, A. Ahmad, I. Grzegory, Y. Kangawa, S. Krukowski, Adsorption of nitrogen at AlN(000-1) surface – decisive role of structural and electronic factors. *Surf. Sci.* 713, 096503 (2021).  
<https://doi.org/10.1016/j.susc.2021.121891>
- [138] P. Kempisty, P. Strak, K. Sakowski, Y. Kangawa, and Stanislaw Krukowski, *Ab initio* and thermodynamic picture of Al adsorption of AlN(0001) surface - role of bond

- creation and electron transition contributions. *Appl. Surf. Sci.* 532, 147719 (2020).  
<https://doi.org/10.1016/j.apsusc.2020.147419>
- [139] J. Soltys, J. Piechota, P. Strak, S. Krukowski, Electronic Charge Transfer Contribution in Adsorption of Silicon at the SiC(0001) Surface – A Density Functional Theory (DFT) Study. *Appl. Surf. Sci.* 393, 168 (2017).  
<http://dx.doi.org/10.1016/j.apsusc.2016.10.007>
- [140] P. Kempisty, K. Kawka, A. Kusaba, Y. Kangawa, Polar GaN surfaces under Gallium Rich Conditions: Revised Thermodynamic Insights from Ab Initio Calculations. *Materials* 16, 5982 (2023). <https://doi.org/10.390/ma16175982>
- [141] G. Henkelman, B.P. Uberuaga and H. Jonsson, A climbing image nudged elastic band method for finding saddle points and minimum energy paths. *J. Chem. Phys.* **113**, 9901 – 9904 (2000). <https://doi.org/10.1063/1.1329672>
- [142] G. Henkelman, H. Jonsson, Improved tangent estimate in the nudged elastic band method for finding minimum energy paths and saddle points. *J. Chem. Phys.* **111**, 9978 - 9985 (2000). <https://doi.org/10.1063/1.1323224>
- [143] H. Eyring, The activated complex in chemical reactions. *J. Chem. Phys.* 3, 107 (1935).  
<https://doi.org/10.1063/1.1749604>
- [144] R. Gomer, Diffusion of adsorbates on metal surfaces. *Rep. Prog. Phys.* 53, 917 (1990).  
<https://doi.org/10.1088/0034-4885/53/7/002>
- [145] J. Neugebauer, T. K. Zywietz, M. Scheffler, J. E. Northrup, H. Chen, R.M. Feenstra, Adatom Kinetics On and Below the Surface: The Existence of a New Diffusion Channel. *Phys. Rev. Lett.* 90, 056101 (2003).  
<https://doi.org/10.1103/PhysRevLett.90.056101>
- [146] T. Zywietz, J. Neugebauer, M. Scheffler, Adatom diffusion at GaN(0001) and (000 $\bar{1}$ ) surface. *Appl. Phys. Lett.* 73, 487 (1998). <https://doi.org/10.1063/1.121909>
- [147] A. R. Smith, R. M. Feenstra, D. W. Greve, M.-S. Shin, M. Skowronski, J. Neugebauer, J. E. Northrup, GaN(0001) surface structures studied using scanning tunneling microscopy and first-principles total energy calculations. *Surf. Sci.* 423, 70 (1990).  
[https://doi.org/10.1016/S0039-6028\(98\)00903-0](https://doi.org/10.1016/S0039-6028(98)00903-0)
- [148] S. Porowski, C. Skierbiszewski, Potential of MME for gallium nitride based lasers. *Proc. SPIE* 5968, 59580Z (2005). <https://doi.org/10.1117/12.622908>
- [149] T. Akiyama, T. Kawamura, Ab initio study for adsorption behavior on AlN(0001) surface with steps and kinks during metal-organic vapor-phase epitaxy, *Jpn. J. Appl. Phys.* 63, 02SP71 (2024). <https://doi.org/10.35848/1347-4065/ad1896>

- [150] T. Akiyama, T. Kawamura, Structural Stability of Vicinal AlN(0001) and GaN(0001) Surface with Steps and Kinks under Metal-Organic Vapor-Phase Epitaxy Condition: A First-Principles Study, *Cryst. Growth Des.* 24, 5906 (2024).  
<https://doi.org/10.1021/acs.cgd.4c00121>